Molecular Biological Characterization of Aggressive Paraganglioma

Dissertation

zur Erlangung des akademischen Grades

doctor rerum naturalium

(Dr. rer. nat.)

genehmigt durch die Fakultät für Naturwissenschaften

der Otto-von-Guericke-Universität Magdeburg

von

Dipl. Neurowiss. Stephanie Fliedner

geb. am 30.03.1979 in Bremen

Gutachter:

Prof. Dr. med. Hendrik Lehnert

Dr. Henri Timmers (M.D., Ph.D.)

eingereicht am: 25.01.2011

verteidigt am: 16.05.2011

Zusammenfassung

Paragangliome (PGL) sind chromaffine Zelltumore, zu denen auch die in der adrenalen Medulla auftretenden Phäochromocytome (PHEO) zählen. Eine korrekte Diagnose von PHEO/PGL ist anspruchsvoll, denn die auftretenden Symptome sind nicht eindeutig. Unbehandelte PHEO/PGL können verheerend Folgen haben, da erhöhte Katecholamin-Level zu ausgepraegtem Bluthochdruck, Apoplexie, Herzrhytmusstoerungen und Herzinfarkt führen können. Selbst bei korrekter Diagnose bleibt das Risiko der Metastasenbildung. Bis zu 10 % der Patienten haben bereits zum Zeitpunkt der Diagnose Metastasen. Patienten mit Mutationen der Succinat-Dehydrogenase B (*SDHB*) entwickeln zu 50-97 % Metastasen. Behandlungsoptionen sind begrenzt, sobald Metastasen vorhanden sind, und abhängig von der untersuchten Patientengruppe, beträgt die Chance 5 Jahre zu überleben lediglich 35-60 %.

Ziel dieser Arbeit war die molekularbiologische Charakterisierung von agressiven PHEO/PGL.

Zuerst wurde der Nutzen von Urinpeptiden für die Klassifizierung unterschiedlicher Patientengruppen untersucht. Der Urin von gesunden Kontrollpersonen (Ctr), Patienten mit metastasierenden (*SDHB*-met) und nicht-metastasierenden (offensichtlich benignen, *SDHB*-ben) *SDHB*-mutationsbedingten PHEO/PGL und gesunden *SDHB*-Mutationsträgern (*SDHB*-car) wurde per Kapillarelektrophorese gekoppelt mit Elektrospray Ionisations time-of-flight Massenspektrometrie analysiert. Auf Basis der Unterschiede in detektierten Peptiden zwischen diesen Gruppen wurden potentiell prädiktive Marker für *SDHB*-Mutationen und solche zur Unterscheidung zwischen Patienten mit benignen und metastasierenden *SDHB*-mutationsvermittelten PHEO/PGL identifiziert.

Klassifikation von *SDHB*-car auf Grundlage von 4 Peptiden war erfolgreich bei einer Fehlerrate von 1,8 %. Korrekte Klassifizierung von *SDHB*-met anhand nur eines Peptids war mit einer Fehlerrate von 3,3 % möglich. Das höchst rangierende Peptid konnte als Fragment von Kollagen Typ III identifiziert werden. *SDHB*-ben Patienten und gesunde Mutationsträger konnten anhand von 3 Peptiden bei einer Fehlerrate von 10,5 % separiert werden. Wenn jedoch ein kombinierter Klassifikations-Algorithmus aus Katecholaminspiegel und den 3 höchst rangierenden Peptiden angewandt wurde, konnte eine korrekte Klassifikation zu 100 % erzielt werden. Aufgrund dieser Ergebnisse lässt sich vermuten, dass einige wenige Urinpeptide das Potential haben,

Individuen mit *SDHB*-Mutationen als solche zu identifizieren und gesunde Mutationsträger von Patienten mit metastasierenden PHEO/PGL zu unterscheiden. Darüber hinaus scheint die Messung von 3 Urinpeptiden der korrekten Diagnose von nicht Katecholamin sezernierenden PHEO/PGL, die bei 10 % der *SDHB*-Patienten auftreten, zuträglich zu sein.

Als Zweites wurden Charakteristika der zellulären Proteinexpression in aggressiven PHEO/PGL evaluiert. Dabei wurde besonderes Augenmerk auf Fehlfunktionen des Energiestoffwechsels gelegt. Es ist bekannt, dass PHEO/PGL, die mit SDHx und von-Hippel-Lindau (VHL) Genmutation in Zusammenhang stehen, erhöhte Glycolyse und reduzierte oxidative Phosphorylierung (OXPHOS) zeigen. Trotzdem ist die Tendenz dieser Tumore zu metastasieren sehr unterschiedlich: Metastasenbildung ist selten in VHL-bedingten PHEO/PGL, während *SDHB*-bedingte häufig metastasieren. Differenzielle-2D-Gel-Analyse von ‚mouse PHEO cells' (MPC) und ihren filialen, aggressiveren ‚mouse tumor tissue'-Zellen (MTT) zeigte Expressionsunterschiede verschiedener Energiestoffwechsel-Proteine, unter anderem einiger Untereinheiten des ATP-Synthase-Komplexes. Diese Proteine wurden dann in humanen PHEO/PGL untersucht.

Im Einklang mit einem glykolytischen Phänotyp war die Laktat-Dehydrogenase-Expression in den aggressiven Proben erhöht, mit einem höheren Verhältnis von A- zu B- Untereinheit in MPC verglichen mit MTT und *SDHB* PHEO/PGL verglichen mit normaler Nebenniere. Das Verhältnis von A- zu B-Untereinheits-Expression erwies sich als ähnlich in VHL- und *SDHB*-mutationsbedingten PHEO/PGL, allerdings basierend auf einer verminderten Expression der B-Untereinheit in ersteren verglichen mit normaler Nebenniere, während in letzteren die A-Untereinheit verstärkt exprimiert war.

Entzug von Glukose verringerte die Proliferation von MTT, nicht aber MPC Zellen. Respirometrie zeigte jedoch keinen Unterschied im Sauerstoffverbrauch von Komplex I und II zwischen den Zelltypen. Allerdings konnte eine vermehrte Produktion der Reaktiven Sauerstoffspezies (ROS) an Komplex I festgestellt werden. Untersuchung der OXPHOS-Komplex-Aktivität in humanem PHEO/PGL-Gewebe zeigte, dass die Aktivität von Komplex I, II und II+III relativ zum Gehalt an Mitochondrien in *SDHB*- gegenüber VHL-mutationsbedingten PHEO/PGL geringer ist. Es konnte jedoch kein Unterschied im ROS-Level festgestellt werden. Die vorgelegten Daten zeigen, dass MTT- und *SDHB*-mutationsbedingte PHEO/PGL im Vergleich zu ihren weniger

aggressiven Gegenstücken bestimmte Charakteristika teilen. Es werden mögliche pathogene Mechanismen aggressiver humaner PHEO/PGL in Verbindung mit dem Warburg-Effekt berichtet, die zur Identifikation neuer diagnostischer und prognostischer Marker und potentiellen, neuen Therapieansätzen führen könnten.

Als Drittes wurde eine mögliche Zelloberflächen-Lokalisierung, welche für andere Tumortypen bereits beschrieben wurde, und deren Potential als Ansatzspunkt für die medikamentöse Behandlung untersucht. Ergebnisse konfokaler Mikroskopie zeigten, dass die β Untereinheit der ATP-Synthase auf der Zelloberfläche von MPC und MTT, sowie der primärer Zellen eines *SDHB*-mutationsbedingten PGL zu finden waren, während sie auf der Oberfläche von bovinen primären chromaffinen Zellen praktisch nicht zu detektieren war. Die Oberflächen-Lokalisierung wurde per Immun-Elektronenmikroskopie am Gewebe eines *SDHB*-mutationsbedingten PGL verifiziert. Behandlung von MPC- und MTT-Zellen mit dem ATP-Synthase-Hemmer Resveratrol und mit einem ATP-Syntase β-Antikörper führte zu deutlicher Proliferationsinhibition. Die vorgelegten Daten lassen vermuten, dass PHEO/PGL einen funktionalen ATP-Synthase-Komplex auf der Oberfläche tragen, der Zellüberleben oder Proliferation unterstützt. Daher könnte Zelloberflächen-ATP-Synthase einen neuen Ansatzpunkt für die medikamentöse Behandlung von malignen oder inoperablen PHEO/PGL bieten.

Summary

Paragangliomas (PGLs) are tumors of chromaffin cell origin, including adrenal-derived pheochromocytomas (PHEOs). Diagnosis of PHEO/PGL remains a challenge, because signs and symptoms are not characteristic. If untreated, PGL can have a devastating outcome due to catecholamine excess. Even after proper diagnosis, the risk of metastatic disease remains. In up to 10 % of patients, metastases are present at diagnosis and metastases occur in 50-97 % of patients with underlying succinate dehydrogenase B (*SDHB*) mutations. Once metastatses are present, treatment options are limited.

The work presented here aims at better characterization of metastatic PGL on the molecular biological level. First, the value of urinary peptide patterns was evaluated for classification of selected patient groups to potentially improve diagnostic means. The urine of healthy control persons (Ctr), patients with *SDHB*-derived metastatic (*SDHB*-met) and non-metastatic (*SDHB*–ben) PHEO/PGL and healthy *SDHB* mutation carriers (*SDHB*–car) was analyzed by capillary electrophoreses coupled electrospray ionization mass spectrometry. Based on the differences in urinary peptide patterns, possible predictive markers for *SDHB* mutation and differentiation between *SDHB*-car and *SDHB*-ben or *SDHB*-met were identified.

Classification of *SDHB*-car was successful based on 4 peptides (error rate 1.8 %). *SDHB*-met were correctly classified with an error rate of 3.3 % based on only 1 peptide. The top ranking peptide was identified as a collagen type III fragment. Separation of *SDHB*-car&ben using 3 peptides yielded an error rate of 10.5 %. However, by combining the 3 top-ranked peptides with presence/absence of elevated plasma catecholamine levels, 100 % correct classification was reached. Thus, urinary peptides hold the potential to detect *SDHB* mutation and to distinguish mere mutation carriers from patients with *SDHB*-derived metastatic PHEO/PGL. In addition, our data suggests that combining catecholamine testing with evaluation of 3 urinary peptides may be beneficial in diagnosing non-secreting *SDHB*-derived PGL.

Second, distinct protein expression patterns in aggressive PGL were evaluated. The focus was on further exploring dysfunction in energy metabolism related pathways. PHEO/PGL derived due to *SDH*x and von Hippel-Lindau (*VHL*) gene mutations have previously been associated with strengthened glycolysis and decreased oxidative phosphorylation (OXPHOS). Nevertheless, tumor aggressiveness is distinct: metastases

rarely occur in *VHL*-derived PHEOs/PGLs, while *SDHB*-derived PHEOs/PGLs often metastasize. Differential 2D-gel analysis of mouse PHEO cells (MPC), and their more aggressive filial mouse tumor tissue (MTT) cells, revealed changed expression of several energy metabolism proteins, including ATP synthase. These were then assessed in human PHEOs/PGLs. In support of a glycolytic phenotype, lactate dehydrogenase was elevated with an increased A to B subunit ratio in MTT compared to MPC; this was also the case for *SDHB* relative to human normal adrenal medulla. A to B ratio was similarly elevated in *SDHB*- and *VHL*-derived tumors, however due to an A subunit increase in *SDHB* and B subunit decrease in *VHL*. Glucose starvation reduced proliferation of MTT, but not MPC, confirming increased dependence on glycolysis in the more aggressive cells. However, respirometry revealed no difference in oxygen consumption at complex I and II, while ROS production at complex I was increased in MTT cells. Evaluation of OXPHOS activity in human tissue revealed reduced complex I, II and II+III activity in *SDHB* when normalized to mitochondrial content. However, no difference in ROS levels was observed. These results show that the aggressive MTT and *SDHB*-derived PHEOs/PGLs share certain characteristics when compared to their less aggressive counterparts. Pathogenic mechanisms of aggressive human PHEOs/PGLs related to the Warburg effect, which may lead to identification of new diagnostic and prognostic markers and potential therapeutic targets, are described.

Third, a possible cell surface location of ATP synthase - which has been reported for other cancers - and its potential as therapeutic target was evaluated. Confocal microscopy revealed that ATP synthase was present on the cell surface of MPC and MTT cells as well as primary cells of an *SDHB*-derived PGL, while virtually absent on bovine primary chromaffin cells. Cell surface location of ATP synthase β was verified in tissue of an *SDHB*-derived PGL by immunoelectron microscopy. Treatment of MPC and MTT cells with resveratrol as well as ATP synthase β antibody lead to severe proliferation inhibition. The presented data suggest that PHEO/PGL carry a functional ATP synthase complex on their surface that promotes cell survival or proliferation. Thus, cell surface ATP synthase may present a novel therapeutic target in treating metastatic disease and inoperable PHEO/PGL.

Table of Contents

1 Background – Metastatic Paraganglioma

1.1 Paraganglioma definition

Following the definition of the world health organization, paragangliomas (PGLs) are chromaffin cell tumors developing from the sympathetic and parasympathetic ganglia throughout the abdomen and head and neck area. A PGL arising from the adrenal gland is called pheochromocytoma (PHEO). In addition, here we will distinguish between sympathetic extra-adrenal PGL (eaPGL) and parasympathetic PGL from the head and neck area (HNP). In general PGLs are well curable, however once a patient presents with metastases, treatment options are limited and rarely curative.

Metastatic disease due to PGL can only be diagnosed based on the presence of chromaffin tumors in locations where chromaffin cells are not usually present. Thus, the widely used term 'malignancy', that is spreading of a primary tumor by tissue or vascular invasion or metastasizing, does not necessarily apply to PGL. While tissue or vascular invasion is sometimes observed in PGLs these observations don't correlate well with the severity of the disease and a patient's prognosis. Thus, in contrast to other malignancies, the development of metastases cannot be predicted or evaluated by high vascularization and mitotic rate, or vascular and tissue invasion. Despite huge efforts, currently no gene or protein has been identified as a definite marker or predictor for metastatic disease and no reliable cure has been developed yet.

1.2 Rule of 10 % Overcome

PGL has long been considered as the disease of 10 % (10 % metastatic, 10 % familial, 10 % recurring, 10 % extra-adrenal, 10 % occurring in children). However, improved diagnostic techniques showed that the rule of 10 % does not accurately characterize PGL. Overall, 0-36 % of PGL patients develop metastatic disease, depending on the type of tumor (1) (Table 1). The percentage of PGL with family history has been revised to around 30 % (2, 3). Extra-adrenal tumors have been reported in 15-20 % of patients (4).

1.3 Genetic Predispositions

Up to 30 % of PGL appear to present in a hereditary manner (2, 3). To date, 8 different germline mutations are associated with PGL (*NF1*: von Recklinghausen

Neurofibromatosis Type 1, *RET*: Multiple Endrocrine Neoplasia Type 2, *VHL*: von Hippel-Lindau disease, *SDH-B, -C, -D*: familial PGL syndrome 4, 3, 1, *SDH5* (5) (also referred to as *SDHAF2*): familial PGL syndrome 2, *TMEM127*: familial PGL, respectively). However, *SDH5*/*SDHAF2* mutation seems to be rare and should only be suspected in very young patients with HNP and family history thereof in absence of *SDHB*, *C* and *D* mutation (6). *TMEM127* germline mutation seems to occur in up to 30 % of patients with other mutations predisposing to PGL. All PGL patients presenting with *TMEM127* germline mutation had PHEO. However, during follow up of 4-16 years none of the patients with *TMEM127* germline mutation developed metastases or recurrence (7). In the majority of PGL the underlying dysfunction remains unknown and they are referred to as sporadic.

In search of additional genes that may be involved in the development of PGL, a somatic heterozygous mutation of isocitrate dehydrogenase has been reported in one patient with HNP, but was not found again in a large cohort of apparently sporadic PGL (8). In addition, prolyl hydroxylase 2 (PHD2/ EGLN1) mutation has been reported in a PGL patient who also presented with erythrocytosis (9). So far, this mutation has not been confirmed, neither for other patients with PGL nor erythrocytosis.

Table 1: Predisposition to malignancy in patients with mutation-derived PHEO/PGL

Genetic background	Predisposition to malignancy (%)
NF1	0.7-11 (4, 10, 11)
RET	0-3 (4, 10, 11)
VHL	3-8 (4, 10, 11)
SDHB	50-97 (4, 10-13)
SDHD	0-3 (4, 10-13)

Correlation of patient's presentation with their genetic background revealed a distinct manner of representation with respect to metastatic potential, catecholamine expression, tumor location (14) and ultra-structural appearance (unpublished observations) (Table 1). Patients with *NF1*, *RET* and *VHL* related PGL rarely develop metastases (0-11 %) (4, 10, 11), while patients with *SDHB* germline mutation develop metastases in 50-97 % (4, 10-13) (Table 1). The metastatic potential of PGL that developed due to germline mutation of *SDH5* and *TMEM127* is not yet clear, but suspected to be low.

1.4 Metastatic Paraganglioma: Does Location Play a Role?

PGL tissue from different locations appears similar microscopically. However, the prognosis is quite different for different tumor locations.

Patients with PHEO rarely develop metastases. Also, metastases secondary to HNP seem to be infrequent (15). However, development of metastatic disease in patients with eaPGL and/or multiple PGL has been reported frequently (16). Patients with *SDHB*-derived PGL are more prone to developing metastatic disease. However, the primary tumor location most often found in patients with metastatic disease remains eaPGL (13, 17). This may imply an effect of the tumor environment on the development of metastatic disease.

The majority of PGL related metastases occur in local and distant lymphatic nodes, bones, liver and lungs (18, 19). Thus, PGL cells seem to spread via the lymphatic as well as the hematogenic route. Patients with long bone metastases have a more promising prognosis with up to 20 years of survival after detection of metastases, while patients with soft tissue metastases usually die much sooner (own unpublished observations). The cause for the unfavorable outcome of organ lesions remains to be established.

1.5 Metastatic Paraganglioma in Children

PGL in children is rare, thus studies including a representative cohort of pediatric patients are sparse and often contradictory. Available studies were recently reviewed by Havekes et al. (20).

Pediatric PGL appeared to be related to germline mutation frequently, even in the absence of family history (30 % (21), 39 % (22), 59 % (23), up to 80 % (own unpublished observations). Mutation of the *VHL* gene has been reported as predominant in pediatric patients (22, 24). However, in a large group of children and adolescents with PGL (n=41), we observed a 54 % predominance for an *SDHB* mutation (own unpublished observations).

The primary PGLs in pediatric patients have been reported most frequently to be extra-adrenal (50 %), followed by PHEO (40 %) and HNP (10 %) (21). These numbers mainly agree with our findings (54 %, 36 % and 1 %, respectively). As suggested by the high incidence of extra-adrenal primary tumors and *SDHB* mutation in children, the rate of the development of metastases seems to be higher than in adult patients (47 %

21), 68 % (own unpublished observations), 5 out of 7 patients (25)). In contrast, an Indian study including 11 pediatric patients almost always found the primary tumor to be PHEO (26). No case of metastatic disease was reported for this cohort.

Positive family history or genetic testing, eaPGL, and a tumor diameter > 5 cm have been shown to correlate with the development of metastatic disease in children (21).

Post surgical treatment with ^{131}I-MIBG seems to be beneficial in pediatric patients (25). Thus, if detected early, the prognosis for pediatric patients with metastatic PGL may be more promising than for adult patients.

1.6 Insights into the Pathogenesis of Metastatic Paraganglioma

Cell culture experiments suggest that apoptosis resistance in absence of nerve growth factor (NGF) is common to several hereditary forms of PGL (27). Thus, familial PGL may develop due to impaired culling of neural crest cells during the development of chromaffin tissues. NGF is an essential survival factor for developing neuroendocrine cells. Later in development, NGF becomes scarce, leading to neuronal culling. Survival of cultured cells, with impaired *NF1*, *RET* or *VHL* gene expression, was connected to JunB mediated apoptosis resistance in absence of NGF. For *SDH*x dysfunction, apoptosis resistance was also shown, but here it seems to be caused further downstream in the same pathway. Accumulation of succinate, as appears in presence of *SDHx* mutations, inhibits prolyl hydroxylase (PHD) function. This can stabilize hypoxia inducible factor α (HIFα), promoting pseudo-hypoxic conditions (28, 29). On the other hand, particularly inhibition of PHD3, also called EglN3, has been shown to hamper NGF related survival (27). These results promote a common pathway for the development of PGL, but have not yet been proven in human tumor tissue.

Based on a gene expression profiling study, PGL of different genetic backgrounds could be separated into two groups. *VHL* and *SDHx* mutation-derived tumors shared up-regulation of hypoxia-, angiogenesis- and oxidoreductase imbalance related genes. *RET* and *NF1*-derived tumors clustered separately (30, 31). A more recent study confirmed this expression based clustering into different types of PGL (32).

Hypoxia is common to many tumors. However, it is not yet clear if a (pseudo-) hypoxic state with according up-regulation of angiogenesis and cell proliferation genes is sufficient for tumor development (33, 34). In addition, while common to *SDHx* and some *VHL* related PGL, HIFα stabilization has not been found in von Hippel-Lindau 2C related PGL (35). Thus, HIF stabilization alone, while potentially crucial to *SDHx*

and some *VHL* related tumors, is not a common feature in all *SDHx* and *VHL* related PGL.

Interestingly, (pseudo-) hypoxia was shown to inhibit SDHB protein expression. Accordingly, SDHB protein is absent or low in a number of *VHL*-derived tumors (36).

Although tumors derived based on mutation in the *VHL* and *SDHB* genes share pseudo-hypoxic features, tumor location, symptomatic manifestation, and metastatic potential are very distinct (12, 13, 37). *SDHB*-derived PGL typically present in a more aggressive manner with mainly extra-adrenal primary tumors, occurring at an earlier age with a high likelihood for the development of metastases. Thus *SDHB* mutations have been suggested as marker of poor prognosis (38).

It has been proposed, that the route of hypoxia development in *VHL*- and *SDHx*-derived tumors differs and thus results in up-regulation of distinct target genes (39). It has been reported that in *SDHx* mutation-derived tumors HIF1α expression is more often increased, while in *VHL* mutation-derived PGL HIF2α stabilization seems to be predominant. However, Favier et al. reported that HIF2α is more highly expressed in *SDHx*- and *VHL*-derived tumors, while absent in *RET* and *NF1* related tumors (32).

Another currently debated hypothesis to explain more aggressive behavior of *SDHx* related tumors are elevated levels of reactive oxygen species (ROS). In addition to succinate accumulation in *SDHB* and *D* mutation related PGL, complex II dysfunction has been observed (12, 40) and may lead to inappropriate electron transfer and increased ROS production. Mutation of the *SDHC* gene in model systems was shown to result in high levels of ROS, which lead to an increased frequency of mitochondrial and nuclear gene mutations, promoting tumor development and perhaps an aggressive phenotype (41, 42). In a yeast model, mutation of the *SDHB*-equivalent lead to increased ROS production. However, no mutagenic DNA damage was detected (43). However, *SDHB* silencing in cultured cells showed ambiguous results with respect to ROS production (44, 45). It remains to be examined if ROS production differs between *VHL*- and *SDHx*-derived tumors, because the down-regulation of SDHB protein in *VHL*-derived PGL (36) may also result in increased ROS production.

Dysfunction of complex II in *SDHx*- as well as *VHL*-derived tumors may promote aerobic glycolysis as the main source of energy ((32); own unpublished data). Accordingly, lactic acidosis, which can be a result of decoupled glycolysis and oxidative phosphorylation, has been described in some patients with PHEO (46).

The development of metastatic disease on the molecular level remains to be elucidated for PGL. Suppressed expression of $p16^{INK4A}$ and $p14^{ARF}$ has been reported to promote the development of metastases in Pten knock–out mice (47). In human PGL samples, promoter CpG methylation of the $p16^{INK4A}$ gene alone as well as promoter methylation of at least 3 of the following genes *RASSF1A*, *NORE1A*, $p16^{INK4A}$, *RARB*, *DCR2*, *CDH1* and *APC* (i.e. CpG island methylator phenotype (CIMP)) but not $p14^{ARF}$ has been shown to correlate with aggressive tumor behavior (48, 49). However, the same patient population was used in both studies and out of 6 primary metastatic tumors evaluated, only 3 were positive for $p16^{INK4A}$ hypermethylation or CIMP. All reported samples that had tested positive for *SDHB* mutation showed $p16^{INK4A}$ hypermethylation and CIMP, including 1 primary benign tumor. Thus, hypermethylation seems to primarily correlate with *SDHB* mutation, which has been suggested previously as a predictor for metastatic potential (38). Nevertheless, it may be of great interest to evaluate the molecular connection between *SDHB* mutation and a changed DNA methylation pattern. The consequences on the molecular biology of cells that carry these characteristic DNA methylations may help to explain why *SDHB* related PGL present in a more aggressive manner compared to other PGL.

Mutations of the *SDHB* gene as well as an extra-adrenal tumor environment seem to promote the development of metastases. However, a clear molecular biologic explanation for the more aggressive phenotype has not yet been found.

1.7 Markers for Malignant Paraganglioma

Currently there are no reliable markers for metastatic disease in PGL. The single way to diagnose malignancy is the presence of metastases. Thus, patients with PGL have to be followed-up on ultimately, because metastatic disease or recurrence can appear even after decades free of disease.

Many pathologic markers of malignancy used in other tumors were evaluated for PGL, but to date none could be sufficiently confirmed as a diagnostic or prognostic tool (for a summary see (50-53)). Amongst them were tissue invasion, high vascularization, and staining for specific proteins (e.g. Ki67, hTERT (54)), characteristics that correlate with metastatic disease in other cancers. However, most of them proved to be not predictive of metastases or are controversial in PGL (53). In a recent study that includes 11 tumors of patients that presented with PGL related metastases, Ki67 staining has been shown to have a sensitivity and specificity of 100 % (55). However,

this will have to be evaluated in a larger cohort of patients. In 2002 Thompson introduced the 'pheochromocytoma of the adrenal gland scaled score' (PASS), which is a scoring system based on 17 distinct morphologic features of PHEO to distinguish benign from primary metastatic tumors (56). However, considerable inter- and intra-observer variation suggest that the PASS system is of limited diagnostic and predictive value (57).

Recently, absence of SDHB protein in PGL specimens was suggested as predictive of metastatic disease (58). Absence of SDHB staining was found in some sporadic metastatic lesions in addition to others with known *SDHB* mutations. However, absence or low levels of SDHB protein were previously reported in *VHL* related PGL, which rarely metastasize (36). Thus, the predictive value of metastatic disease based on low SDHB protein levels may be limited to a distinct group of PGL.

Stathmin has been shown to be a good predictive marker in endocrine tumors. In PGL tissue, staining for stathmin was more intense in primary metastatic tumors. However, its stand-alone value as a marker of malignancy is limited, because primary non-metastatic tumors also show stathmin expression. Differentiation between weak and more intense staining may be difficult when examining individual tumors (59).

The most promising diagnostic/predictive marker for metastatic PGL so far seems to be the expression of the HIF 2α regulated SNAIL alone (60), or in combination with its target twist (61). Positive staining for one or both in primary tumors correlates well with the presence of distant metastases. However, these findings have to be carefully evaluated for the different types of PGL.

To date, *SDHB* mutation (particularly with a tumor size > 5 cm) and/or highly elevated levels of normetanephrine (NMN), dopamine (DA), L-3,4-dihydroxyphenylalanine (DOPA), and/or methoxytyramine are the best indicators for the development or presence of metastatic disease (Eisenhofer et al. unpublished observation).

1.8 Diagnosis of Metastatic Paraganglioma

Signs and symptoms of patients bearing metastatic disease cannot be distinguished from those of patients with solitary or multiple PGL. In some cases, symptoms related to tumor burden of metastases are present. Most often patients with metastatic as well as non-metastatic PGL suffer from hypertension caused by the tumor's hypersecretion of catecholamines. As described below, the secretion profile of a tumor can present valuable clues about tumor location and the possibility of multiple lesions or

metastases.

Presence of metastases can be ruled out by imaging studies. However, a possible later development of metastases has to be monitored continuously. Considerations about the imaging approach of choice should be based on the genetic background and biochemical phenotype of each patient, as described below.

1.8.1 Biochemical Phenotype of Metastatic Paraganglioma

Currently, the diagnostic gold standard for PGL is an elevated plasma and/or urine metanephrine level. When a PGL is present, catecholamine levels can also be elevated in plasma and urine, but due to their lower stability they show a lower sensitivity as a diagnostic tool than metanephrines (62). For reliable results it is recommended to collect samples of relaxed patients. For plasma collection, patients should rest in the supine position without a pillow for at least 20 minutes after insertion of the cannula (63).

PGL can be differentiated based on their biochemistry in secreting (adrenergic, noradrenergic, or mixed phenotype) and non-secreting (biochemically silent) tumors. The latter most commonly arise from parasympathetic tissue in the head and neck area (64, 65). Knowledge of the biochemical phenotype is an important diagnostic indicator for tumor localization and possible underlying mutation as well as the presence of metastases (summarized in Table 1 and Table 2).

Metastases are most common in eaPGL, thus a noradrenergic phenotype (elevated norepinephrine (NE) or NMN) is often present in patients with metastatic disease. Metastases frequently appear dedifferentiated, potentially lacking the later enzymes of catecholamine synthesis. Thus, elevated methoxytyramine, DA, and/or DOPA levels can indicate metastatic disease (Eisenhofer et al. unpublished observations). Particularly in patients with *SDHB* mutation, eaPGL, and a primary tumor size of >5 cm metastatic disease is likely. Nevertheless, elevated DA, DOPA or methoxytyramine levels may also occur in solitary HNP (64, 66). A combination of elevated epinephrine (EPI)/metanephrine (MN) with NE/NMN may be caused by a solitary adrenal PHEO or multifocal adrenal and extra adrenal PGL or metastases. Metastatic disease in patients with an adrenergic phenotype is extremely rare.

1.8.2 Current Approaches to Detect Metastatic Paraganglioma

Following detection of elevated catecholamines or their metabolites or if PGL is

otherwise suspected, confirmatory diagnosis and/or localization of PGL and possible metastases is necessary. Tumors can often be localized by computer tomography (CT) and/or magnetic resonance imaging (MRI). Non-specific functional imaging modalities, such as ^{18}F-FDG positrom emission tomography (PET) and octreotide scintigraphy are also applied. However, only functional imaging techniques using tracers that are specifically internalized by catecholamine metabolism related mechanisms may confirm a tumor as PGL (e.g. $^{123/131}$I-MIBG, ^{18}F-FDA, ^{18}F-FDOPA[1], ^{11}C-Epinephrine, ^{11}C-Hydroxyephedrine). Excellent in depth considerations which imaging modality is indicated under particular circumstances are presented elsewhere (e.g. (18, 68)). Here the focus will be on imaging of metastatic lesions in PGL.

Use of functional imaging compounds that target specific receptors generally expressed in PGL - namely the NE and somatostatin (ST) (69) transporters - can lead to false negative results in metastatic lesions. Expression of the NE (70, 71) as well as the ST transporter (72, 73) was shown to be reduced or absent in PGL related metastases. It is believed that cellular dedifferentiation in metastatic lesions is the cause for this. Decreased sensitivity and specificity of targeted functional imaging agents (i.e. the 'flip-flop' phenomenon) is especially pronounced in PGL related to *SDHB* mutation. Thus, the preferred imaging modalities differ for *SDHB* and non-*SDHB* related metastatic disease (74, 75). In *SDHB* related metastatic disease, ^{18}F-FDG PET is preferred. ^{18}F-FDG enters a cell through the glucose transporter (GLUT1). GLUT1 expression and ^{18}F-FDG uptake is elevated in highly metabolically active tissue, such as metastases with increased glycolytic energy production. Glycolytic activity appears to be increased in *SDHx* mutation related PGL, possibly due to mitochondrial dysfunction (own unpublished results). Despite its capability to reliably detect *SDHB* related metastases, an ^{18}F-FDG PET positive signal is not specific for PGL related lesions. When the genetic background is unknown and in non-*SDHB* related PGL, specific imaging of metastases should be attempted via ^{18}F-FDA or ^{18}F-FDOPA PET. Non-*SDHx* related bone metastases have been shown to be most reliably and specifically detected with ^{18}F-FDA, while *SDHB* related bone metastases could be more efficiently detected by non-specific scintigraphy and ^{18}F-FDG PET (76). To date, the most widely used functional imaging modality for PGL is 123I-MIBG imaging.

[1]Carbidopa has been shown to increase the tumor-to-background ratio of 18F-FDOPA uptake in PGL, particularly PHEO (67)

While useful in evaluating a patient as potential candidate for treatment with ^{131}I-MIBG, sensitivity and specificity in the detection of metastases is inferior to ^{18}F-FDA and ^{18}F-FDOPA PET in patients with non-*SDHB* related disease and ^{18}F-FDG in patients with *SDHB* related PGL. Overall, ^{18}F-FDA PET remains the functional imaging approach of choice to detect PGL related metastases (18, 68, 77). Functional PET images of a patient with apparently sporadic disease, presenting with extensive bone metastases 16 years after initial diagnosis of a right adrenal PHEO are shown in Figure 1.

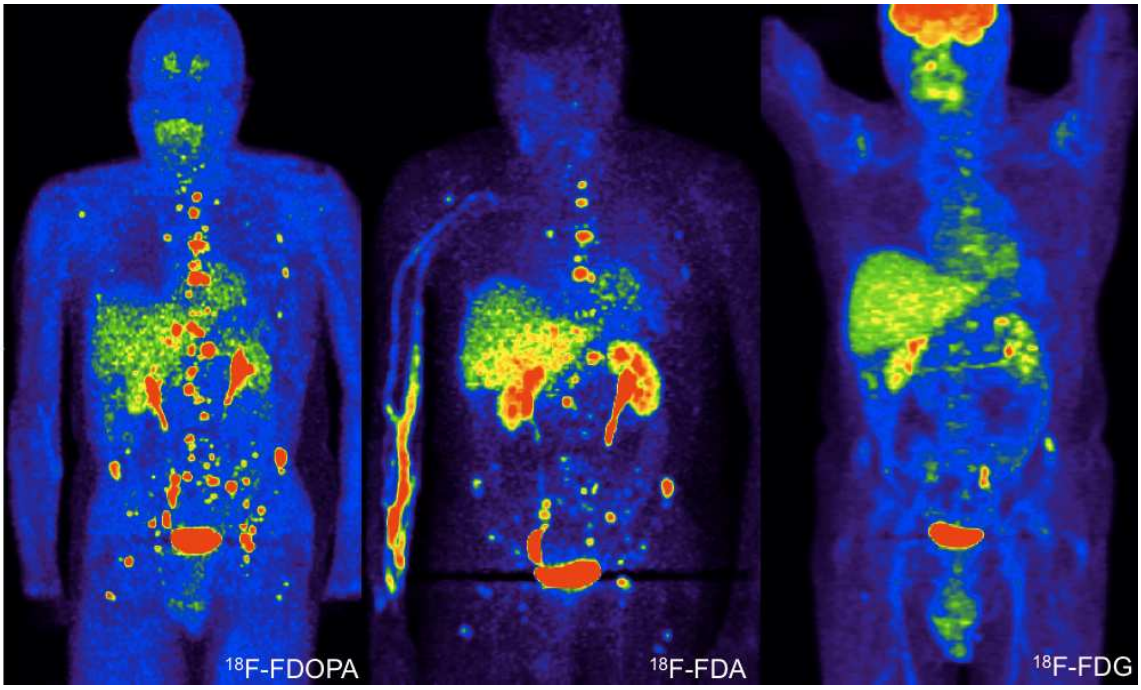

Figure 1: Anterior reprojected functional PET images of a patient with extensive bone metastases, detected 16 years after diagnosis of a right adrenal PHEO. The scans were performed on three consecutive days. Genetic testing for *SDHB*, *C*, and *D* germline mutations or deletion were negative.

1.8.3 Surgical Approaches

Treatment options include palliative tumor resection, to reduce tumor burden and excess In catecholamine related symptoms. Although in benign cases, a laparoscopic approach is preferred, in metastatic PGL this is controversial. Laparoscopy is not advisable when local invasion and/or large tumors are present or organ resection is required (78).

In patients with painful bone metastases and inoperable hepatic lesions, radiofrequency ablation (RFA) and cryoablation may be of benefit. However, before any tumor manipulation, patients have to be medicated with α– and β–blockers and catecholamine

synthesis inhibitors for 7–21 days, to prevent hypertensive crisis during tumor manipulation (phenoxybenzamine, atenolol and metyrosine, respectively) (79). Following pretreatment, RFA has shown to be manageable in patients with secreting PGL (80). More recently, complete ablation of 6 out of 7 metastatic lesions (4 hepatic, 3 bone and 1 ischiatic) in 6 patients suffering from PGL has been presented (81).
Successful cryoablation on a hepatic lesion of a patient with non-secreting metastatic PGL has been reported (82).

1.8.4 Chemotherapy

The most widely used chemotherapeutic regimen is the CVD regimen (cyclophosphamide 750 mg/m^2 body surface on day 1, vincristine 1.4 mg/m^2 body surface on day 1, and dacarbazine 600 mg/m^2 body surface on day 1 and 2, repeated every 21 days), developed by Keiser et al. 1985 (83). However, benefits of CVD therapy for metastatic PHEO appears to be short-term and do not include an increase in patient survival. Particularly in women and patients with primary PHEO, CVD is counter-indicated (84). However, in a patient with *SDHB* mutation related disease, great results were achieved under the CVD regimen (85). Thus, CVD therapy may be considered in patients with fast growing tumors due to *SDHB* mutation, in patients where tumor shrinkage prior to resection is required or in patients whose symptoms related to catecholamine excess cannot be managed otherwise (86).
A recent case study has reported on a patient with metastatic PGL who has been orally treated with temozolomide. The patient received 250 mg temozolomide daily for 5 days, repeated every 28 days. After 21 weeks of treatment, the patient was free of symptoms, with a significant decrease of plasma catecholamine and metanephrine levels. The primary tumor and liver metastases shrank and allowed tumor resection. The authors conclude that treatment of metastatic PGL with temozolomide may be of benefit prior to tumor resection (87).
Temozolomide has also been used in combination with the targeted drug thalidomide for the treatment of metastatic PGL. In a phase II study including 3 patients with metastatic PGL, patients have been treated with 150 mg/m^2 temozolomide for 7 days every other week and 50–400 mg/m^2 daily. One out of 3 patients showed a positive response to the regimen, however cytotoxic effect that caused subjects to end this treatment regimen were observed in patients with other endocrine malignancies (88).

1.8.5 Targeted Therapy

In addition to tumor removal, treatment with targeted radiotherapeutics can be beneficial. The most frequently used radiotherapy is treatment with ^{131}I-MIBG. This treatment option was developed as early as 1984 (83). Feasibility of this treatment for each patient needs to be verified by positive $^{123/131}$I-MIBG imaging. Regimens of high or low doses were performed (> 600 mCi and 100–500 mCi, respectively). Symptomatic response has been reported in as much as 67–98 % of patients, while objective tumor shrinkage/ stable disease or decreased secretion was observed in 27–47 % and 45–67 % of the patients, respectively (89-92). Comparable results with a lower rate of adverse reactions could be achieved in a low dose regimen; hormonal and symptomatic relive for 50 % of patients have been reported (93).

In an attempt to increase the curative effect of ^{131}I-MIBG treatment, recently Ultratrace Iobenguane I-131 has been developed. It is a high-specific activity ^{131}I-MIBG and was shown to result in a lower frequency of adverse effects than regular ^{131}I-MIBG (94). Treatment effects with drastically fewer unlabelled molecules may be a promising improvement for ^{131}I-MIBG therapy. However, its efficacy remains to be evaluated.

Besides radiotherapy, targeting the NET system with ST analogs has been used in the treatment of metastatic PGL (^{90}Y-DOTATOC). Success rate for radiolabelled octreotide analogues is not entirely clear yet, because only a few patients were treated by this means.

Treatment with unlabelled octreotide has also been done. However, it seems to be ineffective with respect to blood pressure, catecholamine- and Chromogranin A release (95). An explanation for the lack of effect may be the relatively low expression of the target of octreotide, the ST2a receptor. While the ST2a receptor was found in only 25 % of PGL samples, the ST3 receptor was found in more than 60 % of cells in 90 % of 52 PGL samples examined (96). Thus, targeting the ST3 receptor may prove a more beneficial approach in the treatment of metastatic PGL.

Treatment of metastatic PGL with the mTOR inhibitor everolimus was attempted with no significant benefit, and thus is not recommended (97, 98).

The most promising approach to date seems to be treatment with multiple tyrosine kinase inhibitors like sunitinib. Reports on 5 patients with metastatic PGL treated with sunitinib are currently available. All 5 patients showed at least a partial response (99-101). A phase II trial is currently being organized. Despite the promising results with

sunitinib, the tyrosine kinase inhibitor imatinib did not prove to be useful in two patients with metastatic PHEO (102).

A recent study showed that the interleukin 13 (IL-13) receptor α2 is expressed on the tumor cell's surface in humans and in a mouse model. Treatment of PGL bearing mice with IL-13 coupled to a truncated *Pseudomonas* exotoxin lead to a significant decrease in tumor size (103). The compound has been successfully tested in several clinical trials (104). Targeting the IL-13 receptor may be a promising new strategy to treat metastatic and inoperable PGL.

Table 2: Presentation, imaging and suggested treatment in PGL by hereditary backgrounds

	Genetic background:	Most common tumor location: primary tumor	metastases	Typical biochemichal phenotype:	Preferred imaging modality for metastases detection:	Suggested treatment:
Metastases common	SDHB*	eaPGL		NA, D	^{18}F-FDA	**fast growing:** Surgery‡, CVD§, experimental treatment
	sporadic	PHEO	bone	A	^{18}F-FDA	
Metastases rare	SDHD	HNP		D	^{18}F-FDOPA†	
	VHL			NA, D		
	RET	PHEO		NA	^{18}F-FDA	**slow growing:** Surgery‡, ^{123}I–MIBG¶
	NF1			A & NA		

Abbreviations: adrenergic (A) (elevated epinephrine (Epi) and/or metanephrine (MN)); noradrenergic (NA) (elevated norepinephrine (NE) and/or normetanephrine (NMN)); dopaminerg (D) (elevated dopamine (DA); L-3,4-dihydroxyphenylalanine (DOPA) and/or methoxytyramine); adrenal PGL (PHEO); extra-adrenal PGL (eaPGL); head and neck PGL (HNP). *Risk of metastatic disease particularly high in children and adolescents. †Mainly studied on primary HNP but potentially similarly effective for metastases. ‡Complete resection of metastases is rarely possible, but resection can have a good palliative effect (avoidance of further organ or bone destruction by tumor growth as well as reduction of catecholamine levels which leads to a decrease in related signs and symptoms). §own unpublished observations suggest that (at least) patients with *SDHB* related fast growing tumors initially respond well. Physicians are recommended not to stop CVD, because resumption of therapy almost always results in chemotherapy resistant tumors (if toxicity occurs, longer intervals between cycles or a reduced dosage can be used).¶High doses may be effective (105), however, additional studies and long-term observations are needed.

In conclusion, tyrosine kinase inhibitors are the most common therapeutic option at present. However, their efficacy may be limited, especially in *SDHB* related metastatic PGL. Perhaps some new tyrosine kinase inhibitors, like axitinib, may be of better value. Ultratrace Iobenguane I-131 showed first promising results, however additional studies are needed. While promising based on preliminary studies, patient trials targeting the ST3 (perhaps in combination with dopamine receptor antagonists) and IL-

13 receptor are needed to evaluate their efficacy. Development of new mTOR pathway inhibitors may be another promising avenue in the treatment of metastatic PGL.

2 Urinary Peptides to Predict SDHB Mutation and SDHB-Derived Metastatic Paraganglioma

2.1 Introduction

Urinary catecholamine analysis is a valuable diagnostic means, when pheochromocytoma (PHEO) or paraganglioma (PGL) is suspected in a patient. While indispensable in specifically diagnosing PHEO/PGL, elevated catecholamines and their metabolites are not very useful in distinguishing patients with removable primary tumors from those presenting with metastases. In addition, PGL can present with a silent phenotype, i.e. non-catecholamine secreting, and thus cannot be diagnosed based on elevated catecholamines or their metabolites.

PHEO/PGL have been associated with germline mutation of the succinate dehydrogenase *A*, *B*, *C* or *D*, (*SDHA, B, C, D*), ret proto-oncogene (*RET*), von Hippel-Lindau (*VHL*) or neurofibromatosis 1 (*NF1*) genes; however the majority of PHEO/PGL occurs in a sporadic manner. Here we focus on current challenges in the diagnosis of *SDHB*-related PHEO/PGL. Up to 10 % of patients with *SDHB*-derived PGL have non-secreting tumors, making diagnosis difficult (13). The risk for metastatic disease is particularly high in patients with *SDHB* mutation-derived PHEO/PGL (50-97 %) (4, 10-13). To date, there are no established markers for malignant potential of PHEO/PGL and malignancy cannot be diagnosed before metastases are present. Currently, there is no satisfactory treatment for metastatic PHEO/PGL and the survival rate is below 5 years.

Upon detection of elevated catecholamine levels, patients often undergo several imaging modalities for tumor localization. Although great improvements in PHEO/PGL imaging have been made, reliable detection of PHEO/PGL metastases, remains challenging due to cellular dedifferentiation. The most successful contrast agent to detect PHEO/PGL metastases, ^{18}F-dopamine (75), is currently only available at very few highly specialized centers. For patients with known *SDHB* mutation the more widely available ^{18}F-fluoro-2-deoxy-D-glucose-positron emission tomography is advised (74). Tumor detection is followed by costly genetic testing for risk evaluation of the patients and their families. Thus, more widely available means to detect metastatic disease in patients with PHEO/PGL and more economic ways to assess the

risk of their family members are very desirable. In addition, a tool to improve the currently difficult diagnosis of biochemically silent PGL is needed.

In recent years, techniques evolved that now allow evaluation of a wide variety of urine constituents, particularly peptides. Urinary peptide analysis has been a successful approach for biomarker discovery in various diseases, including cancer (106). Since urine peptides are extremely stable, even at room temperature, their analysis is highly reproducible (107). CE-MS is a fast, robust method to separate thousands of peptides (108).

In the present study, we analyzed the urinary peptide patterns of patients with *SDHB* derived metastatic (n=11) and non-metastatic (n=7) PHEO/PGL as well as healthy mutation carriers (n=12) and healthy controls (n=25). The aim of this study was to develop characteristic markers or signatures of a small subset of peptides to correctly classify patients with metastatic PHEO/PGL as well as biochemically silent PHEO/PGL and to recognize *SDHB* mutation.

2.2 Material and Methods

2.2.1 Samples

The midstream portion of the second morning urine of patients with metastatic PGL (*SDHB*-met, n=11), non-metastatic (apparently benign) PGL (*SDHB*-ben, n=7), healthy *SDHB* mutation carriers (*SDHB*-car, n=12) and healthy control persons (CTR, n=25) was collected with informed patient's consent under an Eunice Kennedy Shriver National Institutes of Child Health and Human Development IRB approved protocol. Healthy mutation carriers (without any signs or symptoms of PGL) were family members of patients with *SDHB* related PGL who came to our lab for risk assessment. These screening patients underwent genetic testing, patient interview, plasma catecholamine measurement, and imaging (PET/CT/MRI). Patient information is presented in Table 3.

Samples were aliquotted and frozen within 10-120 minutes of collection and stored at -80°C until analysis. If urine appeared turbid, the sample was centrifuged at 500 g for 5 minutes at room temperature and the supernatant was aliquotted. Microscopic analysis of the sediment often revealed squamous cells, salt crystals and/or mucous as the source of turbidity. Samples were shipped on dry ice for proteomic analysis.

2.2.2 Capillary Electrophoresis and Mass Spectrometry

For proteomic analysis, a 0.7 ml aliquot of urine was thawed immediately before use and diluted with 0.7 ml of 2 M urea, 10 mM NH4OH containing 0.02 % SDS, as described (109). To remove higher molecular mass proteins, such as albumin and immunoglobulin G, the sample was ultrafiltered using Centrisart ultracentrifugation filter devices (20 kDa MWCO; Sartorius, Goettingen, Germany) at 3,000 rcf until 1.1 ml of filtrate was obtained. This filtrate was then applied onto a PD-10 desalting column (GE Healthcare, Uppsala, Sweden) equilibrated in 0.01 % NH4OH in HPLC-grade in H_2O (Roth, Germany) to decrease matrix effects by removing urea, electrolytes, salts, and to enrich polypeptides present. Finally, all samples were lyophilized, stored at 4°C, and suspended in HPLC-grade H_2O shortly before CE-MS analyses.

CE-MS analyses were performed using a P/ACE MDQ capillary electrophoresis system (Beckman Coulter, Fullerton, USA) on-line coupled to a micrOTOF MS (Bruker Daltonic, Bremen, Germany) as described previously (108). The ESI sprayer (Agilent Technologies, Palo Alto, CA, USA) was grounded, and the ion spray interface potential was set between –4 and –4.5 kV. Data acquisition and MS acquisition methods were automatically controlled by the CE via contact-close-relays. Spectra were accumulated every 3 s, over a range of m/z 350 to 3000. Accuracy, precision, selectivity, sensitivity, reproducibility, and stability of the CE-MS measurements were demonstrated elsewhere (109).

2.2.3 Data Processing and Cluster Analysis

Mass spectra were processed using MosaiquesVisu software, including peak picking, deconvolution and deisotoping (110). Migration time and peak intensity were normalized using internal polypeptide standards (111). These fragments appear to be the result of normal biological processes, apparently unaffected by any disease state studied to date (greater than 3600 samples analyzed to date) (112). The resulting peak list characterizes each polypeptide by its molecular mass, normalized CE migration time, and normalized signal intensity. All detected polypeptides were deposited, matched, and annotated in a Microsoft SQL database, allowing further analysis and comparison of multiple samples (patient groups).

2.2.4 Sequencing

Candidate biomarkers were sequenced employing LC-MS/MS analysis as described (113). Spectral data were searched against the SwissProt database using the Open Mass Spectrometry Search Algorithm (OMSSA), using an e-value cut-off of 1.00×10^{-2}. All matched sequences were manually validated.

2.2.5 Statistics

Raw peak intensity value of 5616 identified peptides were analyzed. The critical statistical features of these raw values were: a large percentage of 0 values (peptide not detected for the person) and the right-skewness of the non-0 values. The arcsinh transformation was used to convert these raw values. The primary analyses focused on building classifiers that used only a few peptides (typically 1 to 6) since an important aim of this research is to develop rapid, low-cost enzyme immunoassays (EIA) for a handful of peptides. Two standard classification algorithms were used: k-nearest neighbors (KNN) and linear discriminant analysis (LDA) (114). For both we used the default of equal priors, since no good evidence as to the relative proportions of patients in each group for future patients is available. For KNN we used k=3 nearest neighbors (for all problems this is the recommended number, although for the problem of classifying SDHB-car&ben&met (n=30) and Ctr (n=25) k=5 was also an option). We focus on the results using KNN. For the discussed classification problems it may have several advantages: it is a nonparametric approach, making fewer assumptions than LDA; it can discriminate more complicated patterns than LDA; and, an important technical consideration for some analyses, it can be used with larger peptide sets in small sample sets. LDA typically gave very similar estimated numbers of errors and peptide sets as did KNN, although in a few cases there were modest differences. Neither method dominated across all problems, so overall these results are also representative of what LDA achieved.

Three separate, clinically relevant problems were evaluted. The first was whether the urine peptide patterns could discriminate between Ctr and the combined carriers (SDHB-car&ben&met). Among the carriers the most important question was distinguishing those with metastatic disease from the combined group of those with benign disease and healthy carriers. The third question - motivated by the difficulty of diagnosing patients with non-secreting tumors using catecholamine levels – was how well peptides alone could do differentiating SDHB-ben from SDHB-car.

These problems are difficult for statistical classification methods due to the problem of "high dimensionality", where dimensions correspond to the number of peptides (see chapter 18 of (114)). The most critical aspect of these problems is often the choice of which peptides to use in a classifier, rather than the actual classification algorithm (e.g. KNN or LDA); this is especially true in our setting where use of a small set of peptides is mandated.

The standard approach for choosing say 3 peptides to use in a classifier would be to use a standard t-test (or Welch's version) or a nonparametric equivalent like the ranksum on all 5616 peptides and to choose the 3 with the smallest p-values; in these problems, because of the high percentage of 0 values, another option is Fisher's test for comparing the proportions of 0's. Recently specialized extensions of the t-test have been developed, such as Efron's 90 % adjustment rule for the t-statistic; or the "shrinkage t-statistic" by Opgen-Rhein and Strimmer from the University of Munich, which "borrows" variance-estimation information for a peptide from the full set of peptides (115). For the problems presented here, each of these approaches has substantial drawbacks. For the different versions of the t-test (or ranksum test), the large number of 0 values partially invalidates their assumptions and can cause them to give somewhat spurious p-values; Fisher's test avoids this problem, but sacrifices power by discarding all information regarding the non-0 values. To overcome these deficiencies, we devised a multi-step approach for choosing the "best" sets of 1, 2, 3, 4, 6, or more peptides to use in a given problem – in many ways this approach was the heart of the classification method. Because of the use of leave-one-out (LOO) cross-validation (or bootstrap calculations), the approach had to be computationally efficient

The 3-step approach applied to a specific set of data (during cross-validation this would be the LOO subset; denoted as "D" in the following), resulted in a ranking of the 5616 peptides. The peptide with the highest rank was used in building the classifier requiring just 1 peptide; the 3 highest ranked were used in building the classifier for 3 peptides, and so on. Step 1: Welch's t-test for D for each of the 5616 peptides, was computed; the best 50 were chosen as the pool of "competitors" for subsequent steps. Step 2: each of these 50 was used, individually, in a LOO cross-validated LDA-classification of D, and the number of errors recorded. These total error counts provided the rankings of the 50 peptides. Step 3: since often several peptides were tied with the same number of errors an extension of Lachenbruch's procedure (116) for comparing 2 groups when there are a significant proportion of 0 values was

used, since this is the critical feature of our data. The data in D were separated into the 0 and non-0 components and separate tests are done on them: Fisher's on the proportions of 0's and the ranksum on the non-0 values. The squares of normalized versions of these 2 test statistics were summed for the final test statistic.

The assessment of how well a specific classification algorithm will do in future observations is critical. As Hastie, et al. note: "Ideally, if we had enough data, we would set aside a validation set and use it to assess the performance of our prediction model. Since data are often scarce, this is usually not possible." ((114), pp. 241-242). To unbiasedly estimate misclassification error rates, we used 2 recommended approaches: 1) cross-validation, where a certain proportion of observation is set aside at each step, the classifier is built based on those remaining, and then is applied to those left out to count errors made; and 2) Efron's bootstrap approach. In our cross-validation analyses we chose to leave one observation out at each step (LOO), rather than leaving 10% or 20% out because it is a bit less biased and is not subject to random selection problems that are particularly exacerbated in small problems.

For these problems, where the initial step is choosing a small set of peptides from among thousands, the critical feature in doing cross-validation correctly is: the entire process of building the classifier must be cross-validated: this means applying it to both 1) choosing the few peptides; and 2) building the KNN classifier using these peptides. A great many investigators err in neglecting 1). As Hastie et al. strongly warn: "While this point may seem obvious to the reader, we have seen this blunder committed many times in published papers in top rank journals. With the large numbers of predictors that are so common in genomic and other areas, the potential consequences of this error have also increased dramatically…" ((114), p. 247). In our results and tables we use this correct approach, which we call "full" cross-validation.

A final aspect of building classifiers for a given problem, after obtaining these estimates of error rates, is to determine which peptides one should focus on: for developing EIA assays or in understanding possible biological mechanisms behind the disease and gene mutation. Our choices for the "best" 1, 2, 3, 4 or 6 peptides were based on looking at the highest ranked sets of peptides chosen by our 3-step approach at each of the n cross-validated samples. These were quite consistent for the peptides at ranks 1, 2, and 3, and moderately consistent for ranks 4 through 8.

In the Results section, detailing the optimal number of peptides and the set of peptides to use, the number of errors that a specific set of peptides made is given. These are

"partial" cross-validation results, since the classifier has been cross-validated but not the set of peptides. These error estimates will typically be downward biased. They are included only for reference and to allow discussion of which particular patients were erroneously classified using the specific peptide sets; in most cases they gave the same number of errors as the fully cross-validated value, but sometimes the value was a bit smaller. For assessing future performance, even for a specific set of peptides discussed, the reader should use the fully cross-validated values.

It is important to note that these cross-validated error estimates, for the different problems and using different numbers of peptides, have a small to moderate amount of uncertainty. This is due to the generally small numbers of observations available, and is unrelated to the sample reuse used to produce cross-validated estimates – it would occur even with a totally independent validation set. A second consequence of basing the classification algorithms on small sets of data is that they cannot achieve as low error rates as if they were based on much larger sample sets. These caveats are important in assessing the results, particularly for the 2 problems that use only the 30 patients with SDHB mutations. The problem of distinguishing combined SDHB-carriers from normal controls, with 55 observations, fares somewhat better. But even for that problem, if one were to observe 1/55 errors (1.8 %) from a totally independent validation dataset, an upper 90 % confidence interval for the true rate would go up to 6.9 %. For a problem with n=19, and an observed error rate of 0/19 (0 %) in a totally independent sample (e.g. SDHB-ben vs. SDHB-car), the upper 90 % confidence interval would go up to 11.4 %.

Since a basic goal is to develop EIA assays using few peptides, a final question was whether just a few peptides capture most or all of the legitimately "good" peptides in the 5616, or whether there might be a substantially larger number that could potentially yield even lower error rates. Two approaches to addressing this question were used: false discovery rates (FDR); and the "nearest shrunken centroid" classification algorithm (PAMR) developed by Tibshirani et al. (117).

There is a severe multiple comparisons problem in doing the thousands of t-tests to find a top-ranked set of peptides. FDR corrects for this multiplicity of tests, so that at an FDR of say 10 % the expected proportion of null peptides (i.e. those not truly different between the groups) meeting this criterion is at most 10 %. Hastie et al. (114) suggest using a value like 15 % for initial screening (instead of 5 %) in order to reduce the chances of missing a potentially useful peptide (see Section 18.7.1 of (114) for a

detailed discussion of FDR). Two potential drawbacks of FDR are: 1) in problems with small samples, the statistical tests it relies on are likely to have poor power, so after FDR's correction for multiple comparisons it may identify few or no peptides as worthy of further consideration, despite there being peptides that truly are different between the groups; 2) because it is built on doing statistical tests that look for location differences between groups, it is not optimized to find peptides that provide good classification capability; typically these two problems are closely related, but good results for one problem do not necessarily translate into equally good results for the other.

PAMR is a "top-down" classifier, which starts with the full set of peptides and sequentially winnows the set down, estimating via cross-validation at each step the number of classification errors. Typically the result is a U-shaped curve, indicating the optimal number of peptides at its minimum. We used PAMR in 2 problems to compare its optimal number of peptides (and which ones they were) to our "bottom-up" results.

All analyses except PAMR used Release 11 of Stata (StataCorp., College Station, TX, 2010), using either built-in procedures or scripts programmed within Stata or its associated Mata language. PAMR calculations were run under R, using the PAMR package for R (http://www-stat.stanford.edu/~tibs/PAM/Rdist/doc/readme.html). All presented p–values are 2–sided.

Abbreviations for Table 3 (following page): A: adrenal, DA: dopamine, DHPG: dihydroxy phenylglycol, DOPA: L-3,4-dihydroxyphenylalanine, EA: extra-adrenal, Epi: epinephrine, F: female, M: male, na: not applicable, nn: not known, NE: norepinephrine, *SDHB*: succinate dehydrogenase B mutation, *SDHB*p: *SDHB* polymorphism.

Table 3: patient information

Patient ID	Disease Status	Group	Age	Gender	Primary Tumor	Metastases Location	Age at First Symptoms	Centrifuged	Elevated Catecholamines
B01	*SDHB*	ben	56.38	M	l retroperitoneum	na	none, dg at 56	no	silent
B02	*SDHB*	ben	30.01	F	l A	na	27	no	NE, DHPG
B03	*SDHB*	ben	44.35	F	nn	na	nn	yes	NE
B04	*SDHB*	ben	46.73	F	r A	na	28	no	Epi, NE, DOPA
B05	*SDHB*	ben	33.00	M	2 retroperitoneal lesions	na	none, dg @ 34	no	NE, DHPG
B06	*SDHB*	ben	74.93	M	r carotid body	na	none, dg at 74	no	non secreting
B07	*SDHB*	ben	33.23	M	r carotid body	na	none, dg at 33	no	non secreting
H01	*SDHB*	car	40.43	F	na	na	na	no	normal
H02	*SDHB*	car	19.26	F	na	na	na	no	normal
H03	*SDHB*	car	33.51	M	na	na	na	no	normal
H04	*SDHB*	car	26.18	M	na	na	na	no	normal
H05	*SDHB*	car	30.20	M	na	na	na	no	normal
H06	*SDHB*	car	16.36	F	na	na	na	no	normal
H07	*SDHB*	car	49.87	M	na	na	na	no	normal
H08	*SDHB*	car	25.96	F	na	na	na	no	normal
H09	*SDHB*	car	27.93	M	na	na	na	no	normal
H10	*SDHB*	car	44.52	F	na	na	na	no	normal
H11	*SDHB*	car	55.22	F	na	na	na	yes	normal
H12	*SDHB*	car	46.93	F	na	na	na	yes	normal
M01	*SDHB*	met	41.85	M	r close to kidney	bone	40	no	NE
M02	*SDHB*	met	37.27	M	l retroperitoneum	bone	29	no	nn
M03	*SDHB*	met	47.24	F	l carotid body (recurrent), l abdomen	bone	44	no	NE, DA
M04	*SDHB*	met	25.10	M	EA & r Abed	bone, liver, possibly lymphnode	14	no	NE
M05	*SDHB*	met	52.74	M	l carotid body, l retroperitoneum	lymphnode, bones	46	no	DA
M06	*SDHB*	met	29.78	M	abdominal, two lesions	Bone, mediastinum, paratracheal, lymphnode, liver, muscle	22	no	non secreting
M07	*SDHB* p	met	46.44	M	nn	bulky retroperitoneal and liver mets, pancreas, periportal, bone	42	no	NE, DA
M08	*SDHB*	met	34.33	F	l A, l glomus vagale	bone, liver	10	no	Epi, NE, DHPG
M09	*SDHB*	met	31.49	M	l paraspinal mass	Lung, bone, right ischium	24	no	non secreting
M10	*SDHB*	met	41.52	F	retroperitoneal & pelvic mass (recurrent)	liver, r hilum , lung, paravaginal, ileopsas	37	no	DA
M11	*SDHB*	met	43.62	M	l retroperitoneal PGL	lung, bone, pancreas/stomach area	37	no	DOPA

2.3 Results

2.3.1 Data Characteristics

A critical characteristic of the data was the high percentage of 0 values, which had a substantial impact on the subsequent development of statistical methods for classification of patients based on peptide values. For all 55 NIH patients the percentage of peptides not detected (i.e. having 0 peak intensity values) was 75.9 %; for the normal controls the value was a bit lower at 74.1 %, while the 3 groups of *SDHB*-carriers were nearly identical, only varying between 77.2 % and 77.5 %.

The other salient fact about the raw peptide peak intensity values was their extreme skewness: across the 4 patient groups the skewness values, excluding 0-values, ranged from 16.5 to 42.4. After applying the log-like arcsinh transformation, which is able to seamlessly accommodate 0 values, the skewness values were much better behaved, ranging from 0.36 to 0.45 for the non-0 values (Figure 2).

As expected from the results above, the number of detected peptides varied among the 4 patient groups. For all 55 subjects a mean (SE) of 1353±44 peptides was detected. The number of peptides detected was lower in the combined mutation carriers (*SDHB*-met, *SDHB*-ben, and *SDHB*-car) than in the healthy controls (1270±56 and 1453±64 respectively, p=0.035); however among the 3 mutation carrier groups no difference was observed, with the means ranging from 1264 to 1278 (ANOVA p=0.99). A trend was observed that the number of detectable urinary peptides decreased with age in the normal healthy controls (p=0.04); a similar but slightly less pronounced trend was also seen in patients with *SDHB* mutation (p=0.29). However gender had no effect on the number of peptides detected: p=0.61 for gender, after accounting for *SDHB* carrier status. Similarly, among the normal controls the specimens that had been centrifuged (n=12) or not centrifuged (n=13) presented almost identical numbers of peptides (respective means of 1446 and 1461, p=0.91).

2.3.2 Marker for *SDHB* Mutation

The urine peptide patterns detected in the combined carriers significantly differed from those of healthy controls. Using Fisher's test, 18 peptides were identified to significantly differ between the groups at a very stringent false discovery rate (< 0.1 %). With Welch's t-test, which typically yields smaller p-values in peptides differing between the 2 groups, this increased to 40 peptides (Figure 3).

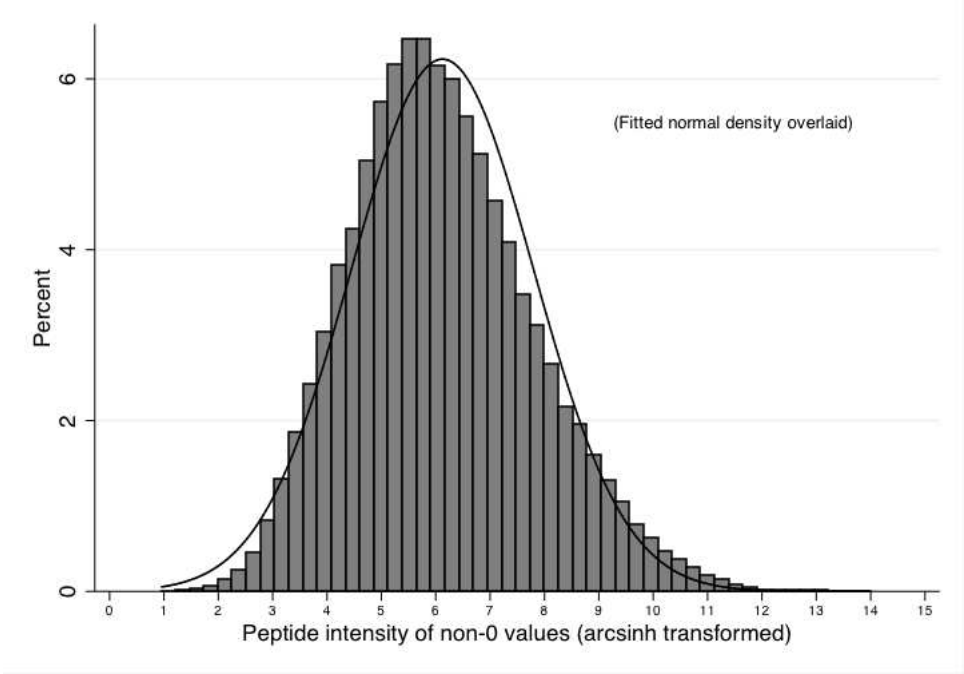

Figure 2: Approximate normality of the non-0 values after the arcsinh transformation.

Table 4: Top 6 peptides classifying combined *SDHB* mutation carriers and patients vs. healthy controls.

Rank	Peptide Number	Molecular Weight	CE Transit Time
1	63183	1860.46	34.22
2	62587	1848.84	27.32
3	71029	2022.89	33.37
4	58137	1751.77	27.72
5	61446	1822.83	27.00
6	62135	1838.82	27.06

The value of individual peptides for correctly classifying all *SDHB* mutation carriers, alone or in small subsets, was evaluated by full cross validation based on the best 1, 2, 3, 4, 6, and 15 peptides. Full LOO cross validation using KNN led to excellent error rates, ranging from 1.8 % to 5.5 % using 3, 4, 6, or 15 peptides. Using just 4 peptides gave an outstanding error rate of just 1.8 % (1/55); adding the two next higher ranking peptides yielded this same error rate. The 6 highest ranked peptides are plotted in Figure 4. Using just a single peptide (63183) gave an excellent fully cross-validated error rate of just 7.3 % (4/55)). The 6 best peptides typically occurring in the full LOO cross-validation are shown in Table 4 with their respective molecular weights and CE-transit times. Partial cross-validations based on using these specific 4 best or 6 best peptides also gave error rates of 1.8 %. Identification of these peptides is still in progress.

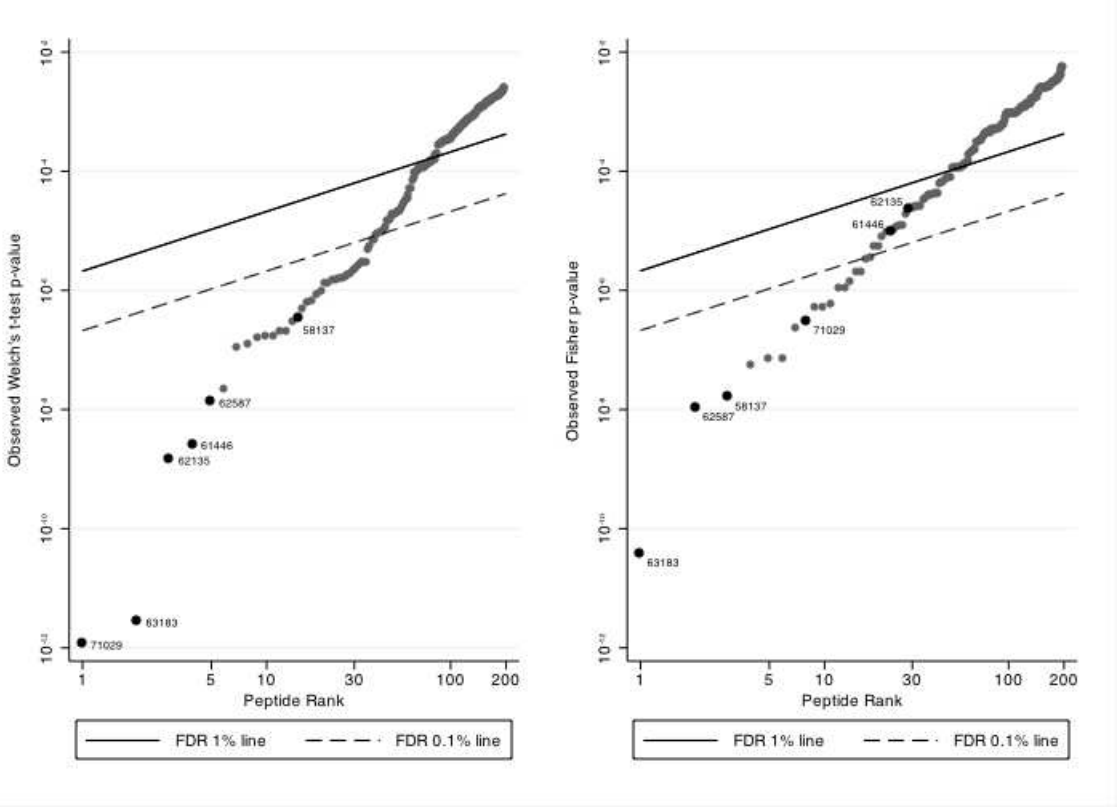

Figure 3: Peptides and their p-values as calculated with Wech's t-test (left) and Fisher's t-test (right) plotted over their rank for classifying healthy controls and the combined *SDHB* mutation carriers

2.3.3 Marker for Metastatic Pheochromocyotmas and Paragangliomas

Full LOO cross-validation led to the conclusion that using the transformed peak intensity values of just two peptides allows excellent classification of *SDHB*-met vs. *SDHB*-ben&car with an error rate of just 3.3 % (1/30; misclassifying the *SDHB*-met patient M10). The 3 highest ranked peptides are depicted in Figure 5. Molecular weights and transit times are presented in Table 5. Restricting the peptide choice to just the single best peptide still gave a very good error rate of 10 % (3/30; misclassifying *SDHB*-ben&car patients H01 and H11, in addition to M10). In the 30 full LOO cross-validation samples the same peptide (76415) was always chosen as the best one; hence in partial cross-validation it gave an error rate of 10 % and made the same 3 errors as noted in the full cross-validation. The results of FDR analysis (Figure 6) provides confirmatory evidence for these results: there are only a few peptides below the FDR 15 % line, and peptide 76415 clearly looks to be the best, meeting FDR 0.2 % criteria. This peptide was identified to be a fragment of the collagen alpha 1 (III) chain (COL31A, aminoacid 886-909).

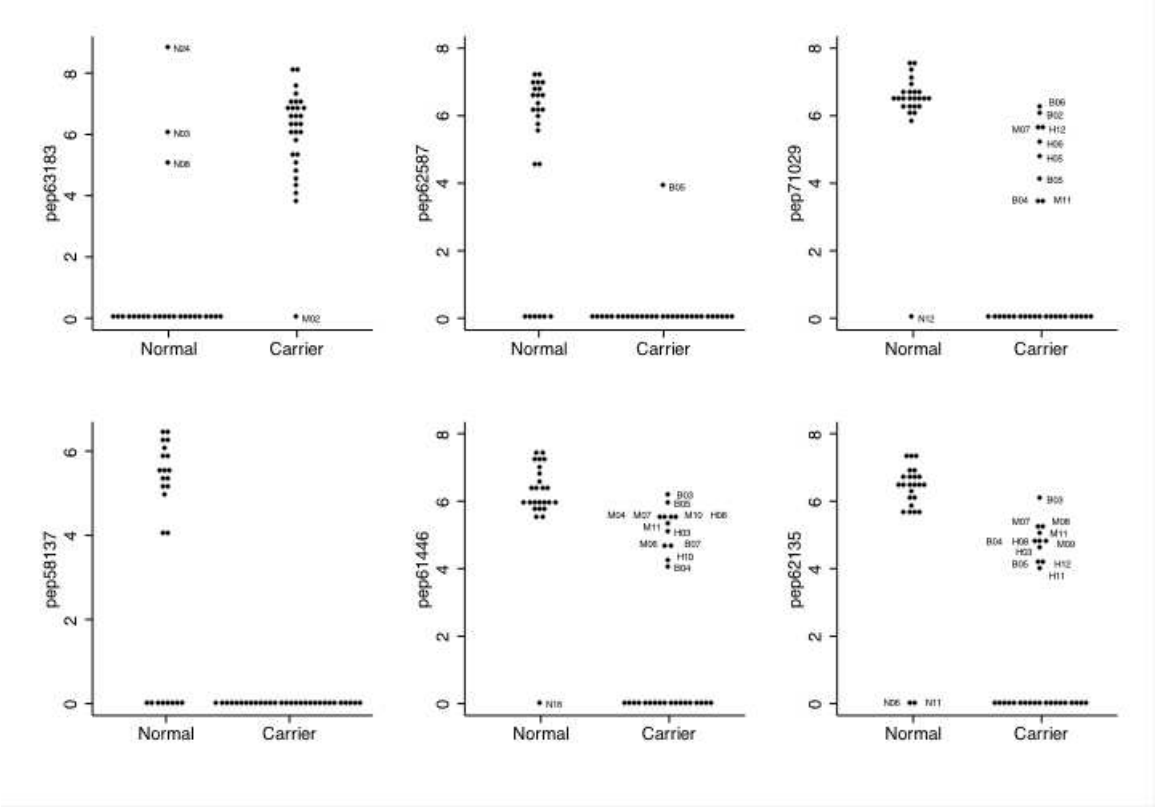

Figure 4: Transformed peak intensity of the 6 highest ranking peptides for differentiation between normal control persons and combied *SDHB* mutation carriers (*SDHB*-car, *SDHB*-ben, and *SDHB*-met)

2.3.4 Distinction of *SDHB* Mutation Carriers and Patients with Apparently Benign Pheochromocytomas and Paragangliomas

To evaluate if further separation of the two groups without metastases was possible based on their urinary peptide pattern, we considered whether small sets of peptides could reliably distinguish the 2 groups of non-metastatic *SDHB* carriers: healthy carriers (*SDHB*-car, n=12) vs. those with benign (non-metastatic) disease (*SDHB*-ben, n=7).

Because of the very small sample sets, one would expect that constructing classifiers with low error rates would be difficult. Applying the fully cross-validated LOO approach on the peptide patterns of these samples correctly classified the patients with an error rate of 10.5 % (2/19) when using 3 peptides (Figure 7). From the FDR plot for this problem (Figure 8), it appears that basing a classifier on roughly 3 peptides is reasonable; also, the set of 3 best peptides based on the fully cross-validated results, given in Table 6, correspond to the 3 shown in the FDR plot. However the 2 errors made were among the 7 *SDHB*-ben patients, classifying them as healthy *SDHB*-car. Furthermore, applying the KNN classifier (using the best 3 peptides listed in Table 6)

to patient M10 (the *SDHB*-met patient misclassified above as not having metastases) classified the patient as a healthy carrier.

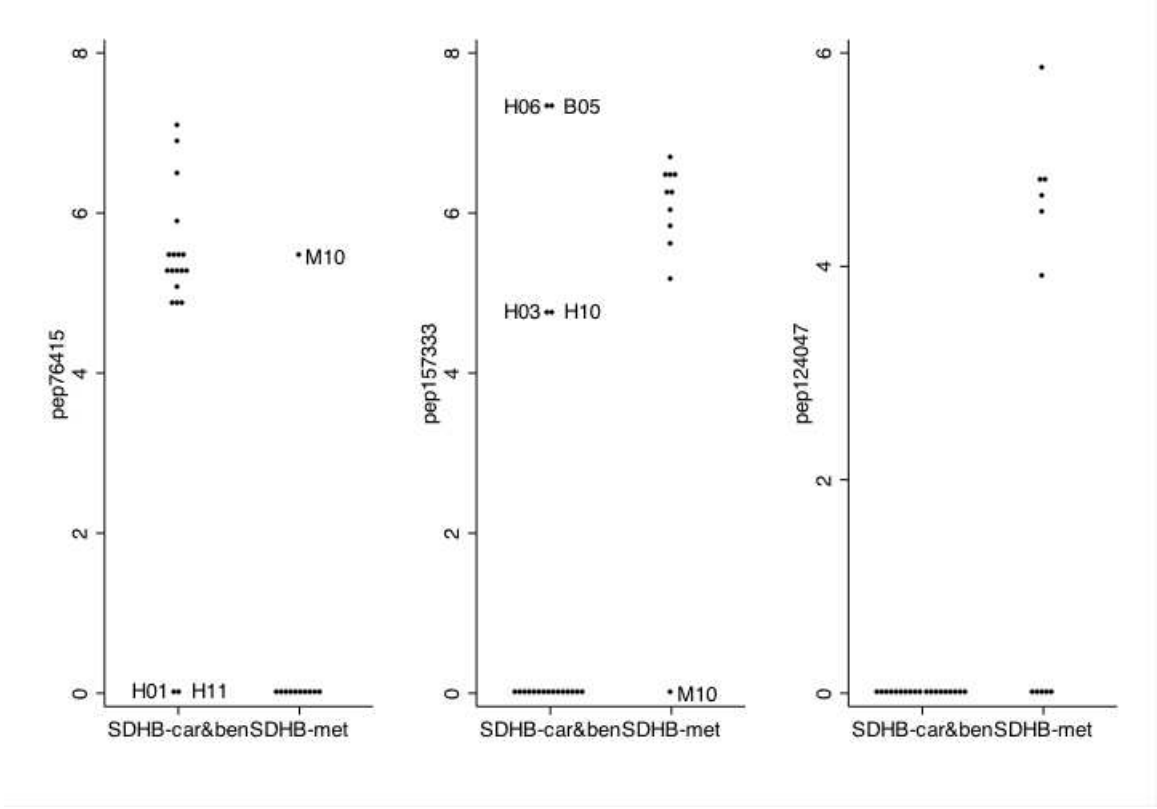

Figure 5: Transformed peak intensity of the 3 highest ranked peptides to distinguish patients with *SDHB*-derived metastatic disease from healthy mutation carriers and patients with *SDHB*-derived non-metastatic PHEO/PGL.

Table 5: Top 3 peptides classifying *SDHB*-met and *SDHB*-car&ben.

Rank	Peptide Number	Molecular Weight	CE Transit Time
1	76415	2117.93	32.97
2	157333	4334.80	20.40
3	124047	3160.47	36.24

Detection of urine or plasma catecholamines currently is the state of the art diagnostic tool to detect potential PHEO/PGL. However in patients with *SDHB* mutation-derived PHEO/PGL, the sensitivity is decreased, because up to 10 % of these PHEO/PGL patients present as biochemically silent (13). Of the *SDHB*-ben patients assessed in this study, 3 out of 7 (43 %; B01, B06, and B07; see Table 3) presented with biochemically silent tumors. Thus, they would have been misdiagnosed based on catecholamine testing only.

Among all 19 *SDHB*-ben or *SDHB*-car patients, catecholamine testing alone would

have classified only 4/7 (57 %) of the *SDHB*–ben patients correctly (patients B01, B06, and B07 were missed).

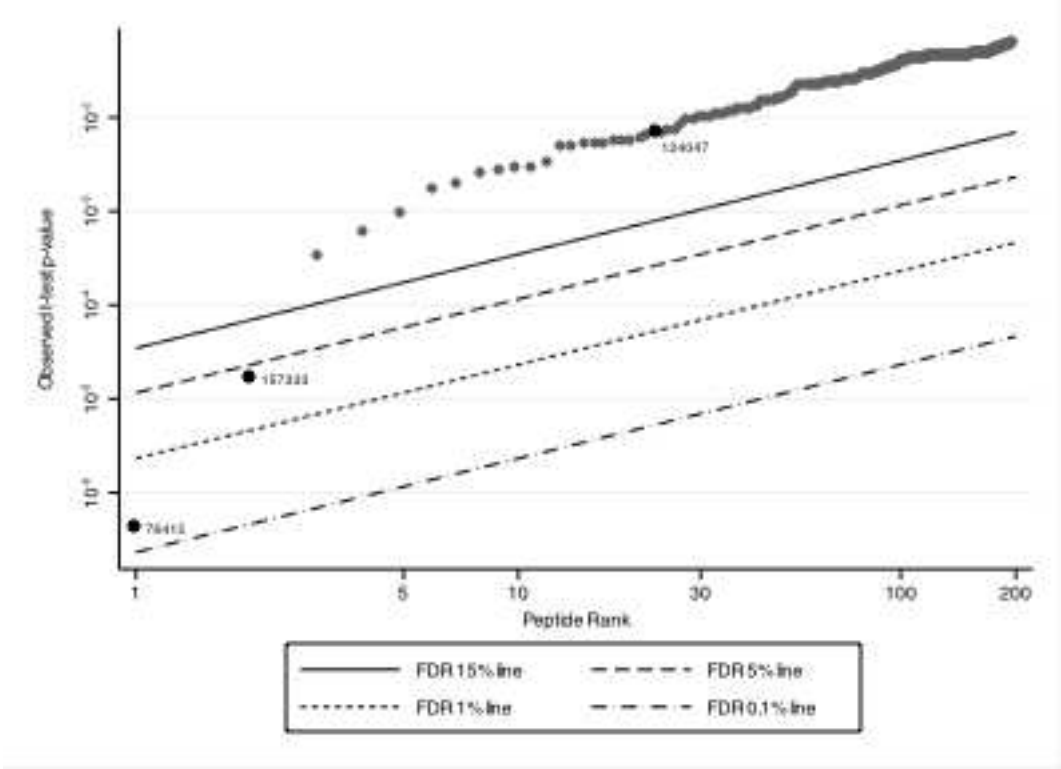

Figure 6: Peptides and their p-values for distinguishing patients with *SDHB*-derived metastatic PHEO/PGL from those with benign disease and healthy mutation carriers as calculated by Fisher's t-test plotted over their rank.

We evaluated a combined classification approach, designed to overcome the difficulties of using peptides or catecholamines alone. In the combined approach we first use the presence/absence of elevated levels of plasma catecholamines or their metabolites (epinephrine, norepinephrine, metanephrine, normetanephrine, dihydroxyphenylalanine, dihydroxyphenylethylene glycol, and/or dopamine) to classify a patient: if any of these was elevated, the patient was called *SDHB*-ben; if none was elevated, the KNN classifier based on using the 3 best peptides was then used to make a final classification as *SDHB*-ben or *SDHB*-car. Using this combination classifier we achieved correct classification of 12/12 *SDHB*-car patients and 7/7 *SDHB*-ben patients using a fully cross-validated LOO error estimate – that is, sensitivity and specificity of both 100 %. This included the correct classification of M10. The same results were seen for the KNN classifier that used the best 4 peptides instead; using the 6 best peptides resulted in an overall error rate of 5.3 %.

This result is based on cross-validation in small samples and is subject to substantial

uncertainty; certainly in any extended use of this combination classification approach in future patients one will not achieve 100 % accuracy. But the combination classifier appears to overcome some of the deficiencies seen in each approach when applied separately. For example, peptide-based KNN classifiers correctly classified 2 of the 3 *SDHB*-ben patients (B01 and B06) missed by catecholamines, regardless of the number of peptides used (1, 2, 3, 4, or 6). And several of them (using 1, 3, or 4) also correctly identified B07 as *SDHB*-ben. Interestingly the overall best peptide (97409), which was ranked 1st in 16 of the 19 full cross-validation samples, correctly identified all 3 of the patients missed by catecholamines as being *SDHB*-ben. Indeed using partial LOO cross-validation for the single peptide 97409 resulted in misclassifying 1/12 healthy carriers and 0/7 patients with benign disease, for an overall error rate of just 5.3 % (1/19); this result does NOT depend on being helped by the catecholamine information

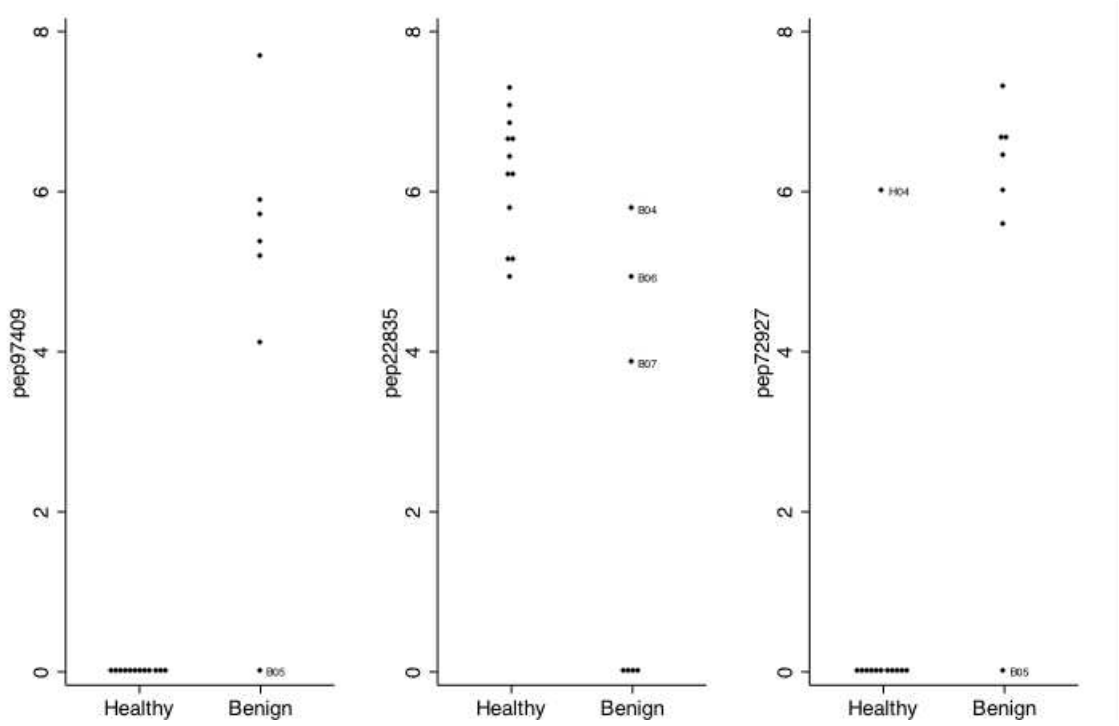

Figure 7: Transformed peak intensity of the best ranked 3 peptides to classify healthy *SDHB* mutation carriers and patients with *SDHB*-derived non-metastatic disease.

Table 6: Top 3 peptides classifying *SDHB*-ben and *SDHB*-car

Rank	Peptide Number	Molecular Weight	CE Transit
1	97409	2542.73	30.68
2	22835	1173.53	37.49
3	72927	2056.92	24.71

(because its error is among the healthy carriers, catecholamines would not help). Of note, this peptide classifies patient M10 as benign, so at least does not make the more severe error of calling this patient a healthy carrier.

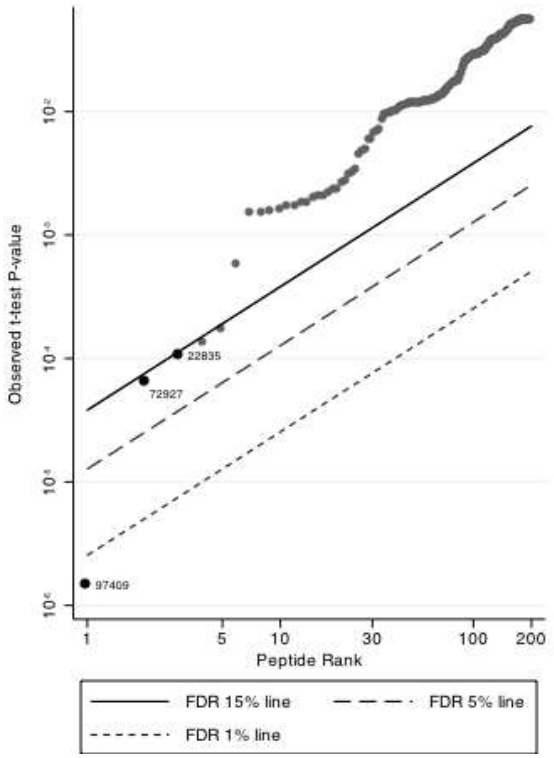

Figure 8: Peptides and their p-values for distinguishing patients with *SDHB*-derived non-metastatic PHEO/PGL from healthy mutation carriers as calculated by Fisher's t-test plotted over their rank.

Further identification of the best peptides used in this classification problem is still in progress. However information is available on another peptide (61510), which was always ranked right behind the best 3 in table 3. Like peptide 97409 peptide 61510 displayed low values in the healthy carriers and much higher values in the patients with benign disease.

These results suggest that these peptides and the catecholamines appear to be providing somewhat independent and complementary information; and although this is based on very limited samples, it is quite encouraging.

2.4 Discussion

Urinary peptide analysis proved potent in the development of new diagnostic means in a variety of diseases, including cancer (106). Here we show, that a small number of

urinary peptides may well classify the patient groups evaluated here into the respective groups: *SDHB*-car&-ben&-met vs. Ctr, *SDHB*-met vs. *SDHB*-ben&car, *SDHB*-ben vs. car. Currently there is only costly genetic testing for diagnosis of *SDHB* mutation, catecholamine testing to diagnose presence of PGL, and very costly functional imaging for the detection of metastatic disease. Although catecholamine testing is a well established tool to diagnose PGL, some *SDHB* patients may be missed due to presenting with biochemically silent tumors. Thus, additional diagnostic means in these questions are highly desirable.

Our results show that classification of *SDHB* mutation was possible with an excellent error rate of 1.8 % based on presence/absence of just 4 urinary peptides for our group of *SDHB*-derived PHEO/PGL patients, healthy mutation carriers and healthy controls. The single misclassified sample was from a healthy volunteer, thus no diseased patients were missed. Further diagnostic evaluation of the individual would allow exclusion of PHEO/PGL. However, the data presented here reflects a select group of patients and healthy mutation carriers. Thus, further validation in a double blind study including *SDHB* as well as other mutation carriers with and without PHEO/PGL are mandated to confirm our promising results and verify its usefulness in a more diverse group of patients.

Our data further suggests that patients with metastatic PGL can be well classified as such based on their urinary peptide pattern. Absence of a fragment of COL3A (AA886-909) peptide 76415, strongly suggests metastatic disease. Interestingly, another fragment of COL3A1 (AA 818-840, peptide 77184) was identified, however it showed similar peak intensities in *SDHB*-met and *SDHB*-ben.

Collagen III is an extracellular matrix component. In healthy tissue, the extracellular matrix supports tissue structure. In aggressive tumors, degradation and realignment of the extracellular matrix have been shown to occur to allow tissue invasion and cell migration (118, 119). However, the process is complex and the exact role of collagen type III has not yet been established.

Various human lung cancer cells have been tested for their spreading ability on collagen type III. Cell spreading of five adenocarcinoma cell lines was reportedly inhibited when grown on collagen type III, while Calu-1 squamous cell carcinoma cell spreading was not affected by collagen type III coating of the growth surface (120), indicating a possible regulatory effect of collagen type III on cell migration.

Increased collagen type III expression has been observed in reactive connective tissue

stroma of neoplasms of the gastrointestinal tract and salivary gland (121) and pancreatic cancer (122). In breast cancer, increased intensity of procollagen mRNA expression and protein deposition has been reported to increase with increasing grade of malignancy. In addition, infiltrating ductal carcinoma and metastases showed irregularly arranged and discontinuous collagen bundles, while those in benign breast lesions appeared well organized (123). Levels of the aminoterminal propeptide of type III collagen (PIIIP) have been evaluated in sera of patients with several types of cancer and amniotic fluid of patients with ovarian cancer (124-129). These studies report that high PIIIP levels correlate with presence of metastases, recurrent disease, or poor survival. Elevated levels of PIIIP in aggressive cancers indicate increased collagen type III metabolism. Thus, collagen type III synthesis and collagenolysis seems to be icreased in aggressive cancers and may follow distinct pathways in metastases and/or metastatic primary tumors compared to non-metastatic primary tumors. Whether a patient's collagen III synthesis is increased in metastatic PHEO/PGL or collagen breakdown in metastatic disease is inhibited or follows a distinct pathway from that in patients with non-metastatic PGL and healthy mutation carriers has yet to be established.

Collagen III is has been reported to regulated by hypoxia inducible factor 1α (HIF1α), which is stabilized in *SDHB*-derived PGL (28, 29). While Duval et al. have reported an inhibitory effect of HIF1α on collagen type III expression (130), Choi et al. have observed decreased mRNA expression of collagen type III upon HIF1α inhibition (131). Whichever effect stabilized HIF in PHEO/PGL may have on collagen type III expression, it should be similar for metastases, primary metastatic, and primary benign tumors, since HIF1α stabilization is not expected to differ between those samples (132). Thus, additional collagen type III metabolism regulators seem to play a role in the distinct collagen type III metabolism suggested by our data.

Collagen type III has been reported to have angiogenic effects (133). However endostatin, a fragment of collagen type XVIII has been shown to act anti-angiogenic and thus can suppress metastatic tumor growth. Here we found that COL3A fragment 76415 is absent in patients with metastatic disease. One may speculate that this fragment is part of a longer peptide or by itself capable of inhibiting metastatic growth, as is endostatin.

The third classification problem we evaluated was the distinction of the remaining

samples once patients with metastatic *SDHB*-derived disease were correctly classified. Differentiation of the samples classified as collected from an individual without metastases (i.e. presenting 76415) based on urinary peptides alone into *SDHB*-derived non-metastatic PHEO/PGL or *SDHB* mutation carrier proved to be less clear-cut. However, including routinely obtained plasma catecholamine data into our algorithm allowed for an excellent separation of healthy *SDHB* mutation carriers and those harboring an *SDHB*-derived PHEO/PGL. Particularly in patients with *SDHB*-derived PHEO/PGL, diagnosis based on elevated catecholamine levels alone can be misleading, since up to 10 % of these tumors are non-secreting (silent) (13). Thus, in state of the art PHEO/PGL diagnosis by testing for elevated catecholamine levels, these patients may easily be overlooked. Here we show, that testing for presence of just 4 urinary peptides may improve correct diagnosis of these patients significantly.

The data presented here are extremely promising and call for development of assays for the identified markers of *SDHB* mutation, *SDHB*-derived metastatic disease, as well as *SDHB*-derived non-metastatic PHEO/PGL. Successful development of such an assay may allow for a cost effective and non-invasive prescreening for patients that are suspected to suffer from *SDHB*-derived PHEO/PGL and for risk assessment of their family members. Collection of spot urine, aliquotting and freezing of samples can be done at any doctor's office, or even at a patient's home. An EIA would be inexpensive and may be used in any diagnostic lab, thus reducing the burden on patients to travel long distances for detection of possible metastases or follow up screening.

3 Warburg Effect's Manifestation in Aggressive Pheochromocytoma and Paraganglioma: Insights from a Mouse Cell Model Conveyed into Human Tumor Tissue

3.1 Introduction

After going unnoticed for decades, Warburg's hypothesis of an increased glycolytic phenotype in tumors is now increasingly recognized. Particularly in highly aggressive tumors a shift from efficient ATP synthesis via oxidative phosphorylation (OXPHOS) to increased glycolysis has been observed (134-136). These changes in energy metabolism have been linked to increased angiogenesis, impaired apoptosis, and generation of an acidic tumor environment (137). Increased glycolysis has been shown to appear through suppression of OXPHOS due to a hypoxic state in tumor areas with poor blood and oxygen supply as well as through mutation of key regulatory genes or increased reactive oxygen species (ROS) levels that lead to a pseudo-hypoxic state under normoxic conditions (138-141). Hypoxia has been recognized as a predictive marker for metastatic disease, therapy resistance and poor outcome in several types of cancer (for an excellent review see (142)).

Recently, mutations of a group of key regulatory genes causing pseudo-hypoxia and a glycolytic phenotype – i.e. the nuclear encoded mitochondrial succinate dehydrogenase (*SDH*) subunits A, B, C, and D – were recognized as tumorigenic. Mutations of the *SDH*x genes can cause pheochromocytoma (PHEO) and paraganglioma (PGL) (143-146). *SDH*x-derived PHEOs/PGLs present a unique type of cancer to study the Warburg effect and its role in aggressive tumors because of their impaired OXPHOS.

In *SDH*x related PHEOs/PGLs, the following dual roles of the *SDH* complex seem to decrease OXPHOS related ATP synthesis. First, its function as complex II in the electron transfer chain of the OXPHOS is impaired, resulting in decreased OXPHOS activity in *SDHB* and *D* (32, 40, 147, 148) and possibly in *A* and C. Second, the SDH complex catalyzes conversion of succinate to fumarate in the Krebs cycle. Accumulation of succinate and/or possibly ROS, due to enzyme malfunction, leads to product inhibition of prolyl hydroxylase (28, 44). Prolyl hydroxylase acts as part of a complex, that also includes the von Hippel-Lindau protein (pVHL), to appropriately degrade hypoxia-inducible factors α (HIFαs) under normoxia. When SDH is

malfunctioning, prolyl hydroxylase cannot adequately tag HIFαs for proteasomal degradation. Stabilized HIFαs then assemble with the constitutively expressed β subunits and together act as transcription factor. HIF responsive genes are activated, which leads to strengthened glycolysis, while OXPHOS activity, particularly complex II expression, is decreased (32, 36).

Another type of PHEOs/PGLs, i.e. *VHL* mutation-derived PHEOs/PGLs, share the pseudo-hypoxic/glycolytic phenotype (36). The study of tumors derived due to *VHL* mutations initially led to the discovery of pseudo- hypoxia and its supporting role in tumor growth (140). Dysfunction or absence of p*VHL* leads to inhibition of HIF α degradation and consequently pseudo-hypoxia.

Despite their similarities in presenting with pseudo-hypoxic/glycolytic phenotypes tumor aggressiveness in *SDH*x and *VHL*-derived PHEOs/PGLs is distinct. Development of metastases in patients with *VHL*, *SDHA*, *C*, and *D*-derived PHEOs/PGLs is rare, while patients with *SDHB* related PHEOs/PGLs frequently present with metastatic disease (10, 13, 149). To date, aggressive tumor behavior of PHEOs/PGLs has not been conclusively studied with respect to energy metabolism. This is partially due to several limitations, including limited availability of *SDHB* related tumors, no successful establishment of an *SDHB* cell line, difficulties in maintaining primary cells from human PHEOs/PGLs in culture, and absence of an *SDHB* animal model.

Recently, mouse PHEO cells (MPC) were established as an excellent tool in the study of the molecular biology of PHEO in vitro and in vivo (103, 150). Tumors identical with PHEOs/PGLs develop after i.v. and s.c. injection of these cells into nude mice. Martiniova et al. recently developed the more aggressive filial mouse tumor tissue (MTT) cells (151). Magnetic resonance imaging and microarray gene expression profiling comparing MPC to MTT revealed changes characteristic for metastatic tumors in MTT. Thus, comparison of the molecular biology of MTT cells to their parental MPC may provide valuable insight into aggressive behavior of PHEOs/PGLs. By focusing on the cell model, typical inter-patient variance in gene expression can be avoided, possibly allowing for an unbiased view of changed molecular pathways. Therefore, I decided to run a comparative protein expression study of MPC and MTT cells. Analysis of the differentially expressed proteins was focused on changes in energy metabolism related pathways. Expression changes detected in the MPC and

MTT cells were then evaluated in human PHEO/PGL tissue of different hereditary backgrounds. Our aim was to evaluate common changes in expression in aggressive types of PHEOs/PGLs in comparison to their less aggressive counterparts. Observed changes related to energy metabolism were further evaluated by measurement of OXPHOS complex activity and ROS production. The results presented here may lead to better identification and understanding of the pathogenesis of aggressive PHEOs/PGLs.

3.2 Material and Methods

3.2.1 Human PHEO/PGL Tissue

PHEO/PGL tissue was collected with informed patient consent at the NIH and at Suburban hospital in Bethesda, MD, under a protocol approved by the NICHD IRB. A summary of patient information is given in Table 7. Genetic testing was performed with informed consent by the patients, following established guidelines for testing (152) and consideration of biochemical phenotypes.

3.2.2 Cell Culture

Mouse pheochromocytoma cells (MPC 4/30PRR) were a generous gift from Dr. Tischler, TUFTS University, Boston. Their more aggressive filial MTT (mouse tumor tissue-derived) cells were generated and maintained as described by Martiniova et al. (151). Briefly, cells of liver tumors, established in nude mice after tail vein injection of MPC, were cultured and showed more aggressive behavior when re-injected than did their parental MPCs.

MPC and MTT cells were maintained at 5 % CO_2, 37°C in RPMI 1640 (Gibco, Grand Island, NY), supplemented with 10 % heat-inactivated horse serum (Hyclone Logan, UT), 5 % fetal bovine serum (Gibco), HEPES (Gibco), and penicillin (10,000 units/ml)/streptomycin (100,000 µg/ml) (Gibco). Medium was changed every other day and cells were passaged when 80-90 % confluence was reached.

3.2.3 2D-sample preparation

To harvest them, cells were incubated in 0.05 % trypsin (Gibco) at 37°C until detachment. Then media was added and cells were collected by centrifugation at 3000 x g for 3 min. Cells were washed in sterile 10 mM phosphate buffered saline (PBS; pH 7.4) and recollected by centrifugation three times.

Cell pellets were covered with 2D-lysis buffer (8 M urea, 4 % CHAPS, 65 mM DTT, 40 mM Tris) and incubated on ice for 30 min. Suspensions were homogenized by sonication at 100 W for 30 seconds on ice. Samples were centrifuged at 20,800 x g for 30 minutes. Protein from an aliquot of supernatant was precipitated with pre–cooled precipitation buffer (1:1 ethanol: acetone containing 0.01% acetic acid) at a 1:1 ratio, followed by incubation at - 20°C over night. The protein pellet was washed in ethanol and dried in a SpeedVac before re-dissolution in 2D-lysis buffer. Protein concentrations were estimated using the Bradford assay (Bio–Rad, Hercules, CA, USA). Samples were kept at - 80°C until analysis.

3.2.4 2D-Gel Electrophoresis

Two-dimensional (2D) gel electrophoresis and image analysis were performed as described by Jiang et al. (153). Briefly, 80 μg protein of four replicate samples per group was separated in two dimensions by isoelectric focusing and sodium-dodecylsulfate-polyacrylamide-gel-electrophoresis (SDS-PAGE) for differential image analysis. Isoelectric focusing was performed using precast IPG dry strips, pH 3-10 NL (Amersham Biosciences, Uppsala, Sweden) in an IPG-Phor^{TM} isoelectric focusing System (Amersham Pharmacia Biotech, Uppsala, Sweden) at a total of 60–70 kVh. After equilibration, IPG strips were placed on 12.5 % polyacrylamide gels. SDS-PAGE was performed in a Hoeffer SE600 electrophoresis unit (Amersham Pharmacia Biotech). Protein was visualized by ammoniacal silver nitrate staining and gels were scanned using a GS–800 calibrated densitometer (Bio–Rad). PDQuest software (Bio–Rad) was used for differential expression analysis. Matched spots with differences in intensity * area in ppM > 1.5, $p < 0.05$ were chosen as spots of interest.

For protein identification, 2D protein separation was repeated with 1 mg total protein (0.25 mg of each replicate) under similar conditions. Protein was reversibly stained using Phastgel Blue R (Amersham Pharmacia Biotech).

3.2.5 Protein Identification

Coommassie stained 2D gel separated protein spots were excised and trypsin digested *in situ* using a modified version of the ABRF protocol (ABRF, *"In-Gel" Digestion Protocol for Proteins in SDS PAGE Gel.* 1997 (http://www.abrf.org/ABRF/ResearchCommittees/intprotseqrescomm.html) without reduction and alkylation of disulfides. Following digestion, peptides were covered with

acid extraction of the gels into 10 µl of 1:1 acetonitrile: 0.1 % TFA.

Initial mass spectrometric analysis was conducted using an ABI 4800 Proteomics Analyzer (Applied Biosystems, Framingham, MA) operated in reflector mode. Unseparated extracted peptide mixtures, 0.5 µl, were applied with an equal volume of matrix, recrystallized HCCA matrix (0.5 mg/ml in 1:1 acetonitrile: 0.1 % TFA and 0.1 M $NH_4H_2PO_4$) containing two internal mass standards, ACTH clip 18-39, MH^+ = 2465.199, and the synthetic peptide RfffR (f= pentafluoro-phenylalanine), MH^+ = 1042.276; in addition to the two internal standards added to the matrix, trypsin autolysis peptides were also used as internal calibrants. Reflector spectra consisting of 400 laser shots were obtained for each peptide mixture and inspected for candidate peptides for MS/MS analysis. Peptides selected for fragmentation analysis were chosen on the basis of both S/N intensity and separation from adjacent peptides using a Timed-Ion-Selector resolution of 300. MS/MS spectra consisting of 3000 laser shots were obtained under unimolecular decomposition conditions using a recently updated default calibration.

Proteins were detected using the Mascot (154) search algorithm for the fragmentation spectra of each sample using the following search constraints:

peptide mass accuracy = 0.15 Da

fragment mass accuracy = 0.06 Da

charge state = +1

in the Swiss Prot database for H. sapiens. Having detected a protein in this manner, its sequence was downloaded and used in conjunction with reflector peptide masses in the algorithm ProteinProcessor. This algorithm digests the protein sequence *in silico* with user-specified modifications to Met and Cys residues allowing one missed cleavage, then attempts to match observed peptide masses within a user-specified tolerance. The algorithm generates files of the digested protein and matched peaks. The latter includes a listing of the total reflector ion signal associated with standards and tryptic autolysis peaks along with the peptides matched against the candidate protein sequence, the accuracy, in ppm, of the match, modifications or missed cleavage and the percentage of sequence coverage along with fraction of total reflector signal; in addition, a listing of unmatched peaks is provided so that the likelihood of additional proteins being in the sample can be assessed. The program is available upon request as either a Perl script or a cgi file.

For some protein digests, the protein of origin could not be identified based on the

MALDI spectra. For those, LC/MS/MS analysis was performed as described previously (155). The resulting tandem mass spectra were extracted using BioWorks, and the MS/MS spectra were analyzed by both Mascot (version 2.2.0; Matrix Science, London, UK) (154) and X! Tandem (version 2007.01.01.2; www.thegpm.org) database search programs. For both search programs, the Sprot_020508 database (selected for Rodentia, 23037 entries) was used with the fragment ion mass tolerance set to 0.60 Da and a 1.2 Da tolerance for the parent ion. The iodoacetamide derivative of cysteine was specified as a fixed modification, and oxidation of methionine was specified as a variable modification. Scaffold (version Scaffold-01_06_19, Proteome Software Inc., Portland, OR) was used to validate MS/MS based peptide and protein identifications. Peptide identifications were accepted if they could be established at greater than 95.0 % probability as specified by the Peptide Prophet algorithm (156), and protein identifications were accepted if they could be established at greater than 99.0 % probability and contained at least 3 identified peptides, using the Protein Prophet algorithm (157).

3.2.6 Ingenuity Pathway Analysis

A list of the identified proteins together with their fold changes was entered into Ingenuity Pathway Analysis (IPA) software to examine whether the identified changes of protein expression suggest impairment of particular established cellular pathways.

3.2.7 Western Blot

For Western blot validation of proteins of interest, MPC and MTT were harvested as described above, using a different lysis buffer (10 mM 3-3-cholamidopropyl dimethylammonio 1-propane sulphate (CHAPS) in PBS, containing a Roche Minitablet protease inhibitor (1 tablet per 5 ml of PBS; Roche Applied Biosciences, Indianapolis, IN)). After sonication, samples were centrifuged at 10,000 x g for 10 min at 4°C. The supernatant was used as protein extract. Human PHEO/PGL tissue was homogenized on ice in the same lysis buffer. After homogenization the crude extracts were treated as described above for the cells. The protein concentration was estimated using the QuantIt protein assay (Molecular Probes Invitrogen, Carlsbad, CA). Samples were diluted to the same concentration, containing 25 % NuPage SDS loading buffer and 10 % NuPage reducing agent. Proteins (20 µg) were separated in 4-12 % Nu-PAGE Bis-Tris gels (Invitrogen, Carlsbad, CA, USA) by reducing sodium-dodecylsulfate

polyacrylamide gel electrophoresis (SDS-PAGE) and transferred to a Immobilon-P PVDF-membrane (Millipore, Billerica, MA, USA). To verify equal protein loading, proteins were stained using the MemCode Reversible Membrane Staining Kit (Pierce Biotechnology, Inc., Rockford, IL). Membranes were blocked in 5 % (w/v) nonfat dry milk, dissolved in 25 mM Tris buffered saline (TBS, pH 7.4) with 0.05 % (v/v) Tween 20 (Sigma–Aldrich, St. Louis, MO) (TBST) for 1 hour or over night. Antibodies were dissolved in 5 % (w/v) Carnation nonfat dry milk (Nestlé USA, Solon, OH) in TBST. Primary antibodies were left on membranes for 1 hour; secondary antibodies remained on membrane for 30 minutes. Before and after antibody incubations, membranes were washed in TBST three times for 5 minutes each. Primary antibodies were as follows: rabbit-anti LDH, rabbit-anti GALK1, mouse-anti ATP-synthase beta, rabbit-anti SOD1 (all Abcam, Cambridge, MA, USA), rabbit-anti ATP5C1 (ProteinTech Group Inc., Chicago, IL), rabbit anti FLC1 (generous gift by Dr. Raoult, NICHD/NIH, Bethesda, MD), mouse-anti Cytochrome C (Zymed, Invitrogen), goat anti β-actin (I-19) (Santa Cruz Biotechnology, Santa Cruz, CA, USA). Secondary antibodies were as follows: HRP conjugated donkey anti-mouse, donkey anti-rabbit and donkey anti-goat IgG (Santa Cruz). Antibody binding was visualized by incubation of the membrane in Super Signal West Pico Chemiluminescent reagent (Pierce Biotechnology, Rockford, IL, USA) followed by exposure to Hyperfilm ECL (Amersham Biosciences GE Healthcare, Pistcataway, NJ, USA).

For Western blot of OXPHOS complex subunits, MPC and MTT mitochondria were isolated in buffer comprising 250 mM sucrose, 10 mM Tris/HCl, 1 mM EDTA and 2 μg/ml aprotinin (pH 7.4) at 4°C. The mitochondrial fraction was dissociated in sample buffer (50 mM Tris/HCl (pH 6.8), 12 % (v/v) glycerol, 4 % SDS, 2 % (v/v) 2-mercaptoethanol and 0.01 % (w/v) Bromophenol Blue) and incubated for 30 min at 37°C, and approximately 10 μg of protein was loaded for each lane. Protein was separated via tricine SDS/PAGE under standard conditions in 12 % polyacrylamide, 0.1 % (w/v) SDS and 5.5 M urea gels.

Transfer of protein to ImmobilonTM-P PVDF membranes (Millipore) was performed semi-dry for 2 h at a constant current of 0.8 mA/cm^2. Membranes were air-dried overnight, rinsed twice with 100 % (v/v) methanol and blocked in PBS and 10 % (w/v) non-fat dried milk for 1 h. Blots were incubated with primary antibodies in PBS, 0.3 % (v/v) Tween 20 and 1 % non-fat dried milk for 2 h. Primary antibodies: complex I

subunit NDUF6B (MS108; 5 μg/ml), complex II SDHA (MS204; 0.4 μg/ml) and SDHB (MS203; 4.5 μg/ml), core 2 subunit of OXPHOS complex III (MS304; 0.6 μg/ml), complex IV subunit Va (MS409; 3 ug/ml), complex V subunit α (ATP-synthase α, MS502; 3,5 μg/ml) (MitoSciences, Eugene, Oregon, USA). Secondary detection was carried out with goat anti-mouse IgG–horseradish peroxidase conjugate (A8924; 1:1000) (Sigma–Aldrich) in PBS, 0.1 % Tween 20 and 1 % non-fat dried milk for 1 h. Blots were finally developed using West Femto Chemiluminescent substrate (Pierce). Signal acquisition was performed using a VersaDoc 4000 imaging system (Bio–Rad), and the resulting digital images were analyzed using the Quantity One application (Bio–Rad).

3.2.8 Quantitative Real Time PCR

Samples of normal adrenal medulla (n=5), *SDHB*- (n=7), and *VHL*- (n = 7) derived PHEOs/PGLs were used. Tissue RNA extraction, reverse transcription and qRT-PCR were performed as previously described (158). Quantitation of *LDHA* and *B* as well as *18S* as internal control was performed using the 7500 RT PCR System and Taqman Gene expression assays (Hs00929956_m1 LDHB, Hs00855332_g1 LDHA, Applied Biosystems, Foster City, CA). Relative expression of *LDHA* and *B* to *18S* was calculated based on the delta Ct method. Oneway ANOVA, with Newman-Keuls correction for multiple comparisons, was used to test the statistical significance of various group comparisons using the Prism 4 software (GraphPad Software Inc., La Jolla, CA, USA).

3.2.9 Glucose Starvation Assay

For improved attachment, 24-well plates were coated with rattail collagen type VII (Sigma–Aldrich, St. Louis, MO). Collagen was dissolved over night in sterile water, containing $2*10^{-6}$ % acetic acid. The solution was diluted to 1 mg/ml with sterile water and added to each well to cover its surface. Plates were allowed to dry in a sterile environment. MPC and MTT cells were seeded at 10,000 cells/well in 1 ml RPMI medium (day –1). After allowing the cells to settle for 24 hours, medium was exchanged to fresh RPMI 1640 (2.0 g/l D-glucose), glucose free RPMI 1640, or high glucose RPMI 1640 (4.5 g/l D-glucose) (all from Gibco) (day0). All media were supplemented as described above. Media were renewed at day 2.

The cell number was assessed in triplicate measurements of three replicates per

treatment group using the Coulter Counter (Beckmann Coulter, Fullerton, CA) from replicate plates at the same time of the day from day -1 to day 4. Statistical evaluation of the data was done using 2-way ANOVA with Bonferroni post-hoc tests using Prism 4 (GraphPad Software Inc).

3.2.10 Mitochondrial Oxygen Consumption and ROS Production (permeabilized cells)

Cells were suspended in medium containing 125 mM sucrose, 65 mM KCl, 2.5 mM KH_2PO_4, 1mM $MgCl_2$, 20 µM EGTA, 20 mM HEPES, 0.1 % Bovine serum albumin, pH 7.4, and 5 mM glutamate/malate or succinate (in the presence of 2 µM rotenone) as substrates and permeabilized with digitonin (30 µg/ml). Oxygen consumption was determined polarographically using a Clark oxygen electrode (World Precision Instruments) in the basal state (S4) and after the addition of 600 µM ADP (S3).

ROS production was measured fluorometrically in permeabilized cells in an assay based on the detection of hydrogen peroxide generated during substrate catabolism in a horseradish peroxidase (HRP) coupled reaction using 10-acetyl-3,7-dihyrdoxyphenoxazine (Amplex Red reagent, Molecular Probes). 10^6 cells were incubated in the respiration medium and the ROS deriving from the mitochondrial respiratory chain were determined after the addition of either 5 mM glutamate/malate or succinate (in the presence of 2 µM rotenone) as substrates. The velocity of H_2O_2 production is calculated from a calibration curve obtained adding known amounts of H_2O_2. All assays were performed at 37°C on instruments equipped with thermostatic control and magnetic stirring. Significance of differences was calculated using Welch's version of the 2-tailed unpaired t-test in Prism 4 (GraphPad Software Inc.).

3.2.11 Tumor Oxphos Complex Activity

Frozen tumor tissue was homogenized and mitochondria were isolated according to standard differential centrifugation procedures (159) in 150 mM KCl, 10 mM Tris/HCl, 2 mM EDTA and 2 μg/ml aprotinin (pH 7.4) at 4 ºC. All samples were stored at −80 ºC.

Activities of respiratory chain complexes NADH:coenzyme Q10 reductase (complex I), succinate:coenzyme Q10 reductase (complex II), succinate:cytochrome c reductase (complex II+III), NADH: cytochrome c reductase (complex I+III), coenzyme Q10:cytochrome c reductase (complex III) and cytochrome c oxidase (complex IV) and

citrate synthase (CS) were measured spectrophotometrically at 37ºC in tissue homogenate or isolated tissue mitochondria as described in (160). Significance of differences was calculated using Welch's version of the 2-tailed unpaired t-test in Prism 4 (GraphPad Software Inc.).

3.2.12 Oxidative Stress (Tissue)

Oxidative stress in the tumor tissue was determined by malondialdehyde (MDA) formation measurement and DHE staining. MDA, an end product of lipid peroxidation, was determined spectrophotometrically by measurement of 2-thiobarbituric acid reactive substances (TBARS), as described previously (161). For DHE staining, 3 consecutive 10 µm thick cryosections of each tumor sample were incubated with 5 µmol/l DHE (Sigma) for 30 minutes at 37°C, washed twice with PBS, mounted and visualized using a confocal microscope (Zeiss, LSM 510 Meta). Significance of differences was calculated using Welch's version of the 2-tailed unpaired t-test in Prism 4 (GraphPad Software Inc.).

3.3 Results

3.3.1 2D-Gels of MPC and MTT Cells and Validation

Image analysis of the silver stained 2D-gels revealed differential intensities (fold change > 1.5, $p < 0.05$) for 127 spots. Spots of interest were narrowed down to 46, based on a scoring system considering spot intensity, ratio between groups and consistency within replicates. Protein identification was successful for 42 of the 46 spots of interest, and revealed 59 different proteins. Peptide sequences used to identify the proteins are listed in the supplemental material along with their Mascot scores and the percent coverage.

Ingenuity Pathway Analysis of the identified proteins and the fold changes of their spot intensity returned the OXPHOS pathway as the canonical pathway with the most significant changes. Four identified spots contained members of OXPHOS complexes: the ubiquinol-cytochrome-c reductase complex core protein 1 (Uqcrc1, OXPHOS complex III, MPC > MTT, Q9CZ13, spot 3405); and the ATP-synthase β, γ and d subunits (OXPHOS complex V, MTT > MPC, P56480, spot 1619; Q91VR2, spot 4120; Q9DCX2, spot 3007) (Figure 9A). Except for the spot representing ATP-synthase d, each of these spots contained additional proteins that potentially influenced the change of intensity between the groups (supplemental material). An increased protein level of

ATP-synthase γ in MTT was verified by western blot, while ATP-synthase β as well as Uqcrc1 did not show a change in protein level (Figure 9B). The glycolysis related protein lactate dehydrogenase B (LDHB, P16125, spot 4312) was identified from a spot with decreased intensity in MTT (fold change = -1.9). Western blot for LDHB verified lower expression in the more aggressive MTT cells. However, Western blot for LDH using an antibody that recognized LDHA (P06151) as well as B showed higher signal intensity in MTT cells (Figure 9B). Thus, overall LDH expression was elevated in MTT, with an increased ratio of expression of LDHA to LDHB.

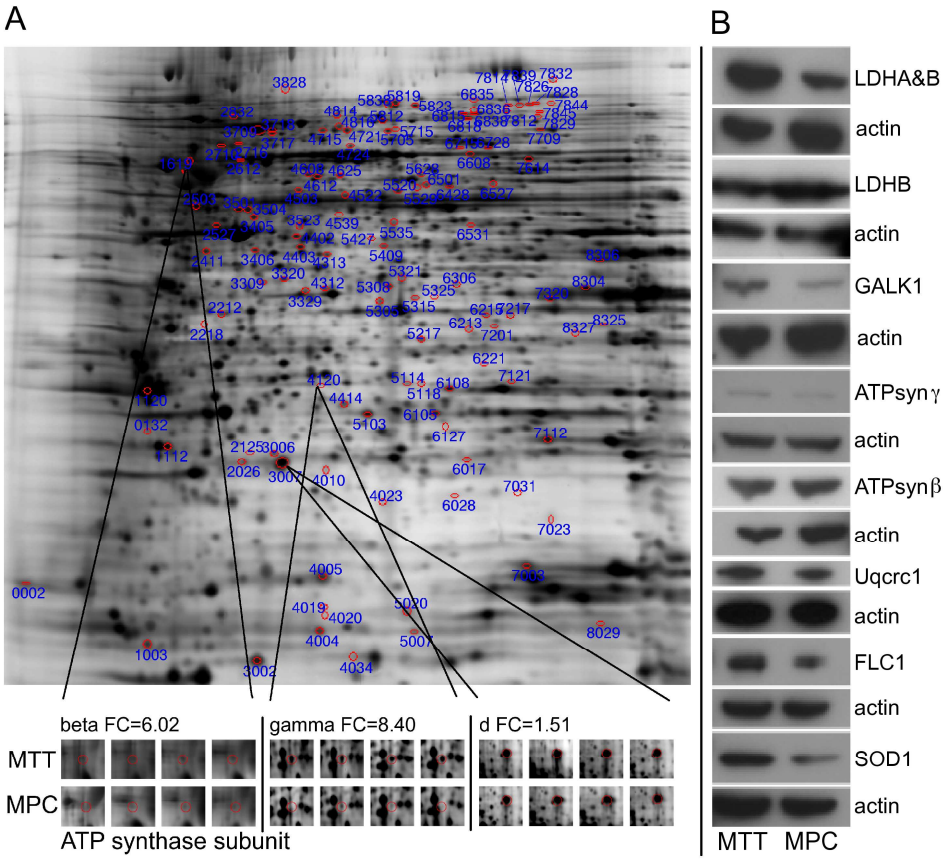

Figure 9: **A** Representative silver staining of 2D-gel. Spots of interest are circled in blue. Magnification of spots containing ATP-synthase subunits are shown to the right for all four MPC and MTT gels. **B** western blot for validation of differential expression of select proteins of interest.

In further support of increased glycolytic activity, galactokinase 1 (GALK1, Q9R0N0, spot 2411) was identified as differentially expressed (fold change 1.5). Western blot for GALK1 verified higher intensity in MTT cells. Three other proteins identified from the same spot were not followed up on.

In addition to pronounced changes in expression of energy metabolism related proteins, changes in expression of proteins related to ROS production were apparent. Ferritin

light chain 1 (FLC1, P29391, spot 4010) as well as copper/ zinc superoxide dismutase (SOD1, P08228, spot 5020) were identified from the spot with the highest fold change between the two cell types. FLC1 and SOD1 were also identified from additional spots, with higher intensity in MTT than MPC (suppl. mat.). With the help of ProteinProcessor, FLC1 truncation could be identified for the lower molecular weight spots (4019 and 4020), based on absence of peptide fragments that were present in the full size FLC1 (spot 4010). Western blot for both SOD1 and FLC1 verified higher expression in the MTT cells (Figure 9B).

3.3.2 Glucose Starvation Assay for MPC and MTT Cells

Altered expression of OXPHOS and glycolysis related proteins suggests an impaired energy metabolism in MTT. Elevated LDH expression with an increased LDHA to LDHB ratio indicates decoupling of glycolysis and OXPHOS in MTT.

To test whether Krebs cycle and/or OXPHOS impairment is more pronounced in MTT than MPC, their proliferation was observed in the presence and absence of glucose for 4 days. This is to show whether there is a difference in the capabilities of MPC and MTT to thrive on glutamine-driven OXPHOS alone or if they depend on glycolysis. MTT cells grown in presence of glucose increased in number more rapidly than MPC, independent of glucose concentration. For MPC, however, the glucose concentration played a role: the number of MPC increased fastest with the highest glucose concentration. Independence of the rate of proliferation of MTT from the level of glucose present indicates that glycolytic activity cannot be further increased by elevated glucose supply in MTT.

To test whether Krebs cycle and/or OXPHOS impairment is more pronounced in MTT than MPC, their proliferation was observed in the presence and absence of glucose for 4 days. This is to show whether there is a difference in the capabilities of MPC and MTT to thrive on glutamine-driven OXPHOS alone or if they depend on glycolysis. MTT cells grown in presence of glucose increased in number more rapidly than MPC, independent of glucose concentration. For MPC, however, the glucose concentration played a role: the number of MPC increased fastest with the highest glucose concentration. Independence of the rate of proliferation of MTT from the level of glucose present indicates that glycolytic activity cannot be further increased by elevated glucose supply in MTT.

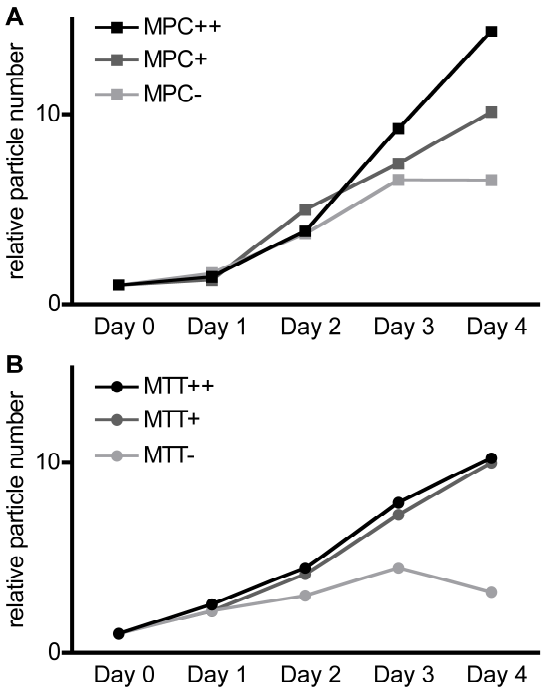

Figure 10: Relative particle number to the first day in culture, counted on 4 consecutive days of culture of: **A** MPC and **B** MTT cells in high glucose media (++, black), regular media (+, dark grey) and glucose free media (-, light grey).

Under glucose deprivation, MPC still increased in number over time, while the number of MTT cells increased more slowly than in the presence of glucose for the first days and started to significantly decline by day 3 (Figure 10). The inability of MTT to proliferate significantly without glucose suggests impairment in the Krebs cycle and/or OXPHOS. However, the fact that MTT slightly increased in number even in absence of glucose suggests that some Krebs cycle and OXPHOS activity remained.

3.3.3 Mitochondrial Oxygen Consumption and ROS production in MPC and MTT cells

To evaluate if and where OXPHOS is impaired in MTT, mitochondrial oxygen consumption was assessed in digitonin-permeabilized cells. No significant differences were observed between the cell lines in either basal state oxygen consumption or ADP-induced oxygen consumption, using either glutamate/malate (complex I) or succinate (complex II) as substrate (Figure 11A). In agreement with this observation, Western blot analysis for several ETC complex subunits – namely NDUFB6 (O95139, Complex I), SDH A and B (P31040, P21912, Complex II), Core 2 (P22695, Complex III), COX V (P20674, Complex IV) and ATP–synthase α (P25705, Complex V) – did not support alterations in protein level (Figure 11C). However, H_2O_2 production with glutamate/malate as substrate was increased, suggesting a non-optimal OXPHOS activity at the level of complex I in MTT (Figure 11B).

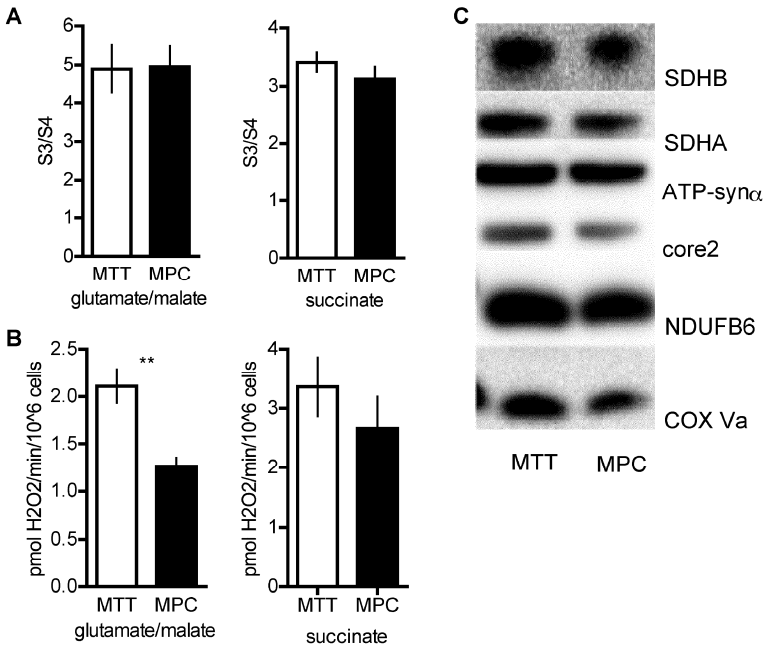

Figure 11: **A** Ratio of ADP-stimulated (S3) and baseline oxygen consumption (S4) in MPC and MTT **B** hydrogen peroxide levels observed after addition of substrate (glutamate/ malate, complex I; succinate, complex II). ** indicates $p < 0.01$. **C** protein expression of select subunits of each complex of the OXPHOS (complex II: SDHA, *SDHB*; complex I: NDUFB6; complex III: core 2; complex IV: COXVa; complex V: ATP-synα).

3.3.4 Differential Expression in Human Pheochromocytomas and Paragangliomas

In the more aggressive MTT cells, an increase in LDH due to an increased expression of LDHA (P00338) was found, while LDHB (P07195) expression was decreased. Expression of LDHA and B was evaluated in tumor tissue by qRT-PCR with specific primers for LDHA and B as well as by 2 Western blots: one with an antibody recognizing LDHA and B, and one specific for LDHB (Figure 12). The LDHA&B as well as LDHB band intensities were normalized to β-actin expression on the respective membranes using image J software. While the mRNA ratio of LDHA to B did not differ between *SDHB*- and *VHL*-derived PHEOs/PGLs , the ratio was significantly higher in both *VHL*- and *SDHB*-derived PHEO/PGL tissues compared to normal adrenal medulla ($p < 0.01$ for both) (Figure 12A). LDHA mRNA levels in *SDHB* were significantly higher than in either normal adrenal medulla or *VHL* ($p < 0.01$ for both), while there was no difference between *VHL* and normal adrenal medulla (Figure 12A). LDHB mRNA levels were significantly decreased comparing *VHL* to normal adrenal medulla and *SDHB* ($p < 0.05$ and $p < 0.01$, respectively) (Figure 12A). In agreement with the mRNA levels, for protein levels the ratio of LDHA&B to LDHB did not significantly differ between *VHL*- and *SDHB*-derived PHEOs/PGLs. The signal of LDHA&B as well as LDHB alone was significantly higher in *SDHB* than *VHL*-derived tissue ($p < 0.001$, $p < 0.01$, respectively) (Figure 12B, C). Thus, while both tumor types

show an increased ratio of LDHA to B, favoring the conversion of pyruvate into lactate, *SDHB*-derived tumors show a significantly increased overall expression of LDH. This indicates an increased efficiency of conversion of pyruvate to lactate in *SDHB*, compared to *VHL*-derived PHEOs/PGLs.

In the 2D-gel comparison of the MPC and MTT cells, we found differences in several ATP-synthase subunits. Western blot of human *VHL*-, *SDHD*- and *SDHB*-derived PHEOs/PGLs, showed a significant increase in ATP synthase β (P06576) expression in *SDHB*- and *D*-derived PHEOs/PGLs compared to the *VHL* samples (Figure 13).

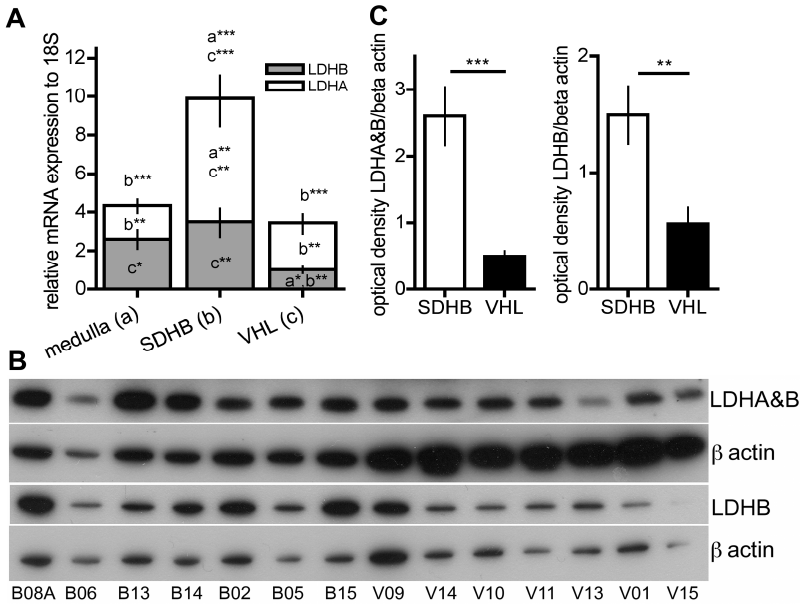

Figure 12: Lactate dehydrogenase expression. **A** relative expression of LDHA and LDHB mRNA in normal adrenal medulla, *SDHB*- and *VHL*-derived PHEO/PGL tissue. **B** Western blot for LDHA&B as well as LDHB for indicated samples. **C** Optical density of bands as assessed with image J software for LDHA&B as well as LDHB from western blots shown in **B**.

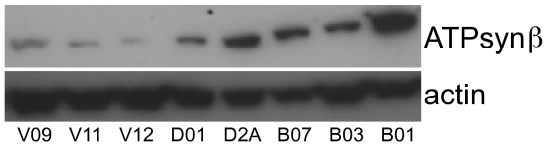

Figure 13: Protein expression of ATP synthase β in *VHL*-, *SDHD*- and *SDHB*-derived PHEO/PGL tissue as indicated.

3.3.5 Mitochondrial Electron Transfer Chain Complex Activity in Human Pheochromocytomas and Paragangliomas

OXPHOS complex activity in frozen *VHL*- (n = 4) and *SDHB*-derived primary PHEOs/PGLs (n = 2), as well as metastases (n = 2), was evaluated. No significant difference in OXPHOS complex activity between *SDHB*-derived primary tumors and metastases was observed; thus the samples were grouped together for comparison to *VHL*-derived PHEOs/PGLs. Comparison of *VHL* and *SDHB*-derived samples revealed a significantly higher activity in *SDHB* of citrate synthase (CS) in tissue homogenates

and isolated mitochondria ($p = 0.04$, $p = 0.05$). In addition complex III activity was significantly increased in *SDHB*-derived tumors ($p = 0.04$). Elevated CS activity can reflect increased mitochondrial content (162). Normalization of complex activity to CS activity revealed a relative decrease in complex I ($p = 0.03$), II ($p = 0.03$) and II+III ($p = 0.03$) in *SDHB*-derived tumors (Figure 14A). Thus, in relation to mitochondrial content, OXPHOS activity seems to be decreased in *SDHB* compared to *VHL*-derived tumors. However, similar levels of complex I+III, III and IV activity in both groups may indicate that OXPHOS is not completely obstructed in *SDHB*.

3.3.6 ROS Production in Human PHEOs/PGLs

The observation of complex II+III disruption in *SDHB* leads us to assume that ROS production may be increased, as was suggested previously for *SDH*x-derived tumors (43, 44, 138, 163). Levels of malondialdehyde as an index of lipid peroxidation, as well as dihydroethidium (DHE) fluorescence, were evaluated in *SDHB* and *VHL*-derived tumor tissue (Figure 14B, C). However, no differences could be observed between the different types of tissue. Protein levels of SOD1 and FLC1 appeared unchanged on Western blot in human PHEOs/PGLs with different genetic backgrounds (data not shown).

3.4 Discussion

Until recently the importance of Warburg's observation of a shift to a glycolytic phenotype in tumor cells has often been underestimated. Now an increasing number of tumors, particularly in aggressive disease, can be linked to a dependence on glycolysis, often related to pseudo-hypoxia and/or OXPHOS dysfunction (164). In the present study we compared aggressive human and mouse PHEOs/PGLs to their less aggressive counterparts and to human normal adrenal medulla. We were able to detect certain overlaps in the characteristics of MTT, aggressive mouse PHEO cells, and *SDHB*-derived tumors, the most aggressive type of human PHEOs/PGLs. Both MTT cells and *SDHB*-derived tumors seem to rely extensively on glycolysis due to significant Krebs cycle and/or OXPHOS dysfunction. For MTT this is shown by decreased proliferation in the absence of glucose.

In addition, increased ROS production at complex I was observed in MTT compared to MPC, indicating inefficiency in OXPHOS.

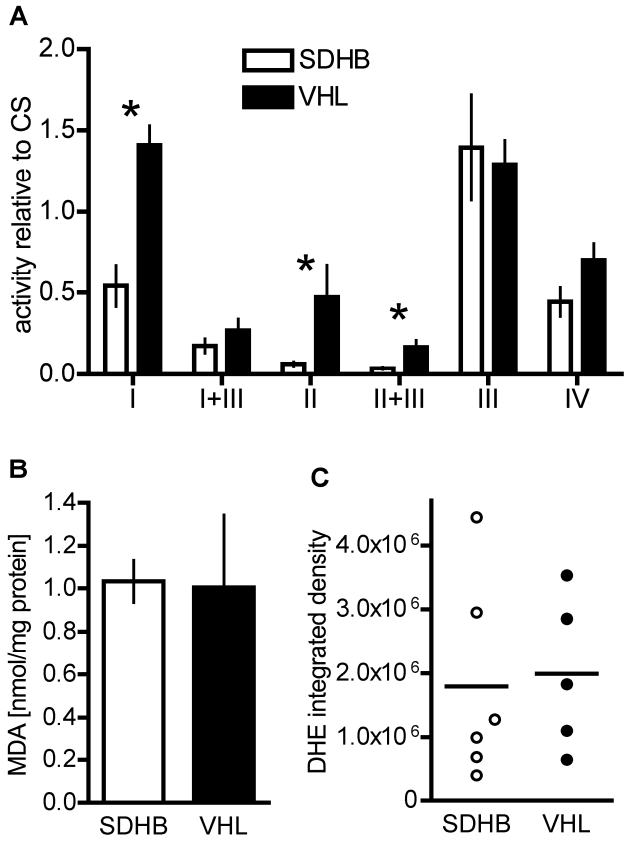

Figure 14: **A** Oxphos complex activity in *SDHB*- and *VHL*-derived (n=4 each) PHEO/PGL tissues. * indicates $p < 0.05$. **B** Malondialdehyde level in *SDHB* (n = 5) and *VHL* (n = 5) tissue as a measure of lipid oxidation. **C** Integrated density of DHE fluorescence in *VHL* (n = 5), *SDHB* (n = 6).

In human *VHL*-, as well as *SDHB*-derived PHEOs/PGLs, OXPHOS complex expression and activity have previously been shown to be decreased (32, 36). In the present study we showed that complex I, II and II+III activity, in relation to the mitochondrial content, is more severely reduced in *SDHB* than in *VHL*. Recently we observed that indeed the number of mitochondria is significantly increased in *SDH*x related PHEOs/PGLs compared to *VHL* and multiple endocrine neoplasia related, as well as sporadic PHEOs/PGLs (unpublished observation). Thus, transfer of electrons from complex II to III seems to be more severely impaired in *SDHB* than in *VHL*, suggesting inefficient, but not completely obstructed, OXPHOS capability.

While more prominent in *SDHB*, decreased OXPHOS activity is also present in mainly benign *VHL*-derived tumors; thus, this change alone may not entirely account for the more aggressive phenotype occurring due to *SDHB* mutations. However, in addition we observed a prominent increase in LDH expression in MTT cells and *SDHB*-derived PHEOs/PGLs in comparison to MPC and *VHL*/normal adrenal medulla, respectively.

LDH is a tetramer of LDHA and LDHB subunits, converting lactate into pyruvate and vice versa, depending on complex composition. Close coupling of glycolysis and OXPHOS is supported as long as the amount of LDHB outweighs or matches that of

LDHA. However, if LDHA is more prevalent, it promotes decoupling with increased lactate production.

The ratio of LDHA&B to B protein was increased in MTT compared to MPC, while in both types of human PHEOs/PGLs, the ratio of LDHA to B was similar (Figure 12). Thus, in *VHL*-derived PHEOs/PGLs an increased LDHA to B ratio is due to suppression of LDHB, potentially related to hypoxic conditions or promoter methylation, as has been observed previously (165). In contrast, in *SDHB*-derived PHEOs/PGLs LDHA expression was increased. In conclusion, in both *SDHB* and *VHL*-derived PHEOs/PGLs the conversion of pyruvate into lactate is more likely than the reverse reaction, presumably with a higher efficiency in *SDHB*-derived tumors due to a higher overall level of LDH.

Resulting high cytosolic lactate levels have been reported to lead to an acidic tumor environment, presumably supporting aggressive tumors by protecting them from the host's immune response and destabilizing the surrounding extracellular matrix, thereby enhancing tumor growth and spread (166). Tumor-generated high lactate levels have also been shown to increase the risk of metastases, recurrence and/or were correlated with reduced patient survival (167-170). Increased LDHA levels seem to be mandatory in tumor initiation as well as tumor maintenance (171, 172). Thus, targeting LDHA has been proposed as a promising therapeutic approach to treat cancers rich in LDHA, with presumed low systemic toxicity (173).

As an HIF target gene, LDHA has previously been shown to be prominent in *VHL* deficient cells as well as in cases of leiomyomatosis, derived due to fumarate hydratase deficiency (173). Favier and colleagues recently reported increased LDH activity in *VHL* compared to *SDH* and *RET*/*NF1* related PHEOs/PGLs (32, 36). It remains unclear why, with an increased mRNA and protein level of LDHA observed in our study, LDH complex activity should be reduced in *SDHB* related PHEOs/PGLs compared to those due to *VHL*. Additional experiments on LDH enzyme activity on fresh tumor tissue of *SDHB* and *VHL* tissue will be necessary to resolve this discrepancy.

In the study presented here, we show that the aggressive MTT cells exhibit a more glycolytic phenotype, accompanied by expression changes in glycolysis and OXPHOS related proteins, i.e. LDH, GALK1, and ATP-synthase γ. In addition, MTT appeared more dependent on glucose, while elevating glucose supply did not enhance cell proliferation. Thus, MTT cells possibly run at full glycolytic capacity. Despite maintenance of OXPHOS complex I and II activity, ROS production at complex I was

significantly increased in MTT. This was accompanied by increased SOD1 expression, which potentially protects the cells from high ROS levels. SOD1 deoxygenates superoxide to the less oxygenating H_2O_2. Recently, in addition to being found in the cytosol, SOD1 has been detected in the inter-membrane space of mitochondria (174). Up-regulation of SOD1 in MTT may indicate that the site of ROS production at complex I is directed towards the inter-membrane space. However, additional experiments are required for confirmation.

Increased ROS production was proposed as a cause for the aggressive behavior of *SDHB*-derived tumors (43, 138). However, we were not able to detect a difference in ROS levels and SOD1 expression (data not shown) between *SDHB*- and *VHL*-derived tumors. Possibly ROS production is equally increased in both tumor types. Another possible explanation is that high ROS levels may be blunted by an increased expression of LDHA in *SDHB*-derived tissue. LDHA has been shown to have a ROS scavenging effect (175). The detection of lipid oxygenation and DHE fluorescence in tumor tissue applied here reflect the oxygenation state of the whole cell. However, measurement of specifically OXPHOS related ROS generation remains to be evaluated.

Decreased growth under glucose deprivation in MTT shows that OXPHOS is impaired and that MTT cells are more dependent on glycolytic energy generation than MPC. In contrast, judged by the silver-stained 2D gels, protein levels of several ATP-synthase (complex V) subunits appeared to be more highly expressed in MTT than MPC. Increased expression of subunit γ was confirmed by Western blot. For ATP-synthase d no commercial antibody was available, so confirmation was not attempted. However, because ATP-synthase d was the sole protein identified from its spot, the change in expression level indicated by the 2D-gel is assumed to be accurate. There was no apparent difference in ATP-synthase α and β subunit expression. Possibly changes in protein levels of additional proteins identified from the spot representing ATP-synthase β contributed to the 6-fold change between MPC and MTT. Unlike in *SDHB*- and *VHL*-derived tumor tissue, the number of mitochondria did not seem to differ between MTT and MPC in electron microscopy images as well as based on mitotracker staining (unpublished observations). It remains unclear why expression of two subunits of the ATP-synthase complex are elevated in MTT (γ and d), while protein levels of α and β subunit remained unchanged between the different cell types. Possibly synchronous expression regulation is disrupted in MTT, leading to elevated expression of individual

subunits of ATP-synthase, possibly causing complex malfunction.

In human PHEOs/PGLs, we observed an increased expression of ATP-synthase β in *SDHB*- and *D*-related tissue, compared to *VHL*-derived tissues (Figure 13). In contrast, decreased expression of ATP-synthase β has been proposed as a marker of aggressive disease in colon, breast, and lung adenocarcinoma as well as squamous lung carcinomas (176). Possibly tumor aggressiveness is not necessarily related to a decrease of ATP-synthase β expression, but to a general dysfunction of the ATP-synthase complex. ATP-synthase dysfunction may be initiated by down-regulation of individual complexes as well as impaired complex assembly, which in turn may lead to increased complex subunit expression in an attempt to rescue complex function. Further experiments are required to evaluate the role of possible ATP-synthase dysfunction in PHEOs/PGLs.

Cells generally make up for a decrease in OXPHOS activity, as observed here in MTT and *SDHB* and previously reported for *SDHD* and *VHL*, by an increase in glycolytic ATP generation. Consistently the expression of the glycolysis related proteins GALK1 and LDHA were shown to be elevated in MTT. While energetically inefficient in a healthy cell, under certain conditions GALK1 can increase the amount of glucose that can be utilized in a cell (177). GALK1 phosphorylates galactose into galactose-1-phosphate, which is broken down into glucose and lactose in subsequent reactions. Thus, increased GALK1 activity promotes utilization of glucose from galactose in the generation of glycolytic ATP.

Additional observations based on the cell model that were not observed in human PHEOs/PGLs, but that may play a role in the development of a more glycolytic phenotype in MTT were an increased expression of the smaller subunit of ferritin, FLC1, as well as truncated versions thereof.

High levels of FLC1 have been shown to protect cells from oxidative stress (178). Ferritin serves as iron storage compartment in binding excess iron, preventing the cell from its toxic effects. Increased Fe^{3+} induces ferritin expression, thus an increased amount of ferritin is very likely to reflect high iron levels. The oxphos pathway is sensitive to changes in iron level in different ways: High iron levels cause mitochondrial membrane damage (179), as well as decreased activity of complex I+III, II and IV (180, 181). Decreased Fe^{2+} levels inhibit pVHL, which prevents degradation of HIF-1α and β, leading to a state of pseudo hypoxia (as seen in *SDHB*-, *C*-, *D*- and

VHL-derived PHEOs/PGLs). Iron is also required in the Fenton reaction, which further reduces highly reactive H_2O_2, the product of superoxide reduction by SOD to prevent cell damage. However, catalase and glutation transferase can catalyze H_2O_2 reduction in the absence of iron. It remains to be examined, whether the observed increase in FLC1 expression leads to decreased cytosolic and/or mitochondrial Fe^{2+} levels or if increased levels of truncated FLC1 impair the iron binding capacity of ferritin, thus leading to increased ferritin expression.

The data presented here suggest, that Krebs cycle and/or OXPHOS are more severely impaired in *SDHB*- than *VHL*-derived PHEOs/PGLs; and more severely impaired in MTT compared to MPC. While higher ROS production was recorded in MTT, there was no indication for differences in ROS levels comparing *SDHB*- to *VHL*-derived PHEOs/PGLs. In addition, elevated LDH expression with an increased ratio of LDHA to LDHB may distinguish aggressive PHEOs/PGLs from their less aggressive counterparts. Thus, targeting LDHA provides a promising treatment option for aggressive, *SDHB*-derived PHEOs/PGLs.

Table 7

ID	Genetic backgroud	Age	Gender	Type	Tumor site	Biochemistry	Oxphos	DHE	MDA	Western blot	qRT-PCR
B01	*SDHB*	31	M	s p	left peri-aortic mass, medial and caudal to kidney	DA, DOPAC	x	x	x	x	x
B02	*SDHB*	13	M	s p	right periadrenal	nd				x	
B03	*SDHB*	35	M	m p	retroperitoneal	NE, NMN, DHPG				x	x
B04	*SDHB*	35	F	met met	liver	NE, NMN, DHPG		x		x	x
B05	*SDHB*	30	F	s p	left adrenal	NE, NMN, DOPA, DHPG		x	x	x	
B06	*SDHB*	41	M	met met	spine	NMN	x			x	
B07	*SDHB*	53	M	s p	nasopharingeal	NE, NMN, DA	x			x	x
B08A	*SDHB*	36	F	met met	abdomen, right lower quadrant, lymph node	NE, NMN, DOPA	x			x	
B08B	*SDHB*	36	F	met met	lung	NE, NMN, DOPA					x
B09	*SDHB*	47	F	s p	right adrenal	MN, NMN, NE, DOPA, DHPG		x	x	x	
B10	*SDHB*	10	F	m p	left iliac bifurcation	NMN, NE, DA		x	x		
B11	*SDHB*	33	M	p met	retroperitoneal	NMN, NE			x		
B12	*SDHB*	39	M	met met	lung	NMN, NE		x			
B13	SHDB	38	M	p met	abdomen, left suprarenal	DOPAC				x	x
B14	*SDHB*	44	M	p met	retroperitoneal	NMN				x	
B15	*SDHB*	15	M	s p	retroperitoneal	non secreting				x	
B16	*SDHB*p	23	M	p met	bladder	NE					x
D01	*SDHD*	61	M	s p	right adrenal	NMN		x		x	
D02	*SDHD*	32	M	m p, inv	bilateral adrenal	DHPG, DA, NE, NMN				x	
$M01R_{CC}$	na	61	M	NAM	na	na					x
$M02_{nn}$	na	nn	nn	NAM	na	na					x
$M03_{MOH}$	na	53	F	NAM	na	na					x
$M04_{AKT}$	na	72	F	NAM	na	na					x
$M04_{BKT}$	na	72	F	NAM	na	na					x
V01	*VHL*	32	M	b p	bilateral adrenal	NE				x	
V02	*VHL*	26	F	m p	celiac mass	NMN				x	
V03	*VHL*	32	M	b p	left adrenal	NE, NMN		x	x		
V04	*VHL*	28	M	s p	left adrenal	NE, NMN		x	x		
V05A	*VHL*	23	M	m p	right adrenal	NE, NMN, DHPG, DOPA	x	x	x		
V05B	*VHL*	23	M	m p	carotid body	NE, NMN		x	x		
V05C	*VHL*	23	M	s p	left adrenal	NE, NMN					x
V06	*VHL*	39	M	m p	left para-aortic	NE, NMN	x				x
V07	*VHL*	52	F	m p	right retrocaval mass	NMN	x				x
V08	*VHL*	16	M	b p	bilateral adrenal	NE, NMN	x	x	x		x
V09	*VHL*	43	F	b p	right adrenal	NE				x	
V10	*VHL*	31	M	b p	bilateral adrenal	MN, NMN, DOPA				x	x
V11	*VHL*	19	M	m p	left adrenal	NE				x	
V12	*VHL*	13	M	b p	right adrenal	nd				x	x
V13	*VHL*	39	F	b p	bilateral adrenal	NE, DOPA				x	
V14	*VHL*	39	M	m p	right adrenal	NMN, DA				x	
V15	*VHL*	39	F	s p	right adrenal	NMN				x	
V16	*VHL*	47	F	b p	bilateral adrenal	NE					x

Abbreviations: b p: bilateral primary tumors, DA: dopamine, DHPG: dihydroxy phenylglycol, E: extra-adrenal, F: female, inv: invasive, M: male, met met: metastatic metastases, m p: multiple primary tumors, MN: metanephrine, na: not applicable, NAM: normal adrenal medulla, nd: not done, NE: norepinephrine, NMN: normethanephrine, p met: primary metastatic, s p: solitary primary tumor, *SDHB*: succinate dehydrogenase B mutation, *SDHB*p: *SDHB* polymorphism. Same sample ID with different letters to follow indicates samples removed from the same patient; subscript abbreviations stand for cause of resection of normal adrenal medulla: RCC: renal cell carcinoma, MOH: multiorgan harvest, KT: kidey transplantation.

4 Cell Surface ATP synthase: Potential as a Therapeutic Target in Metastatic Pheochromocytoma and Paraganglioma

4.1 Introduction

F1Fo-ATP synthase (ATP synthase) is an ubiquitous enzyme complex in eukaryotes. In general it is localized to the mitochondrial inner membrane. There it utilizes the proton gradient across the inner mitochondrial membrane that is built by the complexes of the electron transfer chain to catalyze the final step in the mitochondrial oxidative phosphorylation of ADP to ATP. Within the past decade, ATP synthase has been shown to play a role in cancer (182-184) and was suggested as therapeutic target, particularly when expressed on the cell surface (185, 186).

Initially cell surface ATP synthase was discovered on endothelial cells as a target of angiostatin (187). Angiostatin was shown to inhibit tumor angiogenesis and thus was evaluated as a promising therapeutic agent for starving tumor cells. However, clinical trials where not as successful as hoped for (188).

Recently, cell surface ATP synthase was also discovered on some other cell types, including certain tumors, neurons, adipocytes, heart (189), liver, clonal β-cells (INS-1) and T-cells. It has been suggested as a direct target to treat tumor cells. Inhibition of cell surface ATP synthase with angiostatin, aurovertin, resveratrol and antibodies against the α and β subunits of ATP synthase effectively and specifically killed corresponding cells, especially under low pH conditions. Cell types on which surface ATP synthase has been found, drugs that have been effectively used to target it and its possible functions have recently been reviewed (190).

Although the role of cell surface ATP synthase is still unclear, it has been suggested that it benefits tumor cells thriving on aerobic glycolysis in surviving their high acid generation by shuttling protons out of the cell to create both, a physiological intracellular pH and an acidic extra-cellular environment (191). An acidic micro-environment may trigger local destabilization of the extracellular matrix, facilitating tumor growth and tissue invasion (191). Due to the acidic micro-environment surrounding many tumors, cell surface ATP-synhtase inhibition holds the potential to specifically kill tumor cells, either directly or by killing endothelial cells of the

microvessels that nourish the tumor.

As in most cancers, currently treatment options for metastatic pheochromocytomas (PHEOs) and paragangliomas (PGLs), i.e. catecholamine producing tumors of the sympathetic nervous system, are limited and rarely curative. Thus, specific new therapeutic targets for the treatment of inoperable and metastatic PHEOs/PGLs need to be detected.

Like all cells in the body, PGL cells receive the majority of their energy from ATP. Recently, the energy metabolism in PHEOs/PGLs was much considered. It has been shown that certain types of PHEOs/PGLs exhibit a glycolytic phenotype. In particular PHEOs/PGLs derived due to von Hippel-Lindau syndrome (*VHL*) or succinate dehydrogenase subunit B, C, and D (*SDHB/C/D*) mutation were shown to have a decreased activity in the oxidative phosphorylation as well as increased glycolytic activity (32, 132), (own unpublished observation), thus, are susceptible for a low extracellular pH. Despite these similarities, the metastatic potential of these types of PHEO/PGL is distinct: patients with *VHL* related PHEOs/PGLs almost never develop metastatic disease, while tumors due to *SDHB* mutation are at high risk to develop metastases. Recently we have shown an increased expression of ATP synthase β in *SDHB*- compared to *VHL*-derived primary tumors (own unpublished observation). Thus, we aimed to evaluate potential cell surface localization of ATP synthase in PHEOs/PGLs and its potential as a therapeutic target.

Currently, no human PHEO or PGL cell line exists, thus we evaluated the location of ATP synthase in mouse PHEO cells (MPC) as well as the more aggressive filial mouse tumor tissue (MTT) cells and cells from a human primary *SDHB*-derived retroperitoneal PGL via immuno-cytochemistry. Bovine primary chromaffin cells were used as negative control tissue. The results were validated in another human *SDHB*-derived primary PGL electron microscopically. Targeting of cell surface ATP synthase with resveratrol and an ATP synthase β antibody was attempted.

Cell surface ATP synthase may present a specific therapeutic target for the treatment of metastatic disease as well as in cases of inoperable PGLs.

4.2 Material and Methods

4.2.1 Ethics Statement

Tissue collection and genetic testing was performed with written patients consent under

a protocol approved by the Eunice Kennedy Shriver National Institutes of Child Health and Human Development institutional review board.

4.2.2 Human Samples

PHEO/PGL tissue was collected at the NIH and at Suburban hospital in Bethesda, MD. A summary of patient information is given in Table 1. Genetic testing was performed following established guidelines for testing (152) and consideration of biochemical phenotypes.

4.2.3 Cell Culture

Mouse PHEO cells (MPC 4/30PRR) were a generous gift from Dr. Tischler, TUFTS University, Boston. Their more aggressive filial MTT (mouse tumor tissue-derived) cells were generated and maintained as described by Martiniova et al. (151). Briefly, cells of liver tumors, established in nude mice after tail vein injection of MPC, were cultured and showed more aggressive behavior when re-injected than did their parental MPCs.

MPC and MTT cells were maintained at 5 % CO_2, 37°C in RPMI 1640 (Gibco, Grand Island, NY), supplemented with 10 % heat-inactivated horse serum (Hyclone Logan, UT), 5 % fetal bovine serum (Gibco), HEPES (Gibco), and penicillin (10,000 units/ml)/streptomycin (100,000 µg/ml) (Gibco). Medium was changed every other day and cells were passaged when 80-90 % confluence was reached.

4.2.4 Human Primary Paraganglioma Cells

Tissue was collected from a retroperitoneal PGL of a 15 year old male patient with *SDHB* germline mutation and placed in culture media. Central viable parts of tumor specimens were used for primary culture. Dissected tissues were washed three times in ice-cold PBS and minced into 1 mm^3 squares. Tissue was then dissociated in 0.025 % trypsin and DNase I at 37°C for 20 min. The digested fluid was passed through a 40 µm cell strainer to obtain a single cell suspension. Cells were seeded on poly-D-lysine coated chamber slides in a concentration of 5,000 cells/cm2. Cells were grown in DMEM supplemented with 10 % FBS for at least one week before consequent experiments.

4.2.5 Bovine Primary Chromaffin Cells

Bovine primary chromaffin cells were harvested and separated as previously described

(192). Cell identity was verified by immunocytochemical staining for tyrosine hydroxylase as described below.

4.2.6 Immunocytochemistry

Immunocytochemistry was performed in the same way for mouse MPC, MTT, bovine primary chromaffin cells and human primary *SDHB*-derived PGL cells.

Lab-Tek^{TM} II chamber slide (Nalge Nunc International, Rochester, NY, USA) surfaces were evenly covered with 0.1 mg/ml rat tail collagen type VII (Sigma-Aldrich) in cell culture grade H_2O with 0.01 % acetic acid. Chamber slides were allowed to air dry in a fume hood. When dry, 0.5 mill cells/ml (MPC and MTT) or 0.25 mill cells/ml (bovine primary chromaffin cells and primary *SDHB*-derived cells) were seeded in DMEM culture media supplemented as described above. Mitochondria were labeled during 15 min incubation with 500 nM MitoTracker® Red CM-H2XRos at 37°C (Invitrogen, Molecular Probes, Eugene OR, USA). After washing the cells in PBS, they were fixed in 4 % paraformaldehyde solution. Cells were permeabilized with methanol, pre-cooled to -20°C for 3 minutes. Cells were blocked in 10 % donkey serum (Jackson ImmunoResearch Laboratories, Inc., West Grove, PA, USA) for 1 h before incubation in a 1:1000 dilution of monoclonal anti ATP synthase β antibody (ab14730) from abcam (Cambridge, MA, USA) or sheep anti-tyrosine hydroxylase (Enzo Life Sciences, Plymouth Meeting, PA, USA) antibody for 4 h. The secondary antibodies were Alexa Fluor® 647 donkey anti-sheep and Alexa Fluor® 488 donkey anti-mouse (Invitrogen, Molecular Probes). The labeled cells were cover-slipped in a 0.12 M tris solution consisting of 30 % glycerol, 12 % Mowiol 4-88 (Calbiochem®, EMD Chemicals, Inc., Gibbstown, NJ, USA), 2.5 % 1,4-diazobicyclo-[2.2.2]-octane (DABCO) (Sigma-Aldrich), pH 6.8. Images were taken with a Zeiss 510 inverted microscope.

4.2.7 Immunoelectron Microscopy

Tissue of an *SDHB*-derived cardiac PGL of a male 53 years old patient with multiple tumors was selected for immunoelectron microscopy. A carotid body tumor invading the nasopharinx was removed 2 month previously, but there were no signs for metastatic disease. Tissue was cut from a paraffin block and labeled as previously described (193). The same ATP synthase β antibody was used as for immuno-cytochemistry (ab14730, abcam) at 1:500. Identity of the examined tissue as PGL was

confirmed by presence of secretory granules.

4.2.8 in vitro Drug Response

MPC and MTT cells were cultured at 1 mill cells/ml in collagen I coated 96 well plates (Biocoat, Becton Dickinson Labware, Bedford, MD) in DMEM media, supplemented as described above. After 24 h, media was exchanged to the respective drug solutions in pH 6.5 and pH 7.0 supplemented DMEM. Monoclonal anti-ATP synthase β antibody (Novus Biologicals, Littleton, CO, USA) and non-immune IgG: 50, 25, 10 μg/ml, oligomycin (Cell Signaling Technology, Dauvers, MA, USA): 10 μg/ml, resveratrol (Sigma-Aldrich Corp., St. Louis, MO, USA): 100, 50, 10, 5 μM.

Cell proliferation was measured with the CellTitre-Flour cell viability assay (Promega, Madison WI, USA) after 24 h for antibody and over 4 consecutive days (24, 48, 72, 96 h) for resveratrol with the cell proliferation kit II (XTT) (Roche Diagnostics Corporation, Indianapolis, IN USA) following manufacturer recommendations. Drug solutions were exchanged every 48 h.

Statistical significance was evaluated in Prism 4 (GraphPad Software Inc., La Yolla, CA, USA) with one-way ANOVA for different antibody and IgG solutions comparison to vehicle with Dunnett's multiple comparison post-hoc test for the different cell types. Differences between cell types were evaluated by one-way ANOVA and differeces between pH were evaluated with unpaired T-test for each cell type. To estimate significance of the effect of the different resveratrol solutions on the subsequent days of measurement two-way ANOVA with Bonferonni post-hoc test was used for each cell type and pH separately.

4.3 Results

Fluorescent labeling for ATP synthase β lead to a strong signal in the mitochondria of both, MPC and MTT cells as shown by overlapping red (mitotracker) and green (ATP synthase β antibody) which appears as a yellow signal. In addition, positive signal for ATP synthase β that was spatially unrelated to the mitochondria was detected (Figure 15). In non-permeabilized cells there was no overlap in staining of ATP-syntase beta and the mitochondria (Figure 15). In absence of primary antibody, no signal was detected in the green channel (Figure 15).

When examining bovine primary chomaffin cells with the same methods, we detected only minute amount of ATP synthase β signal that was not related to the mitochondria

(Figure 16). To assure chromaffin cell origin, cells from the same batch were labeled with anti-tyrosine hydroxylase antibody (Figure 16).

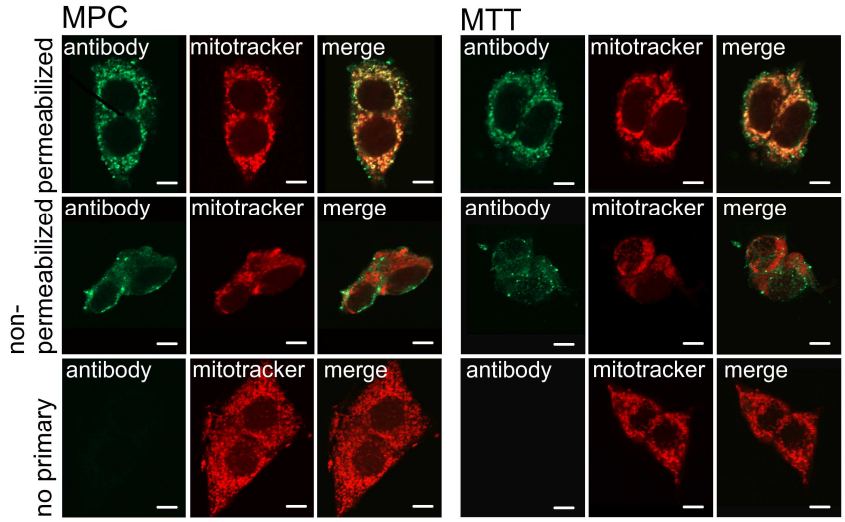

Figure 15: Separate confocal microscopy channels of MPC (left three columns) and MTT (right three columns) cells labeled with ATP synthase β antibody (AB, green signal, left) and mitotracker (MT, red signal, center) and overlap (right). Top panel shows results for permeabilized cells, center panel shows non-permeabilized cells and bottom panel shows negative control (no primary antibody). Both, MPC and MTT show strong positive staining for ATP synthase β that greatly, but not entirely overlaps with the mitochondria (top row). Signal for ATP synthase β on non-permeabilized cells does not overlap with mitochondrial staining, indicating cell surface location of ATP synthase β (second row). Application of secondary antibody only did not lead to any detectable signal (bottom row). Scale bar indicates 10 μm.

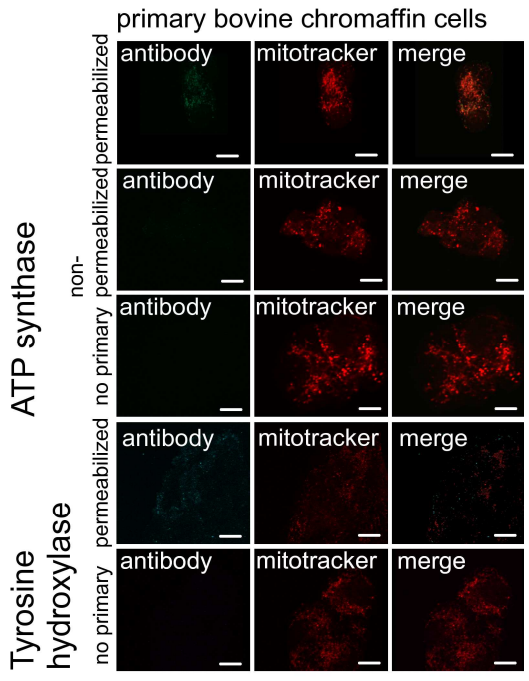

Figure 16: Confocal images of bovine primary chromaffin cells labeled with mouse anti-ATP synthase β antibody in permeabilized cells (top row), non-permeabilized cells (second row), and negative control (anti-mouse antibody only, third row). Merged channels for ATP synthase β and mitotracker show complete overlap in permeabilized cells (top row), while no signal for ATP synthase β was evident in non-permeabilized cells (second row) or the negative control (third row). Forth and Fifth row show labeling for sheep anti-TH and negative control (anti-sheep only), respectively. Positive staining for TH confirms chromaffin cell origin. Thus, cell surface localization of ATP synthase β was non-detectable in primary chromaffin cells. Scale bar indicates 10 μm.

In addition, primary cells of a human retroperitoneal *SDHB*-derived PGL were evaluated for cell surface localization of ATP synthase β. The cell surface signal of ATP synthase β in the non-permeabilized human primary PGL is not as pronounced as in the MPC and MTT cells, however stronger than in the bovine primary chromaffin cells (Figure 17A).

To support cell surface localization of ATP synthase in human PGL tissue, immuno-gold labeling of another *SDHB*-derived PGL was performed. As expected, transmission electron microscopy revealed presence of gold particles in the cytosol in vicinity to mitochondria. In addition, accumulation of gold particles at the plasmalemmal membrane was observed (B).

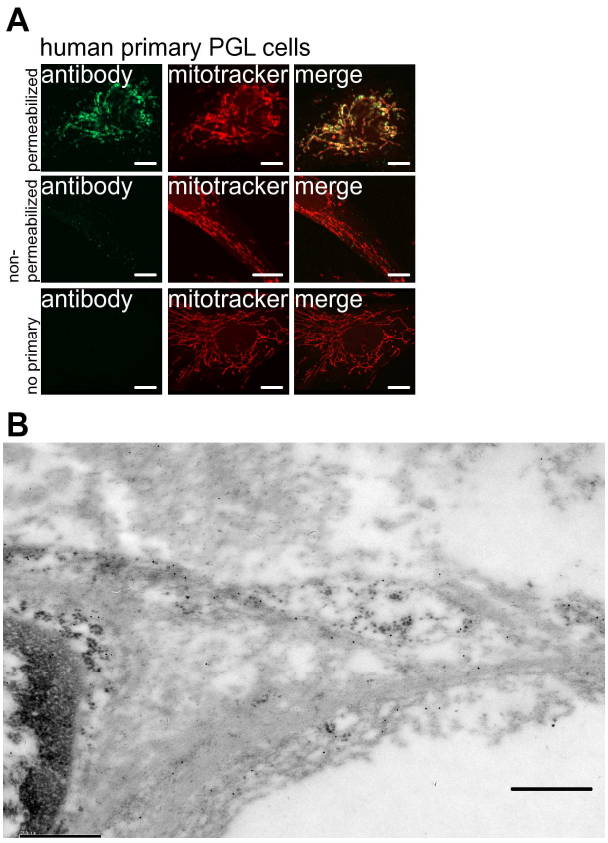

Figure 17: Cell surface ATP synthase in human PGL. **A** Confocal images of *SDHB*-derived primary PGL cells labeled with mouse anti-ATP synthase β antibody in permeabilized cells (top row), non-permeabilized cells (second row), and negative control (anti-mouse antibody only, third row). Merged channels for ATP synthase β and mitotracker show overlap in permeabilized cells. However, focal regions of ATP synthase β signal do not correspond to mitochondria (top row). Focal regions of positive ATP synthase β signal were also evident in non-permeabilized cells, while no overlap with the mitochondrial staining is evident (second row). Signal for the green channel was absent on the negative control (third row). Scale bar indicates 10 µm. **B** Electron microscopy image of an *SDHB*-derived PGL labelled for ATP synthase β with immuno-gold. Black dots indicate location of ATP synthase β within the cytosol and on the cell membrane. Scale bar indicated 500 nm.

The effect of treating MPC and MTT cells with an antibody against ATP synthase β in pH 7.0 and pH 6.5 media for 24 hours was determined fluorometrically. Cell proliferation in MPC and MTT cells was significantly decreased when treated with 50 µg/ml antibody (MPC pH 6.5 and pH 7.0: $p < 0.05$, MTT pH 6.5 and pH 7.0:

$p < 0.01$) (Figure 18). There was no difference in effect between the different pH media or cell types. Oligomycin has been used as a positive control and showed a slightly higher decrease in proliferation than the highest dose of ATP synthase antibody.

Next we evaluated the response of MPC and MTT cell proliferation to treatment with the ATP synthase inhibitor resveratrol (5 μM, 10 μM, 50 μM, 100 μM) in pH 7.0 and pH 6.5 media over 4 days. The relative cell number compared to vehicle (0.1 % ethanol in media) decreased with increasing dose and treatment duration (Figure 19). A concentration of 100 μM significantly decreased proliferation compared to media from day 2 on under all conditions (MPC: day 2, day 3 and day 4 $p < 0.001$ for both pH conditions; MTT: day 2 $p < 0.01$, day 3 and day 4 $p < 0.001$ for both pH conditions). Treatment with 50 μM resveratrol lead to significantly decreased cell proliferation for all tested conditions in MPC and MTT from day 3 on ($p < 0.01$). On day 4, MPC in pH 6.5 media also showed significantly decreased proliferation for 5 and 10 μM resveratrol ($p < 0.01$). MTT also showed a significant reaction to 5 μM resveratrol on day 4 under both pH conditions ($p < 0.01$). No difference between MPC and MTT cells was obvious. The efficacy of resveratrol was independent of different pH conditions (Figure 20).

4.4 Discussion

Within the past 15 years more and more evidence for an important role of ATP synthase dysregulation in cancer appeared. In several cancers up- or down-regulation of specific ATP synthase subunits has been shown (176, 182, 194-196), but in addition, its localization on the cell surface in tumor supporting endothelial cells (187) as well as on tumor cells themselves (197-200) were observed. However, some other normal cells/ tissues have been reported to carry ATP synthase on their surface (e.g. neurons/ brain, adipocytes/ fat, hepatocytes/ liver) (190). Nevertheless, targeting cell surface ATP synthase on tumor supporting endothelial cells and/or directly on tumor cells with angiostatin, ATP synthase antibodies, resveratrol, aurovertin, sangivamycin, and other drugs has been shown to be efficient in killing tumor cells (190).

Here we show, that ATP synthase β is present on the cell surface of PHEO/PGL cells in vitro on MPC and MTT cells and human primary PGL cells as well as tumor tissue of an *SDHB*-derived tumor, while virtually absent on bovine primary chromaffin cells. Bovine chromaffin cell origin was assured by positive labeling of tyrosin hydroxylase (Figure 15). Cell surface signal was intense for MPC and MTT cells, while appearing

punctate in the human primary PGL cells as has been observed in other human tumor cells (198).

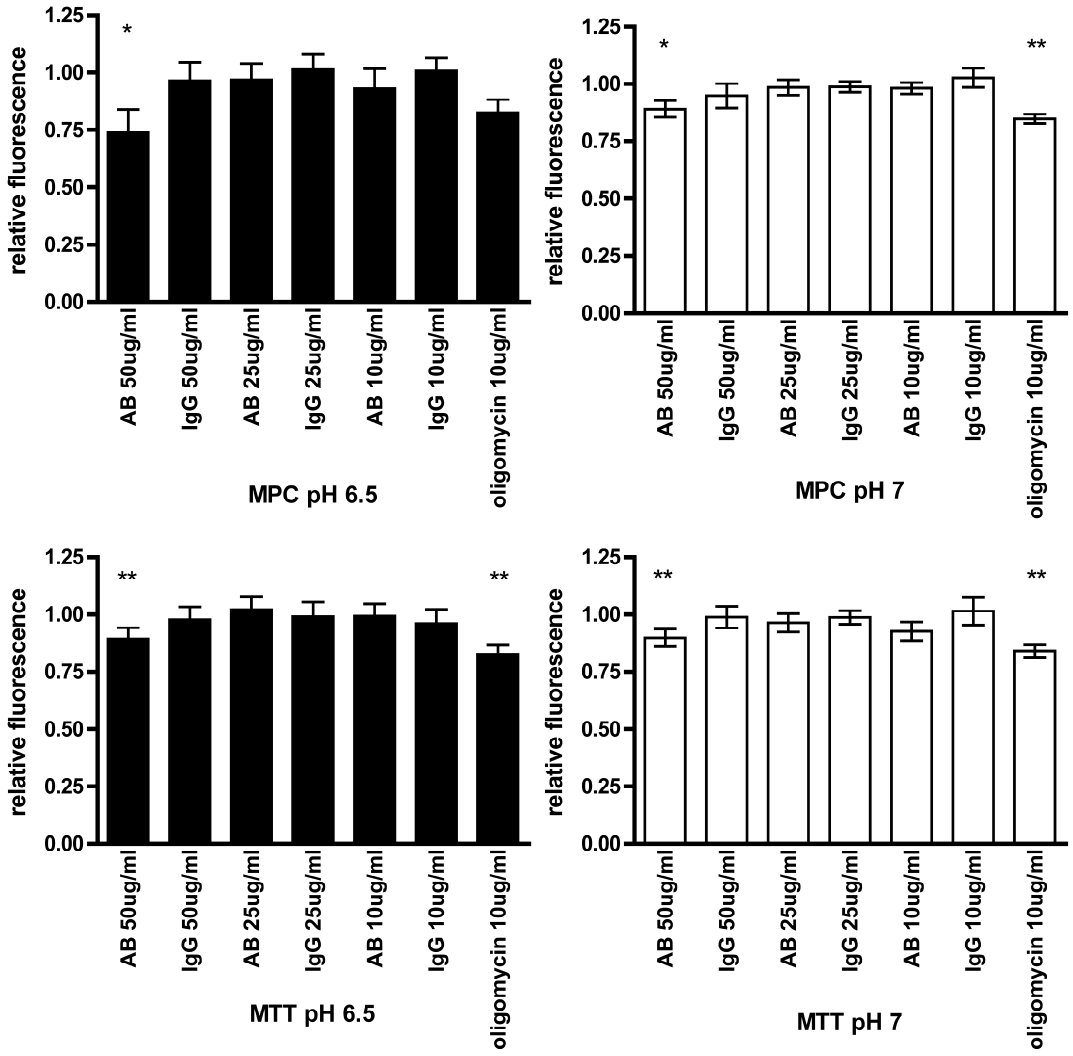

Figure 18: Fluorescence of MPC (top) and MTT (bottom) cells, treated for 24 h with indicated concentrations of anti ATP synthase antibody (AB), non-immun IgG and oligomycin, relative to vehicle in pH 6.5 (left) and pH 7.0 solution (right), detected with the Cell-titre fluor assay (Promega). Under all test conditions, 50 μg/ml AB inhibited proliferation with slightly less efficiency than oligomycin. *: $p < 0.05$, **: $p < 0.01$.

Assuming that presence of ATP synthase β on the surface of PHEO/PGL cells represents a functional ATP synthase complex as has been observed in other tumors (201, 202), we evaluated the effect of in vitro treatment of the mouse PHEO cells with an ATP synthase β antibody and resveratrol. ATP synthase antibody was effective in inhibiting proliferation at the highest applied concentration of 50 μg/ml by at least

10 % within 24 h of treatment. However, lower antibody concentrations and non-immune IgG had no effect on proliferation. It is unlikely that the applied antibody penetrates the cell membrane, so the effect is likely due to inhibition of the cell surface ATP synthase. Resveratrol dosed at 100 μM inhibited proliferation of MPC and MTT up to 75 % on the second day of treatment and 30 % on treatment day 4 compared to vehicle. A dose of 50 μM inhibited proliferation to about 75 % and 50 % on day 3 and 4, respectively (Figure 19). Resveratrol has been shown to have a cytostatic effect on cells carrying cell surface ATP synthase (203). In addition, resveratrol has been shown to target a wide variety of molecular pathways, exhibiting chemopreventive and chemotherapeutic effects in a variety of cell and animal models of cancer (for excellent recent reviews see (204-206)). Clinical trials showed that cancer preventive effects are promising while toxicity seems to be negligible (207-209). In models of neurodegerative diseases using PC12 or neuroblastoma cells, resveratrol was shown to be neuroprotective in attenuating damage by reactive oxygen species (210, 211).
However, neuroblastoma cell proliferation was also effectively inhibited by resveratrol (e.g. (212)). In addition, resveratrol showed to be cardioprotective (213) and improve longevity (214). Bauer and collaborators showed that at least 127 different pathways may be affected by resveratrol (215). Most described resveratrol targets are located inside the treated cells. For example, resveratrol was shown to interact with estrogen (216) and androgen (217) receptors and affect their expression as well as that of their target genes, suggesting a beneficial effect in breast and prostate cancer. Amongst effects on additional transcription factors, resveratrol was shown to decrease hypoxia inducible factor α levels and metastatic potential in colon carcinoma cells (218). However, to our knowledge currently there is no study presenting how the hydrophilic resveratrol may penetrate intact cell membranes to reach its intracellular targets. Thus, it's effects may be permeated by cell surface targets. Interaction of resveratrol with ATP synthase has been previously reported (219). Gledhill and colleagues reported that resveratrol binds to the α and β subinits of the complex, inhibiting ATPase as well as ATP-syntase activity (220, 221). Treatment of human umbilical vein cells that carry ATP synthase on the surface with resveratrol was shown to inhibit proliferation based on inhibited cell surface ATP synthesis (222). The possibility of resveratrol penetrating into the cells was rendered unlikely by the authors, since intracellular ATP levels were barely affected. Thus, the authors conclude that the efficacy of the drug was related to

its inhibition of cell surface ATP synthase. Thus, we assume that the detected ATP synthase β subunit on the cell surface represents a functional ATP synthase complex, that promotes PHEO/PGL survival. However, additional cell surface or intracellular targets for ATP synthase antibody and resveratrol cannot be ruled out.

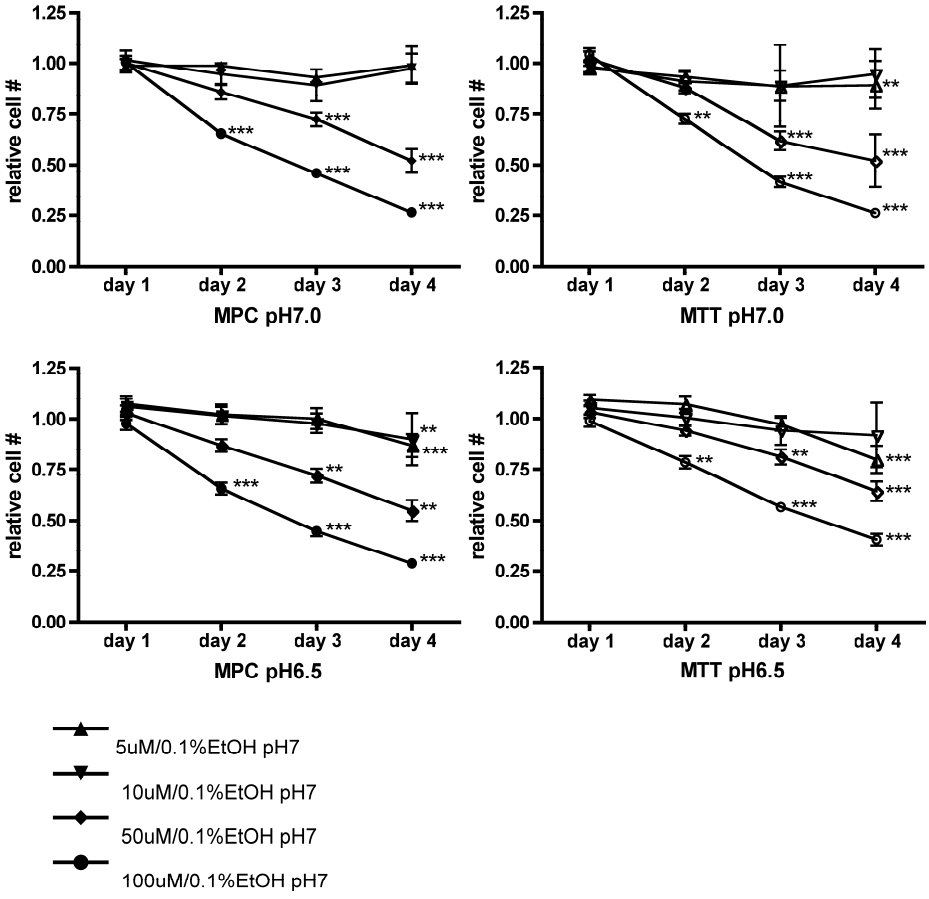

Figure 19: Signal of MPC (top) and MTT (bottom) cells treated with indicated concentrations of resveratrol in pH 6.5 (left) and pH 7.0 (right) for four consecutive days relative to vehicle, as assessed by MTT assay. Cell proliferation was inhibited by day two under all tested conditions with 100 μM resveratrol. 50 μM significantly decreased proliferation by day three. **: $p < 0.01$, ***: $p < 0.001$. Relative fluorescence compared to vehicle for indicated concentrations of resveratrol under different pH conditions. No difference between pH conditions is evident for neither cell type.

Previously, low extracellular pH as expected for glycolytic tumor cells has been shown to enhance toxicity of cell surface ATP synthase inhibition with angiostatin and ATP synthase antibodies (223). Thus, we applied the treatments in low pH media (pH 6.5) as well as neutral media (pH 7.0). However, we did not observe any pH related difference in effect of the treatments with neither ATP synthase β antibody nor resveratrol.

In the present study we show that ATP synthase is localized to the cell surface of

mouse and human PHEO/PGL cells. Targeting cell surface ATP synthase on MPC and MTT cells in vitro efficiently inhibited cell proliferation, indicating a functional ATP synthase complex on their surface. Thus, targeting cell surface ATP synthase may provide a promising new target in the treatment of metastatic and inoperable PHEO/PGL.

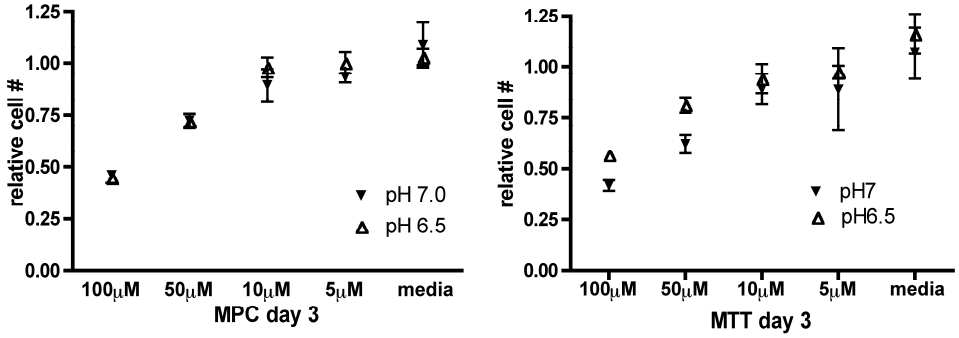

Figure 20: Relative fluorescence compared to vehicle for indicated concentrations of resveratrol under different pH conditions. No difference between pH conditions is evident for neither cell type

Bibliography

1. O'Riordain DS, William F. Young J, Grant CS, Carney JA, Heerden JAv 1996 Clinical Spectrum and Outcome of Functional Extraadrenal Paraganglioma. World Journal of Surgery 20:916-922

2. Opocher G, Schiavi F, Iacobone M, Toniato A, Sattarova S, Erlic Z, Martella M, Mian C, Merante Boschin I, Zambonin L, De Lazzari P, Murgia A, Pelizzo MR, Favia G, Mantero F 2006 Familial nonsyndromic pheochromocytoma. Ann N Y Acad Sci 1073:149-155

3. Bryant J, Farmer J, Kessler LJ, Townsend RR, Nathanson KL 2003 Pheochromocytoma: the expanding genetic differential diagnosis. J Natl Cancer Inst 95:1196-1204

4. Lenders JW, Eisenhofer G, Mannelli M, Pacak K 2005 Phaeochromocytoma. Lancet 366:665-675

5. Hao H-X, Khalimonchuk O, Schraders M, Dephoure N, Bayley J-P, Kunst H, Devilee P, Cremers CWRJ, Schiffman JD, Bentz BG, Gygi SP, Winge DR, Kremer H, Rutter J 2009 SDH5, a Gene Required for Flavination of Succinate Dehydrogenase, Is Mutated in Paraganglioma. Science 325:1139-1142

6. Bayley JP, Kunst HP, Cascon A, Sampietro ML, Gaal J, Korpershoek E, Hinojar-Gutierrez A, Timmers HJ, Hoefsloot LH, Hermsen MA, Suarez C, Hussain AK, Vriends AH, Hes FJ, Jansen JC, Tops CM, Corssmit EP, de Knijff P, Lenders JW, Cremers CW, Devilee P, Dinjens WN, de Krijger RR, Robledo M 2010 SDHAF2 mutations in familial and sporadic paraganglioma and phaeochromocytoma. Lancet Oncol 11:366-372

7. Qin Y, Yao L, King EE, Buddavarapu K, Lenci RE, Chocron ES, Lechleiter JD, Sass M, Aronin N, Schiavi F, Boaretto F, Opocher G, Toledo RA, Toledo SP, Stiles C, Aguiar RC, Dahia PL 2010 Germline mutations in TMEM127 confer susceptibility to pheochromocytoma. Nat Genet 42:229-233

8. Gaal J, Burnichon N, Korpershoek E, Roncelin I, Bertherat J, Plouin PF, de Krijger RR, Gimenez-Roqueplo AP, Dinjens WN 2010 Isocitrate dehydrogenase mutations are rare in pheochromocytomas and paragangliomas. J Clin Endocrinol Metab 95:1274-1278

9. Ladroue C, Carcenac R, Leporrier M, Gad S, Le Hello C, Galateau-Salle F, Feunteun J, Pouyssegur J, Richard S, Gardie B 2008 PHD2 mutation and congenital

erythrocytosis with paraganglioma. N Engl J Med 359:2685-2692

10. Amar L, Bertherat J, Baudin E, Ajzenberg C, Bressac-de Paillerets B, Chabre O, Chamontin B, Delemer B, Giraud S, Murat A, Niccoli-Sire P, Richard S, Rohmer V, Sadoul JL, Strompf L, Schlumberger M, Bertagna X, Plouin PF, Jeunemaitre X, Gimenez-Roqueplo AP 2005 Genetic testing in pheochromocytoma or functional paraganglioma. J Clin Oncol 23:8812-8818

11. Gimenez-Roqueplo AP, Lehnert H, Mannelli M, Neumann H, Opocher G, Maher ER, Plouin PF 2006 Phaeochromocytoma, new genes and screening strategies. Clin Endocrinol (Oxf) 65:699-705

12. Gimenez-Roqueplo AP, Favier J, Rustin P, Rieubland C, Crespin M, Nau V, Khau Van Kien P, Corvol P, Plouin PF, Jeunemaitre X 2003 Mutations in the SDHB gene are associated with extra-adrenal and/or malignant phaeochromocytomas. Cancer Res 63:5615-5621

13. Timmers HJ, Kozupa A, Eisenhofer G, Raygada M, Adams KT, Solis D, Lenders JW, Pacak K 2007 Clinical presentations, biochemical phenotypes, and genotype-phenotype correlations in patients with succinate dehydrogenase subunit B-associated pheochromocytomas and paragangliomas. J Clin Endocrinol Metab 92:779-786

14. Mannelli M, Castellano M, Schiavi F, Filetti S, Giacche M, Mori L, Pignataro V, Bernini G, Giache V, Bacca A, Biondi B, Corona G, Di Trapani G, Grossrubatscher E, Reimondo G, Arnaldi G, Giacchetti G, Veglio F, Loli P, Colao A, Ambrosio MR, Terzolo M, Letizia C, Ercolino T, Opocher G, Network tIPP 2009 Clinically Guided Genetic Screening in a Large Cohort of Italian Patients with Pheochromocytomas and/or Functional or Nonfunctional Paragangliomas. J Clin Endocrinol Metab 94:1541-1547

15. Boedeker CC, Neumann HP, Maier W, Bausch B, Schipper J, Ridder GJ 2007 Malignant head and neck paragangliomas in SDHB mutation carriers. Otolaryngol Head Neck Surg 137:126-129

16. Burnichon N, Rohmer V, Amar L, Herman P, Leboulleux S, Darrouzet V, Niccoli P, Gaillard D, Chabrier G, Chabolle F, Coupier I, Thieblot P, Lecomte P, Bertherat J, Wion-Barbot N, Murat A, Venisse A, Plouin PF, Jeunemaitre X, Gimenez-Roqueplo AP 2009 The succinate dehydrogenase genetic testing in a large prospective series of patients with paragangliomas. J Clin Endocrinol Metab 94:2817-2827

17. Brouwers FM, Eisenhofer G, Tao JJ, Kant JA, Adams KT, Linehan WM, Pacak

K 2006 High frequency of SDHB germline mutations in patients with malignant catecholamine-producing paragangliomas: implications for genetic testing. J Clin Endocrinol Metab 91:4505-4509

18. Yu J-P, K. 2002 Management of malignant pheochromocytoma. The Endocrinologist 12:291-299

19. Lehnert H, Mundschenk J, Hahn K 2004 Malignant pheochromocytoma. Front Horm Res 31:155-162

20. Havekes B, Romijn JA, Eisenhofer G, Adams K, Pacak K 2009 Update on pediatric pheochromocytoma. Pediatr Nephrol 24:943-950

21. Pham TH, Moir C, Thompson GB, Zarroug AE, Hamner CE, Farley D, van Heerden J, Lteif AN, Young WF, Jr. 2006 Pheochromocytoma and paraganglioma in children: a review of medical and surgical management at a tertiary care center. Pediatrics 118:1109-1117

22. Barotini M, Levin G, Sanso G 2006 Characteristics of Pheochromocytoma in a 4- to 20-Year-Old Population. Annals of the New York Academy of Sciences 1073:30-37

23. Neumann HP, Bausch B, McWhinney SR, Bender BU, Gimm O, Franke G, Schipper J, Klisch J, Altehoefer C, Zerres K, Januszewicz A, Eng C, Smith WM, Munk R, Manz T, Glaesker S, Apel TW, Treier M, Reineke M, Walz MK, Hoang-Vu C, Brauckhoff M, Klein-Franke A, Klose P, Schmidt H, Maier-Woelfle M, Peczkowska M, Szmigielski C, Eng C 2002 Germ-line mutations in nonsyndromic pheochromocytoma. N Engl J Med 346:1459-1466

24. Ciftci AO, Tanyel FC, Senocak ME, Buyukpamukcu N 2001 Pheochromocytoma in children. J Pediatr Surg 36:447-452

25. Hammond PJ, Murphy D, Carachi R, Davidson DF, McIntosh D 2010 Childhood phaeochromocytoma and paraganglioma: 100% incidence of genetic mutations and 100% survival. J Pediatr Surg 45:383-386

26. Ganesh HK, Acharya SV, Goerge J, Bandgar TR, Menon PS, Shah NS 2009 Pheochromocytoma in children and adolescents. Indian J Pediatr 76:1151-1153

27. Lee S, Nakamura E, Yang H, Wei W, Linggi MS, Sajan MP, Farese RV, Freeman RS, Carter BD, Kaelin WG, Jr., Schlisio S 2005 Neuronal apoptosis linked to EglN3 prolyl hydroxylase and familial pheochromocytoma genes: developmental culling and cancer. Cancer Cell 8:155-167

28. Pollard PJ, Briere JJ, Alam NA, Barwell J, Barclay E, Wortham NC, Hunt T,

Mitchell M, Olpin S, Moat SJ, Hargreaves IP, Heales SJ, Chung YL, Griffiths JR, Dalgleish A, McGrath JA, Gleeson MJ, Hodgson SV, Poulsom R, Rustin P, Tomlinson IP 2005 Accumulation of Krebs cycle intermediates and over-expression of HIF1alpha in tumours which result from germline FH and SDH mutations. Hum Mol Genet 14:2231-2239

29. Selak MA, Armour SM, MacKenzie ED, Boulahbel H, Watson DG, Mansfield KD, Pan Y, Simon MC, Thompson CB, Gottlieb E 2005 Succinate links TCA cycle dysfunction to oncogenesis by inhibiting HIF-alpha prolyl hydroxylase. Cancer Cell 7:77-85

30. Dahia PL, Hao K, Rogus J, Colin C, Pujana MA, Ross K, Magoffin D, Aronin N, Cascon A, Hayashida CY, Li C, Toledo SP, Stiles CD 2005 Novel pheochromocytoma susceptibility loci identified by integrative genomics. Cancer Res 65:9651-9658

31. Dahia PL, Ross KN, Wright ME, Hayashida CY, Santagata S, Barontini M, Kung AL, Sanso G, Powers JF, Tischler AS, Hodin R, Heitritter S, Moore F, Dluhy R, Sosa JA, Ocal IT, Benn DE, Marsh DJ, Robinson BG, Schneider K, Garber J, Arum SM, Korbonits M, Grossman A, Pigny P, Toledo SP, Nose V, Li C, Stiles CD 2005 A HIF1alpha regulatory loop links hypoxia and mitochondrial signals in pheochromocytomas. PLoS Genet 1:72-80

32. Favier J, Briere JJ, Burnichon N, Riviere J, Vescovo L, Benit P, Giscos-Douriez I, De Reynies A, Bertherat J, Badoual C, Tissier F, Amar L, Libe R, Plouin PF, Jeunemaitre X, Rustin P, Gimenez-Roqueplo AP 2009 The Warburg effect is genetically determined in inherited pheochromocytomas. PLoS One 4:e7094

33. Mack FA, Rathmell WK, Arsham AM, Gnarra J, Keith B, Simon MC 2003 Loss of pVHL is sufficient to cause HIF dysregulation in primary cells but does not promote tumor growth. Cancer Cell 3:75-88

34. Kondo K, Kim WY, Lechpammer M, Kaelin WG, Jr. 2003 Inhibition of HIF2alpha is sufficient to suppress pVHL-defective tumor growth. PLoS Biol 1:E83

35. Hoffman MA, Ohh M, Yang H, Klco JM, Ivan M, Kaelin WG, Jr 2001 von Hippel-Lindau protein mutants linked to type 2C VHL disease preserve the ability to downregulate HIF. Hum Mol Genet 10:1019-1027

36. Dahia PL 2006 Transcription association of VHL and SDH mutations link hypoxia and oxidoreductase signals in pheochromocytomas. Ann N Y Acad Sci 1073:208-220

37. Srirangalingam U, Khoo B, Walker L, MacDonald F, Skelly RH, George E, Spooner D, Johnston LB, Monson JP, Grossman AB, Drake WM, Akker SA, Pollard PJ, Plowman N, Avril N, Berney DM, Burrin JM, Reznek RH, Kumar VKA, Maher ER, Chew SL 2009 Contrasting clinical manifestations of SDHB and VHL associated chromaffin tumours. J Endocr Relat Cancer 16:515-525

38. Amar L, Baudin E, Burnichon N, Peyrard S, Silvera S, Bertherat J, Bertagna X, Schlumberger M, Jeunemaitre X, Gimenez-Roqueplo AP, Plouin PF 2007 Succinate dehydrogenase B gene mutations predict survival in patients with malignant pheochromocytomas or paragangliomas. J Clin Endocrinol Metab 92:3822-3828

39. Pollard PJ, El-Bahrawy M, Poulsom R, Elia G, Killick P, Kelly G, Hunt T, Jeffery R, Seedhar P, Barwell J, Latif F, Gleeson MJ, Hodgson SV, Stamp GW, Tomlinson IPM, Maher ER 2006 Expression of HIF-1{alpha}, HIF-2{alpha} (EPAS1), and Their Target Genes in Paraganglioma and Pheochromocytoma with VHL and SDH Mutations. J Clin Endocrinol Metab 91:4593-4598

40. Gimenez-Roqueplo AP, Favier J, Rustin P, Rieubland C, Kerlan V, Plouin PF, Rotig A, Jeunemaitre X 2002 Functional consequences of a SDHB gene mutation in an apparently sporadic pheochromocytoma. J Clin Endocrinol Metab 87:4771-4774

41. Ishii T, Yasuda K, Akatsuka A, Hino O, Hartman PS, Ishii N 2005 A mutation in the SDHC gene of complex II increases oxidative stress, resulting in apoptosis and tumorigenesis. Cancer Res 65:203-209

42. Ishii N, Ishii T, Hartman PS 2007 The role of the electron transport SDHC gene on lifespan and cancer. Mitochondrion 7:24-28

43. Smith EH, Janknecht R, Maher LJ, III 2007 Succinate inhibition of {alpha}-ketoglutarate-dependent enzymes in a yeast model of paraganglioma. Hum Mol Genet 16:3136-3148

44. Guzy RD, Sharma B, Bell E, Chandel NS, Schumacker PT 2008 Loss of the SdhB, but Not the SdhA, subunit of complex II triggers reactive oxygen species-dependent hypoxia-inducible factor activation and tumorigenesis. Mol Cell Biol 28:718-731

45. Cervera AM, Apostolova N, Crespo FL, Mata M, McCreath KJ 2008 Cells silenced for SDHB expression display characteristic features of the tumor phenotype. Cancer Res 68:4058-4067

46. Bornemann M, Hill SC, Kidd GS, 2nd 1986 Lactic acidosis in pheochromocytoma. Ann Intern Med 105:880-882

47. You MJ, Castrillon DH, Bastian BC, O'Hagan RC, Bosenberg MW, Parsons R, Chin L, DePinho RA 2002 Genetic analysis of Pten and Ink4a/Arf interactions in the suppression of tumorigenesis in mice. Proc Natl Acad Sci U S A 99:1455-1460

48. Kiss NB, Geli J, Lundberg F, Avci C, Velazquez-Fernandez D, Hashemi J, Weber G, Hoog A, Ekstrom TJ, Backdahl M, Larsson C 2008 Methylation of the p16INK4A promoter is associated with malignant behavior in abdominal extra-adrenal paragangliomas but not pheochromocytomas. Endocr Relat Cancer 15:609-621

49. Geli J, Kiss N, Karimi M, Lee JJ, Backdahl M, Ekstrom TJ, Larsson C 2008 Global and regional CpG methylation in pheochromocytomas and abdominal paragangliomas: association to malignant behavior. Clin Cancer Res 14:2551-2559

50. Pacak K, Lenders JW, Eisenhofer G 2007 Pheochromocytoma: diagnosis, localisation and treatment: Blackwell Publishing

51. Pacak K, Eisenhofer G, Ahlman H, Bornstein SR, Gimenez-Roqueplo AP, Grossman AB, Kimura N, Mannelli M, McNicol AM, Tischler AS 2007 Pheochromocytoma: recommendations for clinical practice from the First International Symposium. October 2005. Nat Clin Pract Endocrinol Metab 3:92-102

52. Eisenhofer G, Bornstein SR, Brouwers FM, Cheung NK, Dahia PL, de Krijger RR, Giordano TJ, Greene LA, Goldstein DS, Lehnert H, Manger WM, Maris JM, Neumann HP, Pacak K, Shulkin BL, Smith DI, Tischler AS, Young WF, Jr. 2004 Malignant pheochromocytoma: current status and initiatives for future progress. Endocr Relat Cancer 11:423-436

53. Carlsen E, Abdullah Z, Kazmi SM, Kousparos G 2009 Pheochromocytomas, PASS, and immunohistochemistry. Horm Metab Res 41:715-719

54. Elder EE, Xu D, Hoog A, Enberg U, Hou M, Pisa P, Gruber A, Larsson C, Backdahl M 2003 KI-67 AND hTERT expression can aid in the distinction between malignant and benign pheochromocytoma and paraganglioma. Mod Pathol 16:246-255

55. Tavangar SM, Shojaee A, Moradi Tabriz H, Haghpanah V, Larijani B, Heshmat R, Lashkari A, Azimi S 2010 Immunohistochemical expression of Ki67, c-erbB-2, and c-kit antigens in benign and malignant pheochromocytoma. Pathol Res Pract 206:305-309

56. Thompson LD 2002 Pheochromocytoma of the Adrenal gland Scaled Score (PASS) to separate benign from malignant neoplasms: a clinicopathologic and immunophenotypic study of 100 cases. Am J Surg Pathol 26:551-566

57. Wu D, Tischler AS, Lloyd RV, DeLellis RA, de Krijger R, van Nederveen F,

Nose V 2009 Observer variation in the application of the Pheochromocytoma of the Adrenal Gland Scaled Score. Am J Surg Pathol 33:599-608

58. van Nederveen FH, Gaal J, Favier J, Korpershoek E, Oldenburg RA, de Bruyn EM, Sleddens HF, Derkx P, Riviere J, Dannenberg H, Petri BJ, Komminoth P, Pacak K, Hop WC, Pollard PJ, Mannelli M, Bayley JP, Perren A, Niemann S, Verhofstad AA, de Bruine AP, Maher ER, Tissier F, Meatchi T, Badoual C, Bertherat J, Amar L, Alataki D, Van Marck E, Ferrau F, Francois J, de Herder WW, Peeters MP, van Linge A, Lenders JW, Gimenez-Roqueplo AP, de Krijger RR, Dinjens WN 2009 An immunohistochemical procedure to detect patients with paraganglioma and phaeochromocytoma with germline SDHB, SDHC, or SDHD gene mutations: a retrospective and prospective analysis. Lancet Oncol 10:764-771

59. Sadow PM, Rumilla KM, Erickson LA, Lloyd RV 2008 Stathmin Expression in Pheochromocytomas, Paragangliomas, and in other Endocrine Tumors. Endocrine Pathology Volume 19:97-103

60. Hayry V, Salmenkivi K, Arola J, Heikkila P, Haglund C, Sariola H 2009 High frequency of SNAIL-expressing cells confirms and predicts metastatic potential of phaeochromocytoma. Endocr Relat Cancer 16:1211-1218

61. Waldmann J, Slater EP, Langer P, Buchholz M, Ramaswamy A, Walz MK, Schmid KW, Feldmann G, Bartsch DK, Fendrich V 2009 Expression of the transcription factor snail and its target gene twist are associated with malignancy in pheochromocytomas. Ann Surg Oncol 16:1997-2005

62. Pacak K, Eisenhofer G 2007 An assessment of biochemical tests for the diagnosis of pheochromocytoma. Nat Clin Pract Endocrinol Metab 3:744-745

63. Lenders JW, Willemsen JJ, Eisenhofer G, Ross HA, Pacak K, Timmers HJ, Sweep CG 2007 Is supine rest necessary before blood sampling for plasma metanephrines? Clin Chem 53:352-354

64. Timmers HJ, Pacak K, Huynh TT, Abu-Asab M, Tsokos M, Merino MJ, Baysal BE, Adams KT, Eisenhofer G 2008 Biochemically silent abdominal paragangliomas in patients with mutations in the succinate dehydrogenase subunit B gene. J Clin Endocrinol Metab 93:4826-4832

65. Eisenhofer G, Goldstein DS, Sullivan P, Csako G, Brouwers FM, Lai EW, Adams KT, Pacak K 2005 Biochemical and clinical manifestations of dopamine-producing paragangliomas: utility of plasma methoxytyramine. J Clin Endocrinol Metab 90:2068-2075

66. van Duinen N, Steenvoorden D, Kema IP, Jansen JC, Vriends AH, Bayley JP, Smit JW, Romijn JA, Corssmit EP 2010 Increased urinary excretion of 3-methoxytyramine in patients with head and neck paragangliomas. J Clin Endocrinol Metab 95:209-214

67. Timmers HJ, Hadi M, Carrasquillo JA, Chen CC, Martiniova L, Whatley M, Ling A, Eisenhofer G, Adams KT, Pacak K 2007 The effects of carbidopa on uptake of 6-18F-Fluoro-L-DOPA in PET of pheochromocytoma and extraadrenal abdominal paraganglioma. J Nucl Med 48:1599-1606

68. Havekes B, King K, Lai EW, Romijn JA, Corssmit EP, Pacak K 2010 New imaging approaches to phaeochromocytomas and paragangliomas. Clin Endocrinol (Oxf) 72:137-145

69. Krenning EP, Kwekkeboom DJ, Pawels S, Kvols LK, Reubi JC 1995 Somatostatin receptor scintigraphy. In: Freeman LM ed. Nuclear Medicine Annual 1995. New York: Raven Press; 242-244

70. Cleary S, Brouwers FM, Eisenhofer G, Pacak K, Christie DL, Lipski J, McNeil AR, Phillips JK 2005 Expression of the noradrenaline transporter and phenylethanolamine N-methyltransferase in normal human adrenal gland and phaeochromocytoma. Cell Tissue Res 322:443-453

71. Eisenhofer G 2001 The role of neuronal and extraneuronal plasma membrane transporters in the inactivation of peripheral catecholamines. Pharmacol Ther 91:35-62

72. Epelbaum J, Bertherat J, Prevost G, Kordon C, Meyerhof W, Wulfsen I, Richter D, Plouin PF 1995 Molecular and pharmacological characterization of somatostatin receptor subtypes in adrenal, extraadrenal, and malignant pheochromocytomas. J Clin Endocrinol Metab 80:1837-1844

73. Reubi JC, Waser B, Khosla S, Kvols L, Goellner JR, Krenning E, Lamberts S 1992 In vitro and in vivo detection of somatostatin receptors in pheochromocytomas and paragangliomas. J Clin Endocrinol Metab 74:1082-1089

74. Timmers HJ, Kozupa A, Chen CC, Carrasquillo JA, Ling A, Eisenhofer G, Adams KT, Solis D, Lenders JW, Pacak K 2007 Superiority of fluorodeoxyglucose positron emission tomography to other functional imaging techniques in the evaluation of metastatic SDHB-associated pheochromocytoma and paraganglioma. J Clin Oncol 25:2262-2269

75. Timmers HJ, Chen CC, Carrasquillo JA, Whatley M, Ling A, Havekes B, Eisenhofer G, Martiniova L, Adams KT, Pacak K 2009 Comparison of 18F-fluoro-L-

DOPA, 18F-fluoro-deoxyglucose, and 18F-fluorodopamine PET and 123I-MIBG scintigraphy in the localization of pheochromocytoma and paraganglioma. J Clin Endocrinol Metab 94:4757-4767

76. Zelinka T, Timmers HJ, Kozupa A, Chen CC, Carrasquillo JA, Reynolds JC, Ling A, Eisenhofer G, Lazurova I, Adams KT, Whatley MA, Widimsky J, Jr., Pacak K 2008 Role of positron emission tomography and bone scintigraphy in the evaluation of bone involvement in metastatic pheochromocytoma and paraganglioma: specific implications for succinate dehydrogenase enzyme subunit B gene mutations. Endocr Relat Cancer 15:311-323

77. Ilias I, Yu J, Carrasquillo JA, Chen CC, Eisenhofer G, Whatley M, McElroy B, Pacak K 2003 Superiority of 6-[18F]-fluorodopamine positron emission tomography versus [131I]-metaiodobenzylguanidine scintigraphy in the localization of metastatic pheochromocytoma. J Clin Endocrinol Metab 88:4083-4087

78. Zografos GN, Vasiliadis G, Farfaras AN, Aggeli C, Digalakis M 2009 Laparoscopic surgery for malignant adrenal tumors. JSLS 13:196-202

79. Pacak K 2007 Preoperative management of the pheochromocytoma patient. J Clin Endocrinol Metab 92:4069-4079

80. Pacak K, Fojo T, Goldstein DS, Eisenhofer G, Walther MM, Linehan WM, Bachenheimer L, Abraham J, Wood BJ 2001 Radiofrequency ablation: a novel approach for treatment of metastatic pheochromocytoma. J Natl Cancer Inst 93:648-649

81. Venkatesan AM, Locklin J, Lai EW, Adams KT, Fojo AT, Pacak K, Wood BJ 2009 Radiofrequency ablation of metastatic pheochromocytoma. J Vasc Interv Radiol 20:1483-1490

82. Cozzi PJ, Englund R, Morris DL 1995 Cryotherapy treatment of patients with hepatic metastases from neuroendocrine tumors. Cancer 76:501-509

83. Keiser HR, Goldstein DS, Wade JL, Douglas FL, Averbuch SD 1985 Treatment of malignant pheochromocytoma with combination chemotherapy. Hypertension 7:I18-24

84. Nomura K, Kimura H, Shimizu S, Kodama H, Okamoto T, Obara T, Takano K 2009 Survival of patients with metastatic malignant pheochromocytoma and efficacy of combined cyclophosphamide, vincristine, and dacarbazine chemotherapy. J Clin Endocrinol Metab 94:2850-2856

85. He J, Makey D, Fojo T, Adams KT, Havekes B, Eisenhofer G, Sullivan P, Lai

EW, Pacak K 2009 Successful chemotherapy of hepatic metastases in a case of succinate dehydrogenase subunit B-related paraganglioma. Endocrine 36:189-193

86. Huang H Fau - Abraham J, Abraham J Fau - Hung E, Hung E Fau - Averbuch S, Averbuch S Fau - Merino M, Merino M Fau - Steinberg SM, Steinberg Sm Fau - Pacak K, Pacak K Fau - Fojo T, Fojo T Treatment of malignant pheochromocytoma/paraganglioma with cyclophosphamide, vincristine, and dacarbazine: recommendation from a 22-year follow-up of 18 patients.

87. Bravo EL, Kalmadi SR, Gill I 2009 Clinical utility of temozolomide in the treatment of malignant paraganglioma: a preliminary report. Horm Metab Res 41:703-706

88. Kulke MH, Stuart K, Enzinger PC, Ryan DP, Clark JW, Muzikansky A, Vincitore M, Michelini A, Fuchs CS 2006 Phase II study of temozolomide and thalidomide in patients with metastatic neuroendocrine tumors. J Clin Oncol 24:401-406

89. Loh KC, Fitzgerald PA, Matthay KK, Yeo PP, Price DC 1997 The treatment of malignant pheochromocytoma with iodine-131 metaiodobenzylguanidine (131I-MIBG): a comprehensive review of 116 reported patients. J Endocrinol Invest 20:648-658

90. Safford SD, Coleman RE, Gockerman JP, Moore J, Feldman JM, Leight GS, Jr., Tyler DS, Olson JA, Jr. 2003 Iodine -131 metaiodobenzylguanidine is an effective treatment for malignant pheochromocytoma and paraganglioma. Surgery 134:956-962; discussion 962-953

91. Gonias S, Goldsby R, Matthay KK, Hawkins R, Price D, Huberty J, Damon L, Linker C, Sznewajs A, Shiboski S, Fitzgerald P 2009 Phase II study of high-dose [131I]metaiodobenzylguanidine therapy for patients with metastatic pheochromocytoma and paraganglioma. J Clin Oncol 27:4162-4168

92. Gedik GK, Hoefnagel CA, Bais E, Olmos RA 2008 131I-MIBG therapy in metastatic phaeochromocytoma and paraganglioma. Eur J Nucl Med Mol Imaging 35:725-733

93. Shilkrut M, Bar-Deroma R, Bar-Sela G, Berniger A, Kuten A 2010 Low-dose iodine-131 metaiodobenzylguanidine therapy for patients with malignant pheochromocytoma and paraganglioma: single center experience. Am J Clin Oncol 33:79-82

94. Coleman RE, Stubbs JB, Barrett JA, de la Guardia M, Lafrance N, Babich JW

2009 Radiation dosimetry, pharmacokinetics, and safety of ultratrace Iobenguane I-131 in patients with malignant pheochromocytoma/paraganglioma or metastatic carcinoid. Cancer Biother Radiopharm 24:469-475

95. Lamarre-Cliche M, Gimenez-Roqueplo AP, Billaud E, Baudin E, Luton JP, Plouin PF 2002 Effects of slow-release octreotide on urinary metanephrine excretion and plasma chromogranin A and catecholamine levels in patients with malignant or recurrent phaeochromocytoma. Clin Endocrinol (Oxf) 57:629-634

96. Mundschenk J, Unger N, Schulz S, Hollt V, Steinke R, Lehnert H 2003 Somatostatin receptor subtypes in human pheochromocytoma: subcellular expression pattern and functional relevance for octreotide scintigraphy. J Clin Endocrinol Metab 88:5150-5157

97. Druce MR, Kaltsas GA, Fraenkel M, Gross DJ, Grossman AB 2009 Novel and evolving therapies in the treatment of malignant phaeochromocytoma: experience with the mTOR inhibitor everolimus (RAD001). Horm Metab Res 41:697-702

98. Chrisoulidou A, Kaltsas G, Ilias I, Grossman AB 2007 The diagnosis and management of malignant phaeochromocytoma and paraganglioma. Endocr Relat Cancer 14:569-585

99. Joshua AM, Ezzat S, Asa SL, Evans A, Broom R, Freeman M, Knox JJ 2009 Rationale and evidence for sunitinib in the treatment of malignant paraganglioma/pheochromocytoma. J Clin Endocrinol Metab 94:5-9

100. Jimenez C, Cabanillas ME, Santarpia L, Jonasch E, Kyle KL, Lano EA, Matin SF, Nunez RF, Perrier ND, Phan A, Rich TA, Shah B, Williams MD, Waguespack SG 2009 Use of the tyrosine kinase inhibitor sunitinib in a patient with von Hippel-Lindau disease: targeting angiogenic factors in pheochromocytoma and other von Hippel-Lindau disease-related tumors. J Clin Endocrinol Metab 94:386-391

101. Park K-S, Lee J-L, Ahn H, Koh J-M, Park I, Choi J-S, Kim YR, Park TS, Ahn J-H, Lee DH, Kim TW, Lee JS 2009 Sunitinib, a Novel Therapy for Anthracycline- and Cisplatin-refractory Malignant Pheochromocytoma. Jpn J Clin Oncol 39:327-331

102. Gross DJ, Munter G, Bitan M, Siegal T, Gabizon A, Weitzen R, Merimsky O, Ackerstein A, Salmon A, Sella A, Slavin S 2006 The role of imatinib mesylate (Glivec) for treatment of patients with malignant endocrine tumors positive for c-kit or PDGF-R. Endocr Relat Cancer 13:535-540

103. Lai EW, Joshi BH, Martiniova L, Dogra R, Fujisawa T, Leland P, de Krijger RR, Lubensky IA, Elkahloun AG, Morris JC, Puri RK, Pacak K 2009 Overexpression

of interleukin-13 receptor-alpha2 in neuroendocrine malignant pheochromocytoma: a novel target for receptor directed anti-cancer therapy. J Clin Endocrinol Metab 94:2952-2957

104. Joshi BH, Hogaboam C, Dover P, Husain SR, Puri RK 2006 Role of interleukin-13 in cancer, pulmonary fibrosis, and other T(H)2-type diseases. Vitam Horm 74:479-504

105. Fitzgerald PA, Goldsby RE, Huberty JP, Price DC, Hawkins RA, Veatch JJ, Dela Cruz F, Jahan TM, Linker CA, Damon L, Matthay KK 2006 Malignant pheochromocytomas and paragangliomas: a phase II study of therapy with high-dose 131I-metaiodobenzylguanidine (131I-MIBG). Ann N Y Acad Sci 1073:465-490

106. Metzger J, Schanstra JP, Mischak H 2009 Capillary electrophoresis-mass spectrometry in urinary proteome analysis: current applications and future developments. Anal Bioanal Chem 393:1431-1442

107. Decramer S, Gonzalez de Peredo A, Breuil B, Mischak H, Monsarrat B, Bascands JL, Schanstra JP 2008 Urine in clinical proteomics. Mol Cell Proteomics 7:1850-1862

108. Mischak H, Coon JJ, Novak J, Weissinger EM, Schanstra JP, Dominiczak AF 2009 Capillary electrophoresis-mass spectrometry as a powerful tool in biomarker discovery and clinical diagnosis: an update of recent developments. Mass Spectrom Rev 28:703-724

109. Haubitz M, Good DM, Woywodt A, Haller H, Rupprecht H, Theodorescu D, Dakna M, Coon JJ, Mischak H 2009 Identification and validation of urinary biomarkers for differential diagnosis and evaluation of therapeutic intervention in anti-neutrophil cytoplasmic antibody-associated vasculitis. Mol Cell Proteomics 8:2296-2307

110. Neuhoff N, Kaiser T, Wittke S, Krebs R, Pitt A, Burchard A, Sundmacher A, Schlegelberger B, Kolch W, Mischak H 2004 Mass spectrometry for the detection of differentially expressed proteins: a comparison of surface-enhanced laser desorption/ionization and capillary electrophoresis/mass spectrometry. Rapid Commun Mass Spectrom 18:149-156

111. Jantos-Siwy J, Schiffer E, Brand K, Schumann G, Rossing K, Delles C, Mischak H, Metzger J 2009 Quantitative urinary proteome analysis for biomarker evaluation in chronic kidney disease. J Proteome Res 8:268-281

112. Coon JJ, Zurbig P, Dakna M, Dominiczak AF, Decramer S, Fliser D, Frommberger M, Golovko I, Good DM, Herget-Rosenthal S, Jankowski J, Julian BA,

Kellmann M, Kolch W, Massy Z, Novak J, Rossing K, Schanstra JP, Schiffer E, Theodorescu D, Vanholder R, Weissinger EM, Mischak H, Schmitt-Kopplin P 2008 CE-MS analysis of the human urinary proteome for biomarker discovery and disease diagnostics. Proteomics Clin Appl 2:964

113. Good DM, Zurbig P, Argiles A, Bauer HW, Behrens G, Coon JJ, Dakna M, Decramer S, Delles C, Dominiczak AF, Ehrich JH, Eitner F, Fliser D, Frommberger M, Ganser A, Girolami MA, Golovko I, Gwinner W, Haubitz M, Herget-Rosenthal S, Jankowski J, Jahn H, Jerums G, Julian BA, Kellmann M, Kliem V, Kolch W, Krolewski AS, Luppi M, Massy Z, Melter M, Neususs C, Novak J, Peter K, Rossing K, Rupprecht H, Schanstra JP, Schiffer E, Stolzenburg JU, Tarnow L, Theodorescu D, Thongboonkerd V, Vanholder R, Weissinger EM, Mischak H, Schmitt-Kopplin P 2010 Naturally occurring human urinary peptides for use in diagnosis of chronic kidney disease. Mol Cell Proteomics 9:2424-2437

114. Hastie T, Tibshirani, R., Friedman, J. 2009 The Elements of Statistical Learning: Data Mining, Inference, and Prediction (2nd ed.). New York: Springer

115. Opgen-Rhein R, Strimmer K 2007 Accurate ranking of differentially expressed genes by a distribution-free shrinkage approach. Stat Appl Genet Mol Biol 6:Article9

116. Lachenbruch PA 2002 Analysis of data with excess zeros. Stat Methods Med Res 11:297-302

117. Tibshirani R, Hastie T, Narasimhan B, Chu G 2002 Diagnosis of multiple cancer types by shrunken centroids of gene expression. Proc Natl Acad Sci U S A 99:6567-6572

118. Liotta LA 1984 Tumor invasion and metastases: role of the basement membrane. Warner-Lambert Parke-Davis Award lecture. Am J Pathol 117:339-348

119. Friedl P, Wolf K 2009 Proteolytic interstitial cell migration: a five-step process. Cancer Metastasis Rev 28:129-135

120. Hirai K, Shimada H, Ogawa T, Taji S 1991 The spread of human lung cancer cells on collagens and its inhibition by type III collagen. Clin Exp Metastasis 9:517-527

121. D'Ardenne AJ, Burns J, Sykes BC, Bennett MK 1983 Fibronectin and type III collagen in epithelial neoplasms of gastrointestinal tract and salivary gland. J Clin Pathol 36:756-763

122. Ryschich E, Khamidjanov A, Kerkadze V, Buchler MW, Zoller M, Schmidt J 2009 Promotion of tumor cell migration by extracellular matrix proteins in human pancreatic cancer. Pancreas 38:804-810

123. Kauppila S, Stenback F, Risteli J, Jukkola A, Risteli L 1998 Aberrant type I and type III collagen gene expression in human breast cancer in vivo. J Pathol 186:262-268

124. Wiklund TA, Elomaa I, Blomqvist CP, Risteli L, Risteli J 1992 Type III collagen metabolism in soft tissue sarcomas. Br J Cancer 65:193-196

125. Rudnicki M, Jensen LT, Iversen P 1995 Collagen derived serum markers in carcinoma of the prostate. Scand J Urol Nephrol 29:317-321

126. Plebani M, Basso D, Roveroni G, De Paoli M, Galeotti F, Corsini A 1997 N-terminal peptide of type III procollagen: a possible predictor of colorectal carcinoma recurrence. Cancer 79:1299-1303

127. Yudoh K, Matsui H, Kanamori M, Ohmori K, Tsuji H, Tatezaki S 1994 Serum levels of laminin, type IV collagen and type III procollagen peptide as markers for detection of metastasis. Jpn J Cancer Res 85:1263-1269

128. Narita T, Funahashi H, Satoh Y, Takagi H 1993 Procollagen type III N-peptide and type IV collagen 7S-domain in the sera of breast cancer patients. Surg Today 23:682-686

129. Cracchiolo BM, Hanauske-Abel HM, Schwartz PE, Chambers JT, Holland B, Chambers SK 2002 Procollagen-derived biomarkers in malignant ascites of ovarian cancer. Independent prognosticators for progression-free interval and survival. Gynecol Oncol 87:24-33

130. Duval E, Leclercq S, Elissalde JM, Demoor M, Galera P, Boumediene K 2009 Hypoxia-inducible factor 1alpha inhibits the fibroblast-like markers type I and type III collagen during hypoxia-induced chondrocyte redifferentiation: hypoxia not only induces type II collagen and aggrecan, but it also inhibits type I and type III collagen in the hypoxia-inducible factor 1alpha-dependent redifferentiation of chondrocytes. Arthritis Rheum 60:3038-3048

131. Choi HJ, Eun JS, Kim BG, Kim SY, Jeon H, Soh Y 2006 Vitexin, an HIF-1alpha inhibitor, has anti-metastatic potential in PC12 cells. Mol Cells 22:291-299

132. Lopez-Jimenez E, Gomez-Lopez G, Leandro-Garcia LJ, Munoz I, Schiavi F, Montero-Conde C, de Cubas AA, Ramires R, Landa I, Leskela S, Maliszewska A, Inglada-Perez L, de la Vega L, Rodriguez-Antona C, Leton R, Bernal C, de Campos JM, Diez-Tascon C, Fraga MF, Boullosa C, Pisano DG, Opocher G, Robledo M, Cascon A 2010 Research Resource: Transcriptional Profiling Reveals Different Pseudohypoxic Signatures in SDHB and VHL-Related Pheochromocytomas. Mol Endocrinol

133. Ingber DE, Madri JA, Folkman J 1987 Endothelial growth factors and extracellular matrix regulate DNA synthesis through modulation of cell and nuclear expansion. In Vitro Cell Dev Biol 23:387-394

134. Hsu PP, Sabatini DM 2008 Cancer cell metabolism: Warburg and beyond. Cell 134:703-707

135. Gatenby RA, Gillies RJ 2008 A microenvironmental model of carcinogenesis. Nat Rev Cancer 8:56-61

136. Vazquez A, Liu J, Zhou Y, Oltvai ZN 2010 Catabolic efficiency of aerobic glycolysis: The Warburg effect revisited. BMC Syst Biol 4:58

137. Ralph SJ, Rodriguez-Enriquez S, Neuzil J, Saavedra E, Moreno-Sanchez R 2010 The causes of cancer revisited: "mitochondrial malignancy" and ROS-induced oncogenic transformation - why mitochondria are targets for cancer therapy. Mol Aspects Med 31:145-170

138. Baysal BE 2008 Clinical and molecular progress in hereditary paraganglioma. J Med Genet 45:689-694

139. Sudarshan S, Sourbier C, Kong HS, Block K, Valera Romero VA, Yang Y, Galindo C, Mollapour M, Scroggins B, Goode N, Lee MJ, Gourlay CW, Trepel J, Linehan WM, Neckers L 2009 Fumarate hydratase deficiency in renal cancer induces glycolytic addiction and hypoxia-inducible transcription factor 1alpha stabilization by glucose-dependent generation of reactive oxygen species. Mol Cell Biol 29:4080-4090

140. Maxwell PH, Wiesener MS, Chang GW, Clifford SC, Vaux EC, Cockman ME, Wykoff CC, Pugh CW, Maher ER, Ratcliffe PJ 1999 The tumour suppressor protein VHL targets hypoxia-inducible factors for oxygen-dependent proteolysis. Nature 399:271-275

141. Jung SN, Yang WK, Kim J, Kim HS, Kim EJ, Yun H, Park H, Kim SS, Choe W, Kang I, Ha J 2008 Reactive oxygen species stabilize hypoxia-inducible factor-1 alpha protein and stimulate transcriptional activity via AMP-activated protein kinase in DU145 human prostate cancer cells. Carcinogenesis 29:713-721

142. Qing G, Simon MC 2009 Hypoxia inducible factor-2alpha: a critical mediator of aggressive tumor phenotypes. Curr Opin Genet Dev 19:60-66

143. Baysal BE, Ferrell RE, Willett-Brozick JE, Lawrence EC, Myssiorek D, Bosch A, van der Mey A, Taschner PE, Rubinstein WS, Myers EN, Richard CW, 3rd, Cornelisse CJ, Devilee P, Devlin B 2000 Mutations in SDHD, a mitochondrial complex II gene, in hereditary paraganglioma. Science 287:848-851

144. Niemann S, Muller U 2000 Mutations in SDHC cause autosomal dominant paraganglioma, type 3. Nat Genet 26:268-270

145. Astuti D, Latif F, Dallol A, Dahia PL, Douglas F, George E, Skoldberg F, Husebye ES, Eng C, Maher ER 2001 Gene mutations in the succinate dehydrogenase subunit SDHB cause susceptibility to familial pheochromocytoma and to familial paraganglioma. Am J Hum Genet 69:49-54

146. Burnichon N, Briere JJ, Libe R, Vescovo L, Riviere J, Tissier F, Jouanno E, Jeunemaitre X, Benit P, Tzagoloff A, Rustin P, Bertherat J, Favier J, Gimenez-Roqueplo AP 2010 SDHA is a tumor suppressor gene causing paraganglioma. Hum Mol Genet 19:3011-3020

147. Gimenez-Roqueplo AP, Favier J, Rustin P, Mourad JJ, Plouin PF, Corvol P, Rotig A, Jeunemaitre X 2001 The R22X mutation of the SDHD gene in hereditary paraganglioma abolishes the enzymatic activity of complex II in the mitochondrial respiratory chain and activates the hypoxia pathway. Am J Hum Genet 69:1186-1197

148. Douwes Dekker PBH, P.C.W.; Kuipers-Dijkshoorn, N.; Prins, F.A.; van Duinen, S.G.; Taschner, P.E.M.; van der Mey, A. G. L.; Cornelisse, C. J. 2003 *SDHD* mutations in head and neck paragangliomas result in destabilization of complex II in the mitochondrial respiratory chain with loss of enzymatic activity and abnormal mitochondrial morphology. The Journal of Pathology 201:480-486

149. Neumann HP, Pawlu C, Peczkowska M, Bausch B, McWhinney SR, Muresan M, Buchta M, Franke G, Klisch J, Bley TA, Hoegerle S, Boedeker CC, Opocher G, Schipper J, Januszewicz A, Eng C 2004 Distinct clinical features of paraganglioma syndromes associated with SDHB and SDHD gene mutations. Jama 292:943-951

150. Powers JF, Evinger MJ, Zhi J, Picard KL, Tischler AS 2007 Pheochromocytomas in Nf1 knockout mice express a neural progenitor gene expression profile. Neuroscience 147:928-937

151. Martiniova L, Lai EW, Elkahloun AG, Abu-Asab M, Wickremasinghe A, Solis DC, Perera SM, Huynh TT, Lubensky IA, Tischler AS, Kvetnansky R, Alesci S, Morris JC, Pacak K 2009 Characterization of an animal model of aggressive metastatic pheochromocytoma linked to a specific gene signature. Clin Exp Metastasis 26:239-250

152. Erlic Z, Rybicki L, Peczkowska M, Golcher H, Kann PH, Brauckhoff M, Mussig K, Muresan M, Schaffler A, Reisch N, Schott M, Fassnacht M, Opocher G, Klose S, Fottner C, Forrer F, Plockinger U, Petersenn S, Zabolotny D, Kollukch O,

Yaremchuk S, Januszewicz A, Walz MK, Eng C, Neumann HP 2009 Clinical predictors and algorithm for the genetic diagnosis of pheochromocytoma patients. Clin Cancer Res 15:6378-6385

153. Jiang X-S, Tang L-Y, Cao X-J, Zhou H, Xia Q-C, Wu J-R, Zeng R 2005 Two-dimensional gel electrophoresis maps of the proteome and phosphoproteome of primitively cultured rat mesangial cells. Electrophoresis 26:4540-4562

154. Perkins DN, Pappin DJ, Creasy DM, Cottrell JS 1999 Probability-based protein identification by searching sequence databases using mass spectrometry data. Electrophoresis 20:3551-3567

155. Nelson TJ, Backlund PS, Jr., Yergey AL, Alkon DL 2002 Isolation of protein subpopulations undergoing protein-protein interactions. Mol Cell Proteomics 1:253-259

156. Keller A, Nesvizhskii AI, Kolker E, Aebersold R 2002 Empirical statistical model to estimate the accuracy of peptide identifications made by MS/MS and database search. Anal Chem 74:5383-5392

157. Nesvizhskii AI, Keller A, Kolker E, Aebersold R 2003 A statistical model for identifying proteins by tandem mass spectrometry. Anal Chem 75:4646-4658

158. Fliedner SM, Breza J, Kvetnansky R, Powers JF, Tischler AS, Wesley R, Merino M, Lehnert H, Pacak K 2010 Tyrosine hydroxylase, chromogranin A, and steroidogenic acute regulator as markers for successful separation of human adrenal medulla. Cell Tissue Res 340:607-612

159. 1987 Isolation and characteristics of intact mitochondria. In: Darley-Usmar VM, Rickwood, D. and Wilson, M. T ed. Mitochondria: A Practical Approach Oxford, U.K.: IRL Press 3–5

160. Rustin P, Chretien D, Bourgeron T, Gerard B, Rotig A, Saudubray JM, Munnich A 1994 Biochemical and molecular investigations in respiratory chain deficiencies. Clin Chim Acta 228:35-51

161. Carpi A, Menabo R, Kaludercic N, Pelicci P, Di Lisa F, Giorgio M 2009 The cardioprotective effects elicited by p66(Shc) ablation demonstrate the crucial role of mitochondrial ROS formation in ischemia/reperfusion injury. Biochim Biophys Acta 1787:774-780

162. Reisch AS, Elpeleg O 2007 Biochemical assays for mitochondrial activity: assays of TCA cycle enzymes and PDHc. Methods Cell Biol 80:199-222

163. Goffrini P, Ercolino T, Panizza E, Giache V, Cavone L, Chiarugi A, Dima V,

Ferrero I, Mannelli M 2009 Functional study in a yeast model of a novel succinate dehydrogenase subunit B gene germline missense mutation (C191Y) diagnosed in a patient affected by a glomus tumor. Hum Mol Genet 18:1860-1868

164. Gatenby RA, Gillies RJ 2004 Why do cancers have high aerobic glycolysis? Nat Rev Cancer 4:891-899

165. Rossignol F, Solares M, Balanza E, Coudert J, Clottes E 2003 Expression of lactate dehydrogenase A and B genes in different tissues of rats adapted to chronic hypobaric hypoxia. J Cell Biochem 89:67-79

166. DeClerck K, Elble RC 2010 The role of hypoxia and acidosis in promoting metastasis and resistance to chemotherapy. Front Biosci 15:213-225

167. Walenta S, Salameh A, Lyng H, Evensen JF, Mitze M, Rofstad EK, Mueller-Klieser W 1997 Correlation of high lactate levels in head and neck tumors with incidence of metastasis. Am J Pathol 150:409-415

168. Brizel DM, Schroeder T, Scher RL, Walenta S, Clough RW, Dewhirst MW, Mueller-Klieser W 2001 Elevated tumor lactate concentrations predict for an increased risk of metastases in head-and-neck cancer. Int J Radiat Oncol Biol Phys 51:349-353

169. Walenta S, Wetterling M, Lehrke M, Schwickert G, Sundfor K, Rofstad EK, Mueller-Klieser W 2000 High lactate levels predict likelihood of metastases, tumor recurrence, and restricted patient survival in human cervical cancers. Cancer Res 60:916-921

170. Thorn CC, Freeman TC, Scott N, Guillou PJ, Jayne DG 2009 Laser microdissection expression profiling of marginal edges of colorectal tumours reveals evidence of increased lactate metabolism in the aggressive phenotype. Gut 58:404-412

171. Fantin VR, St-Pierre J, Leder P 2006 Attenuation of LDH-A expression uncovers a link between glycolysis, mitochondrial physiology, and tumor maintenance. Cancer Cell 9:425-434

172. Le A, Cooper CR, Gouw AM, Dinavahi R, Maitra A, Deck LM, Royer RE, Vander Jagt DL, Semenza GL, Dang CV 2010 Inhibition of lactate dehydrogenase A induces oxidative stress and inhibits tumor progression. Proc Natl Acad Sci U S A 107:2037-2042

173. Xie H, Valera VA, Merino MJ, Amato AM, Signoretti S, Linehan WM, Sukhatme VP, Seth P 2009 LDH-A inhibition, a therapeutic strategy for treatment of hereditary leiomyomatosis and renal cell cancer. Mol Cancer Ther 8:626-635

174. Okado-Matsumoto A, Fridovich I 2001 Subcellular distribution of superoxide

dismutases (SOD) in rat liver: Cu,Zn-SOD in mitochondria. J Biol Chem 276:38388-38393

175. Brand KA, Hermfisse U 1997 Aerobic glycolysis by proliferating cells: a protective strategy against reactive oxygen species. FASEB J 11:388-395

176. Isidoro A, Martinez M, Fernandez PL, Ortega AD, Santamaria G, Chamorro M, Reed JC, Cuezva JM 2004 Alteration of the bioenergetic phenotype of mitochondria is a hallmark of breast, gastric, lung and oesophageal cancer. Biochem J 378:17-20

177. Garcia Sanchez R, Hahn-Hagerdal B, Gorwa-Grauslund MF 2010 PGM2 overexpression improves anaerobic galactose fermentation in Saccharomyces cerevisiae. Microb Cell Fact 9:40

178. Baldi A, Lombardi D, Russo P, Palescandolo E, De Luca A, Santini D, Baldi F, Rossiello L, Dell'Anna ML, Mastrofrancesco A, Maresca V, Flori E, Natali PG, Picardo M, Paggi MG 2005 Ferritin Contributes to Melanoma Progression by Modulating Cell Growth and Sensitivity to Oxidative Stress. Clin Cancer Res 11:3175-3183

179. Huang HL, Stasyk T, Morandell S, Dieplinger H, Falkensammer G, Griesmacher A, Mogg M, Schreiber M, Feuerstein I, Huck CW, Stecher G, Bonn GK, Huber LA 2006 Biomarker discovery in breast cancer serum using 2-D differential gel electrophoresis/ MALDI-TOF/TOF and data validation by routine clinical assays. Electrophoresis 27:1641-1650

180. Masini A, Ceccarelli D, Giovannini F, Montosi G, Garuti C, Pietrangelo A 2000 Iron-induced oxidant stress leads to irreversible mitochondrial dysfunctions and fibrosis in the liver of chronic iron-dosed gerbils. The effect of silybin. J Bioenerg Biomembr 32:175-182

181. Britton RS, Leicester KL, Bacon BR 2002 Iron toxicity and chelation therapy. Int J Hematol 76:219-228

182. Chang HJ, Lee MR, Hong SH, Yoo BC, Shin YK, Jeong JY, Lim SB, Choi HS, Jeong SY, Park JG 2007 Identification of mitochondrial FoF1-ATP synthase involved in liver metastasis of colorectal cancer. Cancer Sci 98:1184-1191

183. Shin Y-K, Yoo BC, Chang HJ, Jeon E, Hong S-H, Jung M-S, Lim S-J, Park J-G 2005 Down-regulation of Mitochondrial F1F0-ATP Synthase in Human Colon Cancer Cells with Induced 5-Fluorouracil Resistance. Cancer Res 65:3162-3170

184. Willers IM, Cuezva JM 2010 Post-transcriptional regulation of the mitochondrial H(+)-ATP synthase: A key regulator of the metabolic phenotype in

cancer. Biochim Biophys Acta

185. Pedersen PL 2007 The cancer cell's "power plants" as promising therapeutic targets: an overview. J Bioenerg Biomembr 39:1-12

186. Chi SL, Pizzo SV 2006 Cell surface F1Fo ATP synthase: a new paradigm? Ann Med 38:429-438

187. Moser TL, Stack MS, Asplin I, Enghild JJ, Hojrup P, Everitt L, Hubchak S, Schnaper HW, Pizzo SV 1999 Angiostatin binds ATP synthase on the surface of human endothelial cells. Proc Natl Acad Sci U S A 96:2811-2816

188. Beerepoot LV, Witteveen EO, Groenewegen G, Fogler WE, Sim BK, Sidor C, Zonnenberg BA, Schramel F, Gebbink MF, Voest EE 2003 Recombinant human angiostatin by twice-daily subcutaneous injection in advanced cancer: a pharmacokinetic and long-term safety study. Clin Cancer Res 9:4025-4033

189. Lippe G, Bisetto E, Comelli M, Contessi S, Di Pancrazio F, Mavelli I 2009 Mitochondrial and cell-surface F0F1ATPsynthase in innate and acquired cardioprotection. J Bioenerg Biomembr 41:151-157

190. Vantourout P, Radojkovic C, Lichtenstein L, Pons V, Champagne E, Martinez LO 2010 Ecto-F-ATPase: a moonlighting protein complex and an unexpected apoA-I receptor. World J Gastroenterol 16:5925-5935

191. Harguindey S, Arranz JL, Wahl ML, Orive G, Reshkin SJ 2009 Proton transport inhibitors as potentially selective anticancer drugs. Anticancer Res 29:2127-2136

192. Hahm SH, Hsu CM, Eiden LE 1998 PACAP activates calcium influx-dependent and -independent pathways to couple met-enkephalin secretion and biosynthesis in chromaffin cells. J Mol Neurosci 11:43-56

193. Lodish MB, Powell AC, Abu-Asab M, Cochran C, Lenz P, Libutti SK, Pingpank JF, Tsokos M, Gorden P 2008 Insulinoma and gastrinoma syndromes from a single intrapancreatic neuroendocrine tumor. J Clin Endocrinol Metab 93:1123-1128

194. Cuezva JM, Krajewska M, de Heredia ML, Krajewski S, Santamaria G, Kim H, Zapata JM, Marusawa H, Chamorro M, Reed JC 2002 The Bioenergetic Signature of Cancer: A Marker of Tumor Progression. Cancer Res 62:6674-6681

195. He QY, Chen J, Kung HF, Yuen AP, Chiu JF 2004 Identification of tumor-associated proteins in oral tongue squamous cell carcinoma by proteomics. Proteomics 4:271-278

196. Lopez-Rios F, Sanchez-Arago M, Garcia-Garcia E, Ortega AD, Berrendero JR, Pozo-Rodriguez F, Lopez-Encuentra A, Ballestin C, Cuezva JM 2007 Loss of the

Mitochondrial Bioenergetic Capacity Underlies the Glucose Avidity of Carcinomas. Cancer Res 67:9013-9017

197. Shi XJ, Knowles AF 1994 Prevalence of the mercurial-sensitive EctoATPase in human small cell lung carcinoma: characterization and partial purification. Arch Biochem Biophys 315:177-184

198. Yonally SK, Capaldi RA 2006 The F(1)F(0) ATP synthase and mitochondrial respiratory chain complexes are present on the plasma membrane of an osteosarcoma cell line: An immunocytochemical study. Mitochondrion 6:305-314

199. Lindqvist A, Berger K, Erlanson-Albertsson C 2008 Enterostatin up-regulates the expression of the beta-subunit of F(1)F(o)-ATPase in the plasma membrane of INS-1 cells. Nutr Neurosci 11:55-60

200. Lu ZJ, Song QF, Jiang SS, Song Q, Wang W, Zhang GH, Kan B, Chen LJ, Yang JL, Luo F, Qian ZY, Wei YQ, Gou LT 2009 Identification of ATP synthase beta subunit (ATPB) on the cell surface as a non-small cell lung cancer (NSCLC) associated antigen. BMC Cancer 9:16

201. Zhang X, Gao F, Yu LL, Peng Y, Liu HH, Liu JY, Yin M, Ni J 2008 Dual functions of a monoclonal antibody against cell surface F1F0 ATP synthase on both HUVEC and tumor cells. Acta Pharmacol Sin 29:942-950

202. Ma Z, Cao M, Liu Y, He Y, Wang Y, Yang C, Wang W, Du Y, Zhou M, Gao F 2010 Mitochondrial F1Fo-ATP synthase translocates to cell surface in hepatocytes and has high activity in tumor-like acidic and hypoxic environment. Acta Biochim Biophys Sin (Shanghai) 42:530-537

203. Ravera S, Aluigi MG, Calzia D, Ramoino P, Morelli A, Panfoli I 2010 Evidence for Ectopic Aerobic ATP Production on C6 Glioma Cell Plasma Membrane. Cell Mol Neurobiol

204. Pervaiz S, Holme AL 2009 Resveratrol: its biologic targets and functional activity. Antioxid Redox Signal 11:2851-2897

205. Bishayee A 2009 Cancer prevention and treatment with resveratrol: from rodent studies to clinical trials. Cancer Prev Res (Phila) 2:409-418

206. Kundu JK, Surh YJ 2008 Cancer chemopreventive and therapeutic potential of resveratrol: mechanistic perspectives. Cancer Lett 269:243-261

207. Brown VA, Patel KR, Viskaduraki M, Crowell JA, Perloff M, Booth TD, Vasilinin G, Sen A, Schinas AM, Piccirilli G, Brown K, Steward WP, Gescher AJ, Brenner DE 2010 Repeat Dose Study of the Cancer Chemopreventive Agent

Resveratrol in Healthy Volunteers: Safety, Pharmacokinetics, and Effect on the Insulin-like Growth Factor Axis. Cancer Res 70:9003-9011

208. Patel KR, Brown VA, Jones DJ, Britton RG, Hemingway D, Miller AS, West KP, Booth TD, Perloff M, Crowell JA, Brenner DE, Steward WP, Gescher AJ, Brown K 2010 Clinical pharmacology of resveratrol and its metabolites in colorectal cancer patients. Cancer Res 70:7392-7399

209. Boocock DJ, Faust GE, Patel KR, Schinas AM, Brown VA, Ducharme MP, Booth TD, Crowell JA, Perloff M, Gescher AJ, Steward WP, Brenner DE 2007 Phase I dose escalation pharmacokinetic study in healthy volunteers of resveratrol, a potential cancer chemopreventive agent. Cancer Epidemiol Biomarkers Prev 16:1246-1252

210. Jang JH, Surh YJ 2003 Protective effect of resveratrol on beta-amyloid-induced oxidative PC12 cell death. Free Radic Biol Med 34:1100-1110

211. Albani D, Polito L, Batelli S, De Mauro S, Fracasso C, Martelli G, Colombo L, Manzoni C, Salmona M, Caccia S, Negro A, Forloni G 2009 The SIRT1 activator resveratrol protects SK-N-BE cells from oxidative stress and against toxicity caused by alpha-synuclein or amyloid-beta (1-42) peptide. J Neurochem 110:1445-1456

212. Liontas A, Yeger H 2004 Curcumin and resveratrol induce apoptosis and nuclear translocation and activation of p53 in human neuroblastoma. Anticancer Res 24:987-998

213. Das DK, Sato M, Ray PS, Maulik G, Engelman RM, Bertelli AA, Bertelli A 1999 Cardioprotection of red wine: role of polyphenolic antioxidants. Drugs Exp Clin Res 25:115-120

214. Howitz KT, Bitterman KJ, Cohen HY, Lamming DW, Lavu S, Wood JG, Zipkin RE, Chung P, Kisielewski A, Zhang LL, Scherer B, Sinclair DA 2003 Small molecule activators of sirtuins extend Saccharomyces cerevisiae lifespan. Nature 425:191-196

215. Baur JA, Pearson KJ, Price NL, Jamieson HA, Lerin C, Kalra A, Prabhu VV, Allard JS, Lopez-Lluch G, Lewis K, Pistell PJ, Poosala S, Becker KG, Boss O, Gwinn D, Wang M, Ramaswamy S, Fishbein KW, Spencer RG, Lakatta EG, Le Couteur D, Shaw RJ, Navas P, Puigserver P, Ingram DK, de Cabo R, Sinclair DA 2006 Resveratrol improves health and survival of mice on a high-calorie diet. Nature 444:337-342

216. Lappano R, Rosano C, Madeo A, Albanito L, Plastina P, Gabriele B, Forti L, Stivala LA, Iacopetta D, Dolce V, Ando S, Pezzi V, Maggiolini M 2009 Structure-activity relationships of resveratrol and derivatives in breast cancer cells. Mol Nutr

Food Res 53:845-858

217. Shi WF, Leong M, Cho E, Farrell J, Chen HC, Tian J, Zhang D 2009 Repressive effects of resveratrol on androgen receptor transcriptional activity. PLoS One 4:e7398

218. Wu H, Liang X, Fang Y, Qin X, Zhang Y, Liu J 2008 Resveratrol inhibits hypoxia-induced metastasis potential enhancement by restricting hypoxia-induced factor-1 alpha expression in colon carcinoma cells. Biomed Pharmacother 62:613-621

219. Zheng J, Ramirez VD 2000 Inhibition of mitochondrial proton F0F1-ATPase/ATP synthase by polyphenolic phytochemicals. Br J Pharmacol 130:1115-1123

220. Gledhill JR, Montgomery MG, Leslie AG, Walker JE 2007 Mechanism of inhibition of bovine F1-ATPase by resveratrol and related polyphenols. Proc Natl Acad Sci U S A 104:13632-13637

221. Dadi PK, Ahmad M, Ahmad Z 2009 Inhibition of ATPase activity of Escherichia coli ATP synthase by polyphenols. Int J Biol Macromol 45:72-79

222. Arakaki N, Nagao T, Niki R, Toyofuku A, Tanaka H, Kuramoto Y, Emoto Y, Shibata H, Magota K, Higuti T 2003 Possible role of cell surface H+ -ATP synthase in the extracellular ATP synthesis and proliferation of human umbilical vein endothelial cells. Mol Cancer Res 1:931-939

223. Chi SL, Pizzo SV 2006 Angiostatin is directly cytotoxic to tumor cells at low extracellular pH: a mechanism dependent on cell surface-associated ATP synthase. Cancer Res 66:875-882

This dissertation would not have been possible without the help and support of others:
Professor Lehnert, I am deeply grateful that you were my “Doktorvater”. With bringing me to the NIH you gave me the chance of a lifetime. I am deeply grateful for the support you have provided all along the way, especially that you found time for me whenever I needed reassurance.
Professor Pacak, you were my local supervisor over the past (almost) 5 years and I could not have wished for a better. You were demanding, which allowed me to aim high. Over time I found out, that you were not demanding for your own sake, but because you care. If things did not go the way I hoped for, you were always there to help and find alternatives. There are no words to express how grateful I am towards you. You gave me the wings to fly with my ideas, but helped me not to lose focus on reality.
I am especially grateful to Dr. Wesley. On top of having all patience in the world to explain the miracles of statistics to me, he turned out to be a great mentor and friend. Bob, thank you for never letting me feel stupid when I say something silly!
Dr. Yergey, Dr. Backlund, Dr. Mischak and Dr. Zürbig were all the support in the world I could have hoped for in my proteomics work. Al, you allowed me to keep the perspective of what is important in life when I felt like everything is going wrong.
Dr. Kainerstorfer, I would like to thank you for sitting with me through seemingly endless hours of manuscript writing and data analysis. You were there to cheer me up if needed, made more coffee, and helped me to go beyond the limits of what I thought I could possibly do.
Tamara Prodanov, with your pragmatic views of the world, you helped me remember that the sky is the limit and I just have to reach for it. Thank you!
Dr. Biertümpfel, you were the person who most of all helped me build a life in the US. But you were also greatly supportive of my work in solving many issues that seemed impossible to solve for me.
I would also like to thank Dr. Lai, Dr. Martiniova, the nurses of 5NW and 1NW, and all other colleagues I worked with at the NIH.
Without the support of the patients this work would not have been possible. Thank you for donating your blood, urine, and tissue.
And last but not least I would like to thank my parents for always believing in me.